INVESTIGATION OF FERMI-LIQUID EFFECTS
IN SUPERCONDUCTING VANADIUM AND AMORPHOUS GALLIUM
BY SPIN-POLARIZED TUNNELING

by

GARY ALFRED GIBSON

B.S. Physics and Math, Stanford University
(1980)

SUBMITTED TO THE DEPARTMENT OF PHYSICS
IN PARTIAL FULFILLMENT OF THE REQUIREMENTS
FOR THE DEGREE OF

DOCTOR OF PHILOSOPHY IN PHYSICS

at the

MASSACHUSETTS INSTITUTE OF TECHNOLOGY
June, 1988

Signature of Author   ....
Department of Physics
June, 1988

Certified by ....
R.H. Meservey
Senior Scientist, National Magnet Laboratory, MIT
Thesis Supervisor

Certified by ....
P.A. Wolff
Professor, Department of Physics, MIT
Thesis Supervisor

Accepted by ....
G.F. Koster, Chairman
Departmental Graduate Committee
Department of Physics

INVESTIGATION OF FERMI-LIQUID EFFECTS
IN SUPERCONDUCTING VANADIUM AND AMORPHOUS GALLIUM
BY SPIN-POLARIZED TUNNELING

by

GARY ALFRED GIBSON

Submitted to the Department of Physics
on June, 10 1988 in partial fulfillment of the
requirements for the Degree of Doctor of Philosophy in Physics

Abstract

The Fermi-liquid parameter G_0 has been determined in both vanadium and amorphous gallium. $Al/Al_2O_3/V$ and $Al/Al_2O_3/a\text{-}Ga$ tunnel junctions were used to observe the renormalization caused by Fermi-liquid interactions of the spin-splitting of the quasiparticle density of states of these materials in a magnetic field . In both cases this was done by fitting the dynamic tunneling conductance to the theory of Rainer. The results were consistent with critical field measurements made on the same films. To study amorphous gallium an evaporator capable of making and measuring junctions at less than 1 K within the 2 inch bore of a Bitter magnet was used. A large renormalization was observed in amorphous gallium ($G_0 = 0.81 \pm 0.14$), as expected for this strongly-coupled material. To our knowledge this is the largest positive value for G_0 measured in a metal. Correlation effects were also observed in thin, disordered gallium films. In vanadium $G_0 \simeq 0$, indicating the importance of spin-fluctuations. $Fe/Al_2O_3/V$ tunnel junctions were also used to resolve the conductance into the contributions from each electron spin direction and verify this result. The spin-orbit scattering rates, b_{so}, have concurrently been determined. It was found that $b_{so}^{a\text{-}Ga} = 0.18 \pm 0.03$ and $b_{so}^{V} = 0.06 \pm 0.03$.

Thesis Supervisors:

R.H. Meservey
Senior Scientist

P.A. Wolff
Professor of Physics

ACKNOWLEDGEMENTS

Well, the pay isn't great, but you can't beat the working environment.... The years I spent at M.I.T. were enjoyable because of the people with whom I worked. Bob Meservey is all I could ask for in an advisor. He is not only a good scientist; he is a wise and caring teacher. His optimism is infectious. I always felt better (and knew more) about my work after talking to Bob.

I am deeply indebted to Jagadeesh Moodera for the countless times he dropped what he was doing in order to give me a hand. His patience in helping others constantly amazes me. Without him, much of the research at the Francis Bitter National Magnet Lab (and elsewhere!) would grind to a standstill.

I would like to thank Paul Tedrow for many helpful discussions and for suggesting a thesis topic. Paul can always be counted on for an intelligent comment. Thanks are also due my fellow graduate student, Eric Tkaczyk. I have often benefitted from his understanding of a problem.

A number of other people at the Magnet Lab were helpful. Mike Blaho was invaluable for finding parts, fixing equipment, and giving history lessons on World War II. Larry Rubin and Bruce Brandt were very accomodating with Magnet Lab facilities. I hope I have returned all the equipment I borrowed from them. I would also like to thank Richard McNabb for preparing innumerable samples.

Professors Terry Orlando, Peter Wolff and David Rudman were all sources of good advice. In addition, Terry answered many of my questions on Fermi-liquid effects.

Mark Taylor, Jagadeesh Moodera, and Paul Tedrow graciously volunteered to proofread this thesis and provided many helpful suggestions.

Finally, I would like to thank my parents. They taught me the value of an education, and have always supported and encouraged mine.

4

Contents

List of Figures

Chapter 1

Introduction

This thesis is a study of Fermi-liquid effects using superconducting vanadium and amorphous gallium. Consideration of these effects is essential to understanding the properties of superconductors near their transition to the normal state. The properties considered include the critical magnetic field, particularly at low temperature, and the quasiparticle density of states. A comparison with theory of the renormalization of these quantities will be used to determine the Fermi-liquid parameter, G_0. Fermi-liquid theory provides a useful and conceptually economical framework for the description of many of the equilibrium and transport properties of metals and ^3He. The Fermi-liquid parameters are intrinsic to a material and are the same in the superconducting and normal states. Their determination from normal materials is difficult and has only been accomplished for a few elements. The present technique is a powerful method for determining

13

G_0 in materials which undergo a superconducting transition. A large renormalization of the critical field and quasiparticle density of states was observed in amorphous gallium, underscoring the need to incorporate Fermi-liquid effects in understanding the superconducting behaviour of this material. A very small renormalization was found in vanadium, providing strong new evidence for the importance of spin fluctuations in this system. The large renormalization in amorphous gallium is due to its strong electron-phonon coupling. The small effect in vanadium is the result of a strong electron-electron interaction enhanced by spin-fluctuations, which cancels out the effect due to its electron-phonon interaction. For both these materials the data were in excellent agreement with theory. Thus, these materials test the theory both for strong electron-phonon and strong electron-electron interactions.

Near a second-order phase transition to the normal state the density of quasiparticles approaches the normal-state density of electrons and interaction between them becomes important. The effect of the neighboring quasiparticles on a given quasiparticle can be described in terms of an additional field acting on its spin (in addition to the renormalization of its self-energy or effective mass). Since this is equivalent to renormalizing the effective magnetic moment of the quasiparticles, the principal effects of the interaction are the renormalization of the

superconducting properties dependent on this moment. These include the Pauli-limited critical field and the spin-splitting of the quasiparticle density of states in a magnetic field.

The importance of Fermi-liquid effects in high-field superconductivity was first pointed out by Orlando, et al. (1979), Tedrow and Meservey (1979, 1982), and Orlando and Beasley (1981) in their critical field experiments on Pauli limited superconductors. The theoretical foundation for the incorporation of Fermi-liquid effects into clean superfluids was laid by Leggett (1965, 1968, 1975). The extension of the standard high-field theory of superconductivity (Werthamer, et al., 1966; Maki, 1966) to include these effects was performed by Rainer (Alexander, et al., 1985) in the dirty limit using the quasiclassical approach. We will use this theory, which is described in Chapter 2, to analyze our results. Rainer's theory was first used by Tedrow, et al. (1984) and Alexander (1986) to measure the Fermi-liquid parameter, G_0, in aluminum. They did this by fitting the renormalization of the quasiparticle density of states as a function of field to the theory and obtained $G_0 = 0.3$. The most important change due to the Fermi-liquid effects is the renormalization of the effective Zeeman splitting. This and the history of these measurements are also described in Chapter 2.

We have used fits of the dynamic conductance of $Al/Al_2O_3/a$-Ga

tunnel junctions as a function of field and temperature to determine G_0 in amorphous gallium. The large renormalization observed ($G_0 = 0.81$) verifies the importance of Fermi-liquid effects, as well as the accuracy of Rainer's theory in describing them. The large size of the renormalization allows for it to be unambiguously distinguished from the similar effects of spin-orbit scattering. Fitting of the dynamic conductance and critical fields of the gallium junctions is described in Chapter 4. A discussion of the results can be found in Section 6.1.

Amorphous gallium anneals at less than 20 K. Thus, it was necessary to use an evaporator capable of making and measuring these junctions within the 2 inch bore of a Bitter magnet. This experimental equipment is described in Section 3.3. Procedures for making and testing these junctions, as well as the junctions used in the vanadium studies are discussed in Chapter 3.

The dynamic conductance of $Al/Al_2O_3/V$ tunnel junctions was also fit to the theory. Good agreement was found with a value for G_0 of zero. The presence of a zero-bias peak in the conductance at high field aided in making an accurate determination of G_0. Its existence also established an upper bound on the spin-orbit scattering rate of about $b_{so} = 0.12.$[1] This analysis is described in Section 5.2 and discussed in

---

[1]The spin-orbit scattering rate is a phenomenological parameter used in the theory to describe the "$\vec{L} \cdot \vec{s}$" coupling of the electrons to impurity and defect potentials. $b_{so} = \hbar/3\tau_{so}\Delta_0$ where τ_{so} is the spin-orbit scattering time and Δ_0 is the order parameter at zero temperature and field.

Section 6.2.

The low value for G_0 is strong evidence for the importance of spin fluctuations in this material. The enhanced electron-electron interaction due to spin- fluctuations is essentially canceling out the effect of the electron-phonon interaction. This is of great interest because spin-fluctuations are believed to be responsible for the low T_c of vanadium and the lack of superconductivity in elements such as palladium. This is discussed in Section 6.2.

$V/Al_2O_3/Fe$ junctions have also been studied. These junctions allow for the separation of the junction conductance into its "up-spin" and "down-spin" components. This allows a direct measure of the renormalization of the effective Zeeman splitting in a field. Fitting these separated curves to the theory also provides an additional check on the spin-orbit scattering rate and the accuracy of the theory in incorporating Fermi-liquid effects. This experimental technique is explained in Section 3.1. Its application to $V/Al_2O_3/Fe$ junctions is described in Section 5.3 and discussed in Section 6.2. An attempt was also made to make amorphous gallium tunnel junctions with ferromagnetic counterelectrodes. This work is described in Appendix A.

For both vanadium and amorphous gallium the measured value of

G_0 is predicted quite accurately by the simple relation

$$1 + G_0 = (1 + \lambda_{ep} + \lambda_s)(1 - \bar{I})$$

where λ_{ep} is the electron-phonon coupling constant, λ_s is the equivalent mass renormalization for paramagnons, and $(1-\bar{I})^{-1}$ is the Stoner factor. Thus, it seems possible to predict the overall renormalization by simply summing the contributions from the electron-electron and electron-phonon interactions in this simple way.

An interesting consequence of our work with thin, disordered gallium was the observation of correlation effects in its normal state density of states. Both logarithmic and square-root corrections were seen in the energy dependence of the density of states. This depended on the thickness and diffusion constant of the film involved, as well as the temperature. This is in accord with the theories of Al'tshuler and Aronov (1979), McMillan (1981), and Al'tshuler, Aronov, and Lee (1980) and is discussed in Appendix B.

Chapter 2

Fermi Liquid Effects

2.1 Normal Fermi-Liquids

Good reviews of Fermi-liquid theory for normal Fermi-liquids are given in Baym and Pethick (1978) and Wilkins (1980). The underlying assumption behind Landau's Fermi-liquid theory is that the low-lying excited states of a strongly interacting collection of fermions can be modeled as nearly-free particles (Landau 1956, 1958). These "quasiparticle" states are in a one-to-one correspondence with the states of the non-interacting system. They possess a definite momentum, p, and spin, σ. There is a well defined Fermi surface such that in the ground state all states with $p < \hbar k_F$ are occupied. The success of this approach is due to the Pauli exclusion principle. The lifetime of an excited electron close to the Fermi surface is long because the Fermi sea occupies most of the phase space into which it can decay. Landau defined the quasiparticle energy, $E_{\mathbf{p},\sigma}$, as $E_{\mathbf{p},\sigma} = \partial E / \partial n_{\mathbf{p},\sigma}$ where the

19

$n_{\mathbf{p},\sigma}$ are the occupation numbers for the basis states and E is the total energy of the system. Thus, $\delta E = \sum_{\mathbf{p},\sigma} E_{\mathbf{p},\sigma} \delta n_{\mathbf{p},\nu}$. Note that the total energy is not simply the sum of the quasiparticle energies. Both the total energy and the quasiparticle energies are functionals of the occupation numbers. Thus,

$$E_{\mathbf{p},\sigma} = E_{\mathbf{p},\sigma}^0 + \sum_{\mathbf{p}',\sigma'} f(\mathbf{p},\sigma; \mathbf{p}',\sigma') \delta n_{\mathbf{p},\sigma} \qquad (2.1)$$

where f is the scattering amplitude which describes the interaction between quasiparticles and $E_{\mathbf{p},\sigma}^0$ is the quasiparticle energy in the absence of interactions. If we include the spin degrees of freedom in the general case where the spins are not all quantized along the same axis then the distribution function becomes a 2 × 2 matrix in spin space.

$$\tilde{\mathbf{n}}_{\mathbf{p}} = n_p \tilde{\delta} + \vec{\sigma}_p \cdot \vec{\tilde{\tau}}$$

We will use tildes to indicate 2 × 2 matrices. Here $\tilde{\delta}$ is the identity matrix, the $\tilde{\tau}_i$ are the Pauli matrices, and $(\sigma_p)_i = \sum_{\alpha\alpha'} (\tilde{\tau}_i)_{\alpha\alpha'} (\tilde{\mathbf{n}}_{\mathbf{p}})_{\alpha'\alpha}$ is the expectation value of the spin polarization in the i<u>th</u> direction for quasiparticle p. For simplicity, we will use p to indicate both the momentum and spin indices. Clearly, the quasiparticle energy can be written in the form

$$\tilde{\mathbf{E}}_{\mathbf{p}} = E_p \tilde{\delta} + \vec{h}_p \cdot \vec{\tilde{\tau}} \qquad (2.2)$$

since $\tilde{\delta}$ and the $\tilde{\tau}_i$'s span the space of 2 × 2 matrices. In the absence of spin-orbit coupling between the quasi-particles the most general form

for the interaction function is

$$\tilde{\mathbf{f}}_{\mathbf{pp'}} = f_{pp'}\tilde{\delta} + g_{pp'}\vec{\tau} \cdot \vec{\tau}'$$

where we have also assumed rotational symmetry. Thus, Equation 2.1 becomes

$$
\begin{aligned}
E_p &= E_p^0 + 2\sum_{p'} f_{pp'}\delta n_{p'} \\
\vec{h}_p &= \vec{h}_p^0 + 2\sum_{p'} g_{pp'}\delta\vec{\sigma}_{p'}
\end{aligned}
\qquad (2.3)
$$

From the form of Equation 2.2, we now see that the effect of the quasiparticle interaction can be thought of as two-fold. There is an effective internal or 'molecular' field $\vec{h}_p^I$ acting on the quasiparticles' spins (but not coupled to their orbital motion) in addition to the external field $\vec{h}_p^0$ ($\vec{h}_p = \vec{h}_p^0 + \vec{h}_p^I$). In addition, the particles' effective mass is renormalized. Of course, the net self-energy (or effective mass) includes the field.

For a rotationally invariant system the interaction depends only on $|\mathbf{p} - \mathbf{p'}|$. If we consider only low-lying excitations (Fermi-liquid theory is only good for low-lying excitations) then $|\mathbf{p}|, |\mathbf{p'}| \simeq \hbar k_F$, and f depends only on the angle θ between $\mathbf{p}$ and $\mathbf{p'}$. We can then expand f and g in terms of Legendre polynomials,

$$
\begin{aligned}
4N(0)f_{\mathbf{p},\mathbf{p'}} &= \sum_l (2l+1)F_l P_l(cos\theta) \\
4N(0)g_{\mathbf{p},\mathbf{p'}} &= \sum_l (2l+1)G_l P_l(cos\theta)
\end{aligned}
\qquad (2.4)
$$

where $N(0)$ is the density of states at the Fermi surface. The F_l's and G_l's are known as Landau parameters or Fermi-liquid parameters. Fermi-liquid theory provides a useful and conceptually economical way of describing many of the equilibrium and transport properties of metals and ^3He in terms of these parameters. In most cases, only a few parameters are necessary to describe the renormalization of physical quantities due to the interaction between quasiparticles. For example, consider the effect of an applied field, H_a, in the $\hat{z}$ direction. Clearly, if we ignore the coupling of the field to the orbital motion, the change in occupation number and spin polarization (δn_p and $\delta \vec{\sigma}_p$) due to the field are independent of the direction of p. Thus, the $l > 0$ terms drop out of the change in energy, $\delta \tilde{E}_p$, when we integrate over p' in Eq. 2.3 (ie., take the sum over p'). Also, since this pertubation is only coupled to the spins the symmetric terms (the F's) drop out when we sum over spin. Thus, using Eqs. 2.2, 2.3, and 2.4 we see that

$$\tilde{E}_p = E_p \tilde{\delta} + [\vec{h}_p^0 + 2\left(\frac{G_0}{4N(0)}\right) \sum_{p'} \delta \vec{\sigma}_{p'}] \cdot \tilde{\delta} \qquad (2.5)$$

Now,

$$\sum_{p'} \delta \vec{\sigma}_{p'} = \delta n_\uparrow - \delta n_\downarrow$$
$$= 2N(0)\mu_{eff} H_a \qquad (2.6)$$

where $n_\uparrow$ and $n_\downarrow$ are the total number of up and down particles, respec-

tively, and μ_{eff} is the effective magnetic moment[1]. The last equality

follows from equating the chemical potentials of the two spin direc-

tions. Plugging Eq. 2.6 into Eq. 2.5 we get

$$E_{p\uparrow} - E_{p\downarrow} = -2\mu_b H_a + 2G_0 \mu_{eff} H_a$$

$$\equiv -2\mu_{eff} H_a \qquad (2.7)$$

Thus,

$$\mu_{eff} = \frac{\mu_B}{1 + G_0}. \qquad (2.8)$$

The change in the effective mass, m^*, or self-energy of the quasi-

particles can be expressed in terms of the renormalization of the den-

sity of states found from the heat capacity, $N(0)$,

$$C/C_0 = m^*/m = N(0)/N_0(0). \qquad (2.9)$$

Here $N_0(0)$ is the heat capacity density of states in the absence of

Fermi-liquid effects, or the band-structure density of states. Using

Eqs. 2.6, 2.8 and 2.9 we get

$$\chi = \frac{M}{H_a} = \frac{\mu_B(n_\uparrow - n_\downarrow)}{H_a} = 2\mu_B\mu_{eff}N(0) = \frac{(m^*/m)}{1 + G_0}\chi_0 \qquad (2.10)$$

where χ and χ_0 are the Pauli spin susceptibility with and without

renormalization, respectively. For a translationally invariant system

---

[1]Note the perspective this gives on the physical significance of G_0. The change
in energy of the quasiparticles is proportional to G_0 times the change in occupation
numbers for a perturbation which is anti-symmetric in spin: $\delta E_{p\uparrow} = -\mu_B H_a + (n_{p\uparrow} - n_{p\downarrow})\frac{G_0}{2N(0)}$

such as ^3He

$$m^*/m = 1 + F_1$$

Also, the renormalization of the compressibility and sound velocity is readily shown to be

$$\kappa_0/\kappa = v_S^2/v_{S0}^2 = \frac{1 + F_0}{(m^*/m)}$$

Note that the ratio of the effective density of states measured from heat capacity [2] to that obtained from the spin susceptibilty is given by

$$N(\gamma)/N(\chi) = 1 + G_0 \tag{2.11}$$

As we will see below, this difference in the effective densities of states, characterized by the single parameter G_0, is responsible for the many-body effects which have been observed in high-field superconductivity.

The contributions to the renormalization in which we are interested arise from the electron-phonon interaction and the exchange induced electron-electron interaction including spin fluctuations, if present. The renormalization of the effective mass due to the electron-phonon interaction is well known. In the presence of spin fluctuations an additional change in the self-energy arises if the spin-polarization regions are sufficiently large and long-lived. Then, a given up-spin electron will be surrounded (usually) by other up-spin electrons. This

---

[2] $N(\gamma)$ is the same as $N(0)$ from above.

makes it difficult for a down-spin electron to take advantage of the short range electron-phonon attraction produced by the up spin electron. There is an effective exchange potential barrier separating the two spins.

The manner in which the electron-electron and electron-phonon contributions should be added in order to determine the net renormalization is still a matter of debate. Jensen and Andres (1968) have shown that the renormalization of the self-energy of a quasiparticle in the presence of these interactions is given by

$$m^*/m = 1 + \lambda_{ep} + \lambda_s \qquad (2.12)$$

λ_{ep} is the usual electron-phonon coupling constant

$$\lambda_{ep} = 2 \int \frac{\alpha^2 F(\omega)}{\omega} d\omega$$

where α^2 is the square of the electron-phonon matrix element and $F(\omega)$ is the phonon density of states. Similarly,

$$\lambda_s = 2 \int \frac{P(\omega)}{\omega} d\omega$$

is the (equivalent) mass-renormalization parameter for spin-fluctuations with a paramagnon spectral density (the equivalent of $\alpha^2 F(\omega)$) given by $P(\omega)$. Equation 2.12 was derived using the theory of Berk and Schrieffer (1966). Berk and Schrieffer included the contribution of spin-fluctuations in the linearized Eliashberg equation. Leavens and

Macdonald (1983) argued that it is not clear how to add in the Feyn-
mann diagrams which contribute to the paramagnon spectral density.
According to their model calculations, Equation 2.12 is only accurate
when the exchange enhancement factor is large. From their model
Berk and Schrieffer also show that in the static, long wavelength limit
the susceptibility is given by

$$\chi(0,0) = 2\mu_B^2 N(0)/[1 - N(0)\bar{V_c}] \qquad (2.13)$$

This is similar to the expression derived by Wolff (1960) in the random
phase approximation. $\bar{V_c}$ is the Fermi surface average of the Coulomb
exchange potential. The factor $N(0)\bar{V_c}$ is equivalent to the quantity $\bar{I}$
often used in the literature. $(1 - \bar{I})^{-1}$ is the Stoner factor or exchange
enhancement. Combining Equations 2.10, 2.12, and 2.13 we obtain

$$1 + G^0 = (1 + \lambda_{ep} + \lambda_s)(1 - \bar{I}) \qquad (2.14)$$

This equation was also suggested by Orlando and Beasley (1981) in
explaining their V_3Ga critical field data. We will use Equation 2.14 to
make a rough comparison of our measured values for G_0 with known
or estimated values for λ_{ep}, λ_s and $\bar{I}$. It should be noted that Equa-
tion 2.14 is not an expansion to first order in the small parameters,
λ. It is derived from the equivalent of Wigner-Brillouin perturba-
tion theory and, in so far as the theory is correct (see caveat above),
is accurate to all orders in λ. It should also be remarked that, as

pointed out by Daams, Mitrovic, and Carbotte (1981), the electron-phonon coupling constant and the effective Coulomb pseudopotential are themselves both rescaled by the mass renormalization, λ_s.

$$(\lambda_{ep})_{eff} = \frac{\lambda_{ep}}{1 + \lambda_s}$$
$$(\mu^*)_{eff} = \frac{\mu^* + \lambda_s}{1 + \lambda_s} \tag{2.15}$$

One of the major problems in determining Fermi-liquid parameters in normal metals is that it is difficult to know how much of the measured renormalization is due to Fermi-liquid interactions and how much is due to other effects. Fermi-liquid theory deals with the residual interaction between already dressed quasiparticles. In real metals the electrons will interact, for example, with phonons, thereby changing their effective mass. There will also be an orbital contribution to the susceptibility, which will change their apparent magnetic moment[3]. Thus the problem lies in knowing the "bare" quantities, eg. the effective mass in the absence of Fermi-liquid effects. A few Fermi-liquid parameters have been measured in some of the alkali metals by the technique of conduction electron spin resonance and by de Haas van Alphen measurements (see Platzman and Wolff, 1973, for a review). More recently, some have been measured in noble metals (Vier, Tolleth, and Schultz, 1984). They have also been determined

---

[3]If not for this one could easily determine G_0 using Eq. 2.11 from heat capacity and susceptibility measurements.

for ^3He and used to predict the velocities of zero and first sound (see Wilkins, 1980, and references therein).

As we shall see in the next section, superconductors provide an excellent system for studying Fermi-liquid corrections while circumventing the problems associated with knowing the "bare" mass. In section (2.4) we will describe the measurement of the parameter G_0 in superconducting aluminum in recent experiments by Tedrow, *et al.* (1984), and Alexander (1986). The present experiments are an outgrowth of this work.

2.2 Fermi Liquid Effects In Superconductors

Superconductors are good systems for studying Fermi-liquid effects because we can essentially turn the Fermi-liquid interactions on and off by moving toward or away from the phase boundary. This idea is illustrated schematically in Figure 2.1, where we have plotted the effective field acting on the quasiparticles' spins versus the density of quasiparticle excitations. At low temperature and field, far from the phase boundary, the quasiparticle excitations are few and far between and interaction between them is insignificant. As we approach a second order phase boundary the density of quasiparticles approaches the normal state density of electrons and interaction between them
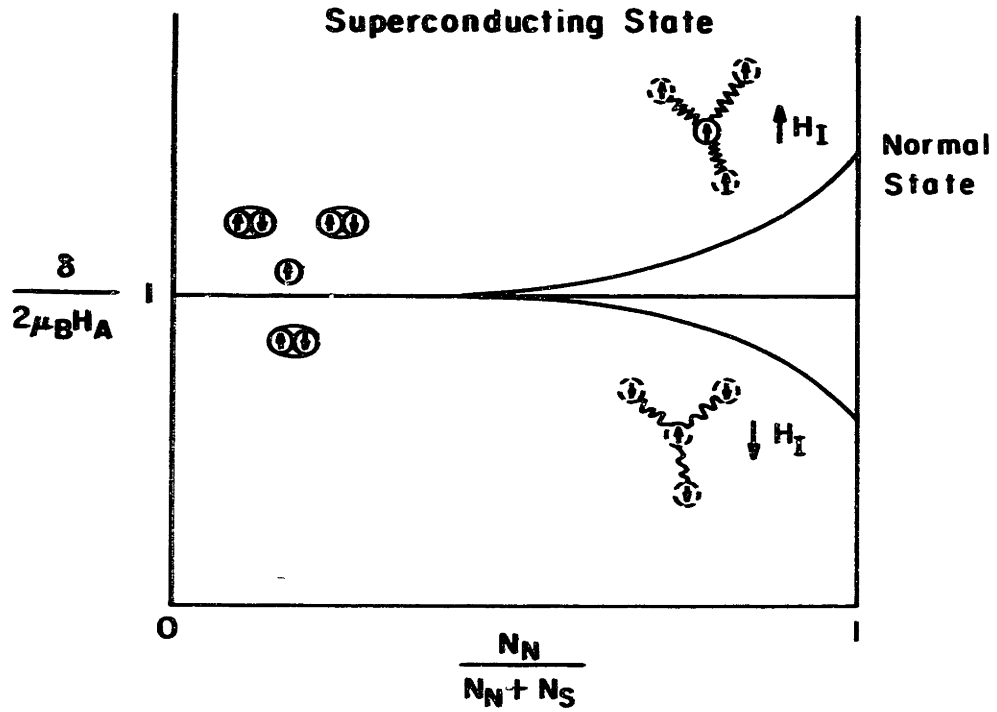
Figure 2.1: Schematic plot of the apparent Zeeman splitting (or the effective field acting on the quasiparticles' spins) versus the applied field (or the density of quasiparticle excitations). In the absence of interaction between the quasiparticles the apparent Zeeman splitting, δ, is equal to $2\mu_B H_A$. The effect of the interaction can either increase or decrease the apparent splitting as the phase boundary is approached.

becomes important[4]. As we will see, the most important contribu-
tions to this interaction come from the electron-phonon interaction
and the electron-electron interaction, including spin-fluctuations if
present. This ability to turn on and off the Fermi-liquid interac-
tions allows us to distinguish them from the other many-body inter-
actions which act to renormalize the self-energy (The quasiparticles
are already dressed with their electronic correlation clouds and with
phonons.). The effect of the Fermi-liquid interaction, as we saw above,
can be described in terms of an additional effective field, which acts
on the quasiparticles' spin, and a renormalized mass. Theoretically
the interaction can be of either sign, ie. the added field can either
add to or subtract from the applied field. We will show below that
in a dirty superconductor the strength of this effective field and the
mass renormalization can be characterized by a single parameter in
the framework of Fermi-liquid theory. It is important to realize that
these Fermi-liquid parameters are intrinsic parameters of the material
and are the same in the superfluid and normal states.

Historically, the need to incorporate Fermi-liquid effects in high
field superconductivity was first pointed out by Clogston (1962). The

---

[4]Here we mean the usual "superconductor quasiparticles" rather than the quasi-
particles of Fermi-liquid theory. The point of this discussion is that interaction
between these "superconductor quasiparticles" necessitates their renormalization.
Thus, in applying Fermi-liquid theory to superconductors one must use quasiparti-
cles which are made up of "superconductor quasiparticles". In what follows "quasi-
particle" refers to "superconductor quasiparticle".

first experimental evidence for their importance was provided by Orlando *et al.* (1979), Tedrow and Meservey (1979, 1982), and Orlando and Beasley (1981). Orlando and coworkers observed that the upper critical fields of thin, parallel oriented films of the A15 superconductors Nb_3Sn and V_3Si were anomalously high at low temperatures. These samples were somewhat Pauli limited, meaning that their critical field is determined by the pair-breaking effect of the field on the spins of the electrons as well as their orbital motion. Spin-orbit scattering, by mixing the spin states of the time-reversed pairs, diminishes this effect, thereby increasing the critical field. However, Orlando and coworkers found that in order to explain their data they had to use spin-orbit scattering rates which were larger than the total scattering rate. They concluded that the Fermi-liquid renormalization due to the electron-phonon interaction must be included. As pointed out by Rainer this changes the Pauli-limited field by

$$H_p/H_p^{BCS} = N(0)/N_0 = (1 + \lambda_{ep})$$

Concurrently, Tedrow and Meservey used the same renormalization to explain their critical field data on Pauli limited aluminum thin films. They used a value for λ_{ep} derived from McMillan's equation (McMillan, 1968), and spin-orbit scattering rates and orbital depairing parameters determined from tunneling conductance data on the same films, to correctly predict their critical fields. In the case of V_3Ga Or-

lando, *et al.*, found that electron-electron interactions, including spin fluctuations, must also be included in the renormalization.

The theoretical foundation for the application of Fermi-liquid theory to isotropic superconductors in the clean limit has been discussed by Leggett (1965, 1968, 1975). We are interested in the dirty limit for our thin, disordered films. We will use the quasiclassical approach developed by Eilenberger (1968) and Larkin and Ovchinikov (1968). This approach has been used by Serene and Rainer (1983) to describe ^3He. The extension of this theory to high-field superconductivity used here is due to Rainer (Alexander *et al.* 1985). The high field properties of superconductors, in particular the superconducting density of states and upper critical field, are calculated from the quasiclassical propagator for the quasiparticle excitations. Impurity, anisotropy and strong-coupling effects can all be incorporated. We are interested in the dirty limit $(l \ll \xi_0)$, where the quasiparticle parameters will be averaged over the Fermi surface.

In the superfluid case we must include the particle-hole, as well as the spin degrees of freedom in our quantum-mechanical description of the propagators. This is necessary because of the pairing interaction, which leads to a wave function which does not conserve particle number and necessitates non-zero off-diagonal elements in the particle-hole space. In what follows we use the notation of Alexander, *et al.* (1985).

Carets are used to indicate 4×4 matrices in Nambu space. This is the product space of the 2×2 spin and particle-hole subspaces. σ_i and τ_i will be used to indicate the Pauli matrices in the spin and particle-hole spaces, respectively. The quasiparticle propagator is then of the form

$$\hat{g}(s, \mathbf{R}; \epsilon) =$$
$$\begin{bmatrix} g(s, \mathbf{R}; \epsilon) + \mathbf{g}(s, \mathbf{R}; \epsilon) & [f(s, \mathbf{R}; \epsilon) + \mathbf{f}(s, \mathbf{R}; \epsilon) \cdot \vec{\sigma}]i\sigma_y \\ i\sigma_y[f^*(-s, \mathbf{R}; -\epsilon^*) - \mathbf{f}^*(-s, \mathbf{R}; -\epsilon^*) \cdot \vec{\sigma}] & g^*(-s, \mathbf{R}; -\epsilon^*) - \sigma_y \mathbf{g}^*(-s, \mathbf{R}; -\epsilon^*) \cdot \vec{\sigma}\sigma_y \end{bmatrix}$$

where s indicates the Fermi surface location of the excitation and ϵ is its energy relative to the Fermi surface. $\hat{g}(s, \mathbf{R}; \epsilon)$ is the solution of Eilenberger's transport equation

$$-i[\epsilon\hat{\tau}_3 - \hat{\sigma}(s, \mathbf{R}; \epsilon) - \hat{\nu}(s, \mathbf{R}), \hat{g}(s, \mathbf{R}; \epsilon)] + \vec{v}_F(s) \cdot \nabla_R \hat{g}(s, \mathbf{R}; \epsilon) = 0$$

and the normalization condition

$$[\hat{g}(s, \mathbf{R}; \epsilon)]^2 = -\pi^2 \hat{1}$$

Here $\hat{\nu}$ represents external perturbations such as a magnetic field. $\hat{\sigma}$ denotes the self-energy, including the electron-electron and electron-phonon interactions. As in the case of the normal Fermi liquid (see *Eq.* 2.2), the change in the self-energy of the quasi-particles due to these interactions takes the form of an effective field acting on renormalized ('dressed') particles. Ignoring impurity terms, the mean-field part of the pertubation is a linear functional of the propagator $\hat{g}$ to

leading order in T_c/Θ_D (weak coupling) and $1/k_F \xi_0$. Its diagonal terms in particle-hole space are

$$\nu_{mf}(s, \mathbf{R}) = T \sum_{\epsilon_n} \int d^2 s' n(s') A^s(s, s') g(s', \mathbf{R}; i\epsilon_n)$$

$$\vec{\nu}_{mf}(s, \mathbf{R}) = T \sum_{\epsilon_n} \int d^2 s' n(s') A^a(s, s') \vec{g}(s', \mathbf{R}; i\epsilon_n) \qquad (2.16)$$

The ϵ_n are the Matsubara frequencies and are merely a mathematical convenience for calculating the temperature dependent Green's functions. $A^s(s, s')$ and $A^a(s, s')$ are the generalization to anisotropic Fermi surfaces of the Landau parameters defined earlier. Note that the Fermi-surface average of the interaction $A^s(s, s')$ is

$$A_0^a = \int d^2 s\, d^2 s'\, n(s) n(s') A^a(s, s') = \frac{G^0}{1 + G^0}$$

As shown by Usadel (1970) in the dirty limit ($l/\xi_0 \ll 1$) Eilenberger's transport equation simplifies to

$$[\epsilon \hat{\tau}_3 - \hat{\vec{\sigma}}_{mf} - \hat{\vec{v}}_{spin}(\mathbf{R}) - \hat{\vec{\sigma}}_{s.o.}(\mathbf{R}; \epsilon), \hat{g}(\mathbf{R}, \epsilon)]$$
$$+ D\{\partial_i \otimes [\hat{g}(\mathbf{R}; \epsilon) \partial_i \otimes \hat{g}(\mathbf{R}; \epsilon)]\} = 0 \qquad (2.17)$$

The bar indicates an average over the Fermi surface. $\partial_i \otimes$ is the ith component of the gauge invariant gradient operator in Nambu space. D is a Fermi surface averaged (isotropic) diffusion constant. $\hat{\vec{v}}_{spin}$ describes the perturbation due to the coupling of the external field to the quasiparticle spin. $\hat{\vec{\sigma}}_{s.o.}$ is the spin-orbit scattering part of the self-energy. This spin-orbit scattering is analogous to that in the simple

hydrogen atom problem. Grain boundaries, impurities, defects, and interfaces can all lead to potentials which yield a "$\vec{L} \cdot \vec{s}$" coupling term in the hamiltonian. We will combine these effects together into a single phenomenological spin-orbit scattering time, τ_{so}. Thus, the spin-orbit scattering rate will be an additional fitting parameter in the theory.

If we consider a thin film parallel to the magnetic field, the order parameter and propagator are approximately independent of position and Usadel's equation can be further simplified. This along with the boundary conditions at the film's surfaces leads to a set of equations which must be solved self-consistently for the total internal field , pair potential, and propagator. The propagator, in turn, can be used to calculate the superconducting density of states. Expanding $\hat{g}(\epsilon)$ in terms of the four linearly independent 4×4 matrices $\hat{\tau}_3, \hat{\Delta}, \hat{h}$, and $\hat{\tau}_3 \hat{\Delta} \hat{h}$

$$\hat{g}(\epsilon) = y_1(\epsilon)\hat{\tau}_3 + y_2(\epsilon)\hat{\Delta} + y_3(\epsilon)\hat{h} + y_4(\epsilon)\hat{\tau}_3\hat{\Delta}\hat{h}$$

where

$$\hat{h} \equiv -\mathbf{h} \cdot \hat{\mathbf{S}} = \begin{pmatrix} -\mathbf{h} \cdot \sigma & 0 \\ 0 & \sigma_y \mathbf{h} \cdot \sigma \sigma_y \end{pmatrix}$$

and $\mathbf{h} = \mu_B \mathbf{H}/\Delta_0$, we have

$$N^{tu}(E, \uparrow) = -2N(0)\frac{1}{\pi}Im[y_1(E + i0^+) + |\mathbf{h}|y_3(E + i0^+)] \quad (2.18)$$

$$N^{tu}(E, \downarrow) = -2N(0)\frac{1}{\pi}Im[y_1(E + i0^+) - |\mathbf{h}|y_3(E + i0^+)]$$

The self-consistent equation for the gap can be linearized near the phase boundary to produce the usual digamma equation obtained from the linearized Ginzburg-Landau equation

$$\ln(T/T_{c0}) + \frac{1}{2}\{1 + b/[b^2 - h_{c2}^2/(1 + G^0)^2]^{1/2}\}\psi(\frac{1}{2} + \rho_-)$$
$$+ \frac{1}{2}\{1 - b/[b^2 - h_{c2}^2/(1 + G^0)^2]^{1/2}\}\psi(\frac{1}{2} + \rho_+) - \psi(\frac{1}{2}) = 0 \quad (2.19)$$

where

$$\rho_-^+ = \frac{\Delta_o}{2\pi T}\{c_F h_{c2}^2 + b \pm [b^2 - h_{c2}^2/(1 + G^0)^2]^{1/2}\}$$

and

$$h_{c2} = \frac{\mu H_{c2}(T)}{\Delta_0}$$

Here

$$c_F = \frac{Dd^2 \Delta_0 \pi^2 \hbar}{6\mu^2 \Phi_0}$$

is the usual pairbreaking parameter for a film of thickness d oriented parallel to a field and

$$b = \frac{\hbar}{3\tau_{s.o.}\Delta_0}$$

is the spin-orbit scattering parameter. Δ_0 is the gap in the absence of any pairbreaking and $\Phi_0 = hc/2e$ is the magnetic flux quantum. For an excellent review of high-field superconductivity in the absence of Fermi-liquid effects see Fulde (1973). Eq.2.19 is derived there from the Ginzburg-Landau equation (with $G^0 = 0$).

2.3   Predictions of the Quasiclassical Theory

In this section we will examine the effect of the renormalization on the critical field and quasiparticle density of states in the dirty (isotropic) limit. An important point is that, in this limit, where we can average the interaction over the Fermi surface, both of these renormalizations are characterized by the single parameter, G_0. In the limit where the interaction of the applied field with the spins dominates the coupling between the orbital motion and the field (eg. a thin, parallel film where c_F can be taken as zero) Eq.2.19 gives the Pauli-limited field,

$$H_p = H_p^{BCS}(1 + G_0) \qquad (2.20)$$

We also find from this theory that as we approach the phase boundary the apparent Zeeman splitting, δ, of the quasiparticle excitations becomes,

$$\delta \xrightarrow{H(T) \to H_c(T)} 2\mu_B H/(1 + G_0) \qquad (2.21)$$

From these relations we see again that the effect of the interaction between quasiparticles is equivalent to adding an extra field which acts on the quasiparticles' spin (in addition to renormalizing their masses; recall Figure 2.1). In general this extra field is given by (Leggett, 1965),

$$H_{int} = H_{ext}\left[\frac{-G_0 Y^2(t)}{1 + G_0 Y(t)}\right]$$

This can be either positive or negative depending on the sign of G_0. Here $Y(t)$ is the Yosida functon. It equals one for $t = T/T_c(H) \geq 1$ and decreases monotonically to zero as t drops to zero[5].

The effect of increasing G_0 on the critical field in the general case where orbital depairing is included (as given by Eq.2.19) is shown in Figure 2.2. Unfortunately, it can be seen from this figure that it is difficult to distinguish the effect of the renormalization from that of changing the spin-orbit scattering rate. Thus it is difficult to determine G_0 from critical field measurements alone. This point has been discussed in detail by Alexander (thesis, 1986).

The best way to determine G_0 is by fitting measured conductance curves to the theory of Rainer[6]. In a superconductor-normal metal tunnel junction the dynamic conductance as a function of bias voltage is simply related to the superconducting density of states, $N_s(V)$ (cf. Wolf, 1985).

$$\frac{dI(V)}{dV} = \frac{dI(0)}{dV} \int N_s(E)[-\frac{\partial}{\partial E} f(E + eV, T)] dE \qquad (2.22)$$

Here, $f(E)$ is the Fermi-Dirac distribution function. At very low temperatures $-\frac{\partial}{\partial E} f = [4KT cosh^2(\frac{E+eV}{2KT})]^{-1}$ is approximately a delta function and $\frac{dI}{dV}(V) \simeq N_s(V)$. The full effect of G_0 on the shape of

---

[5] This is the effective internal field seen by quasiparticles due to their interaction. The full internal field opposing the applied field (including the screening currents) is given by $H_{ext} \left[\frac{(1-G_0)Y(t)-1}{1+G_0Y(t)} \right]$.

[6] Described in the previous section. For further detail see Alexander, *et al.* (1985) and Alexander (1986).
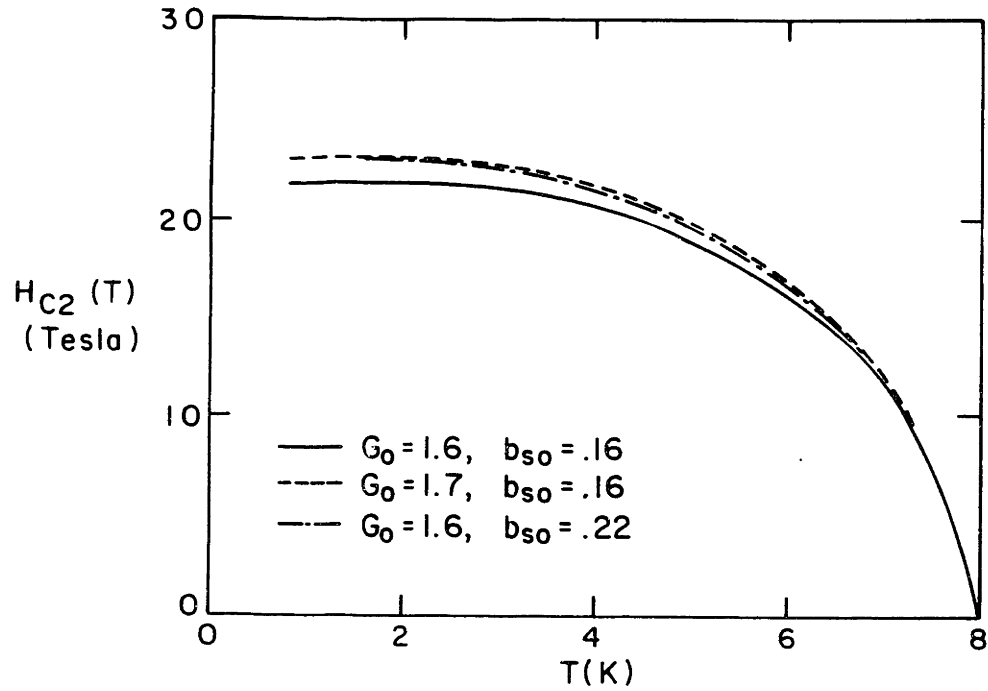
Figure 2.2: The solid curve is the parallel critical field as predicted by Equation 2.19 with $G_0 = 1.6$ and $b_{so} = 0.16$. The dashed curve is for $G_0 = 1.7$ and $b_{so} = 0.16$. The dash-dot curve is for $G_0 = 1.6$ and $b_{so} = 0.22$.

$N_s(V)$ is complicated and depends on the orbital depairing parameter, c, the spin-orbit scattering rate, b, and the critical temperature, T_c. One of the main features of this renormalization is a decrease in the apparent Zeeman splitting. The change in this splitting as a function of field can be measured and compared with that predicted by the theory in order to determine G_0. A caveat must also be issued when considering this approach. In the presence of spin-orbit scattering spin is no longer a good quantum number. As is shown in Figure 2.3, with increasing spin-orbit scattering the spin states are mixed and the apparent splitting of the new time-reversed states (which are no longer purely "up" and "down") decreases. Thus, a direct measurement of the Zeeman splitting can only be used to determine G_0 if the spin-orbit scattering rate is low. A rough guide to the expected spin-orbit scattering rate for an element is its atomic number, Z. Abrikosov and Gorkov (1962) have conjectured that it should go as Z^4. Experimentally this is observed to hold true for a large number of elements including gallium and vanadium (Meservey and Tedrow, 1978). Werthamer (1969) has pointed out that in a superconductor with a short transport scattering length a light-atom impurity or vacancy in a heavy-atom matrix is equivalent to a heavy impurity in a light-atom matrix. Interfaces and grain boundaries may also contribute to the scattering. The nature of the electronic states involved
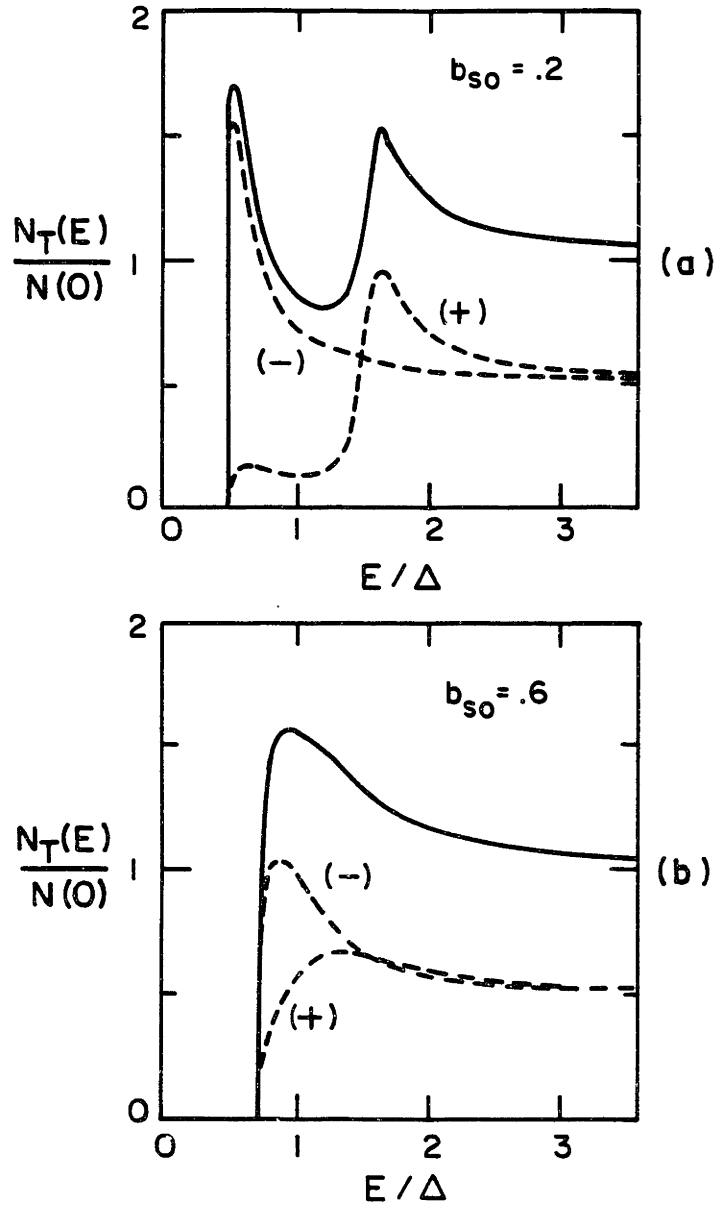
Figure 2.3: Tunneling density of states $N_T(E)/N(0)$ (solid line) as function of E/Δ for $\mu_B H/\Delta = 0.6$. Figures (a) and (b) correspond to $b_{so} = \hbar/(3\tau_{so}\Delta) = 0.2$ and 0.6 respectively. The dashed curves refer to $N_+(E)$ and $N_-(E)$. From Engler and Fulde (1971).

is also, undoubtedly, important. For further discussion of spin-orbit scattering see the end of Section 6.1. A powerful method for directly determining the splitting is the technique of spin-polarized tunneling which will be discussed in section 3.1. We will use this technique, as well as a full fit of the density of states, to study G_0 in vanadium, which has a reasonably low spin-orbit scattering rate.

With a moderate amount of spin-orbit scattering G_0 must be determined by fitting the full shape of the quasiparticle density of states to the theory. The effect on the density of states of changing the spin-orbit scattering rate is not the same as that of changing the renormalization. This will become clearer when we fit the conductance curves for amorphous gallium. In superconductors with a large spin-orbit scattering rate the spin states are completely mixed and it becomes difficult to discern the effects of the renormalization.

2.4   Why Vanadium and Amorphous Gallium ?

Fermi-liquid effects have been studied in thin aluminum films by observing the renormalization of the quasiparticle density of states. Tedrow, *et al.* (1984), obtained $G_0 = 0.3$ by fitting the Zeeman splitting of its two spin components, as a function of applied field, to the theory of Rainer. The Zeeman splitting was measured using the tech-

nique of spin-polarized tunneling, which will be described in the next chapter. Alexander (1986) fitted the full energy dependence of the superconducting density of states to the theory and got a similar result. In this way, the effect of spin-orbit scattering is properly taken into account. As mentioned previously, spin-orbit scattering mixes the spin states and changes the shape of the superconducting density of states. One of the main changes is a reduction in the apparent splitting. The spin-orbit scattering rate in aluminum is small. Thus, directly measuring the Zeeman splitting to determine G_0, as done by Tedrow, *et al.*, is reasonable.

We are interested in studying Fermi liquid effects in vanadium because it is a spin fluctuation system. In aluminum the source of the many-body effects is primarily the electron-phonon interaction. In vanadium, we expect a significant contribution to the renormalization from the Coulomb exchange interaction as well as the electron-phonon coupling. It is of interest to observe the interplay of these two effects. We would like to see whether we can understand the magnitude of the net renormalization in terms of its constituents. Is, for example, Eq. 2.14 correct? The spin-orbit scattering rate in vanadium appears to be fairly low. Thus, it is reasonable to try to determine G_0 directly from measured values of the Zeeman splitting using spin-polarized tunneling. We also have fit the full shape of the superconducting

density of states for $Al/Al_2O_3/V$ tunnel junctions. This further shows the usefulness of the theory in fully describing the effect of the many-body renormalization in high field superconductivity. It also provides a measure of the spin-orbit scattering rate.

It turns out that the net renormalization is fairly small in vanadium just as in aluminum. The stronger electron-phonon coupling in vanadium is essentially cancelled by spin-fluctuations. Our goal in studying amorphous gallium was to observe a really large renormalization. This is expected because of its strong electron-phonon coupling ($\lambda_{EP} \simeq 2.3$). While there are other superconductors with large electron-phonon coupling constants (such as $PbBi$) none has a low enough spin-orbit scattering rate to easily allow this study. The spin-orbit scattering in amorphous gallium is moderately strong and we will use a full fit of the density of states in determining G_0.

Chapter 3

Experimental Techniques and Apparatus

3.1 Spin-Polarized Tunneling

An extremely useful method for directly measuring the apparent Zeeman splitting is the technique of spin-polarized tunneling (Tedrow and Meservey, 1971; Tedrow, *et al.*, 1982). Here a ferromagnetic electrode is used on one side of a tunnel junction. Because of the difference in the densities of states in the ferromagnet for the two spin directions at the Fermi surface, more states of one spin direction are available for tunneling than for the other. We assume that each of these densities of states is constant over the range of energy important in the superconductor. Then the total measured conductance will be the weighted sum of the individual spin conductances in the superconductor. This is illustrated in Figure 3.1. This weighting factor, the polarization, has been determined for a number of ferromagnets (Tedrow and Meser-
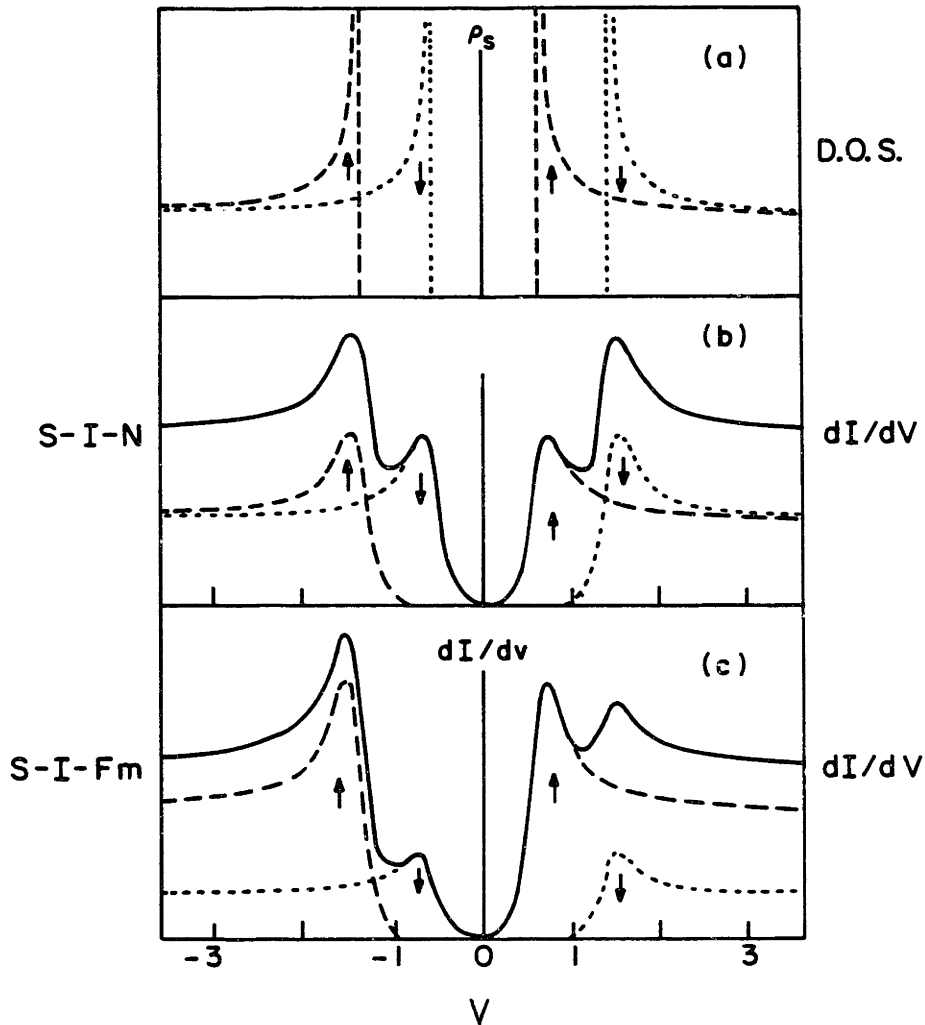
Figure 3.1: (a) "Spin-up" and "spin-down" densities of quasiparticle excitations in a superconductor. (b) Convolution of these densities with Fermi-Dirac temperature distribution to give dynamic conductance of tunnel junction as in Eq. 2.22. Here the counterelectrode is a non-magnetic metal with equal densities of up and down states. (c) Dynamic conductance when the counterelectrode has a spin polarization at the Fermi level. Because of the polarization, there are more electrons of one spin state tunneling than the other, and the overall conductance is asymmetric in the bias voltage.

vey, 1973; Meservey, et al., 1980). If the polarization is known, it is
then a simple matter to separate the measured conductance into its
spin components using the following equations,

$$\left(\frac{dI}{dV}\right)_\uparrow = \frac{a}{2a-1}[a\sigma(V) - (1-a)\sigma(-V)]$$

$$\left(\frac{dI}{dV}\right)_\downarrow = \frac{1-a}{2a-1}[a\sigma(-V) - (1-a)\sigma(V)]$$

Here σ is the measured total conductance and

$$P \equiv \frac{n\uparrow - n\downarrow}{n\uparrow + n\downarrow} = 2a - 1$$

is the polarization.

We will apply this technique to $Fe/Al_2O_3/V$ tunnel junctions to
measure the Zeeman splitting as a function of magnetic field. The
polarization of iron is known to be 44% (Meservey, et al. 1983).
By comparing the result to the theoretical prediction we will derive
a value for G_0. The spin-orbit scattering rate of vanad.   is low
enough to make this feasible. We will also fit the total conductance
of $Al/Al_2O_3/V$ junctions to the full theory.

In the case of amorphous gallium the spin-orbit scattering rate is
too high to allow a direct measurement of the splitting from the spin-
separated conductance curves. However, fitting these spin-separated
curves to the full theory could prove useful. It would provide an inde-
pendent check on the spin-orbit scattering rate. This, in turn, would

allow for more accuracy in determining the Fermi-liquid renormalization. Attempts to make amorphous gallium junctions with ferromagnetic counterelectrodes are discussed in appendix A.1.

3.2   Making and Testing $V/Al_2O_3/Fe$ and $Al/Al_2O_3/V$ Tunnel Junctions

In this section we will describe the preparation and testing of both $V/Al_2O_3/Fe$ and $Al/Al_2O_3/V$ tunnel junctions.

A large number of barrier materials and preparation techniques were tried in an attempt to make vanadium tunnel junctions with a ferromagnetic counterelectrode. Barriers included Al_2O_3 and MgO (produced both by electron-beam evaporation and by oxygen glow-discharge of thermally evaporated Al and Mg), Si, SiO, and combinations of these. The only successful junctions were those with fairly thick ($\geq 45\text{Å}$) glow-discharged aluminum barriers. We attempted to seed the growth of more uniform layers of the other materials with elements such as tantalum, to no avail. We tried these barriers on Fe, Co, Ni, and an Fe-Co alloy. We also tried depositing each of these barriers on top of the vanadium without success. Most of the junctions were either shorted or had an extremely high resistance. A few had a reasonable resistance but did not show a superconducting tunneling characteristic. The successful ferromagnetic junctions were

made in a diffusion pumped vacuum system with a base pressure of 2×10^{-7} torr. First, vanadium "cross-strips" were deposited onto room-temperature glass substrates (see Figure 3.2a). The substrate was then cooled to liquid nitrogen temperature and the cross-strips were overcoated with $45 - 55$ Å of *Al*. The edges of the cross-strips were masked with a thick layer of either Al_2O_3 or SiO (~ 300 Å) to prevent shorting. After warming to room-temperature the samples were glow-discharged, *in situ*, in an oxygen plasma for approximately 50 seconds to form an Al_2O_3 barrier. Next, 300 Å Fe "long-strips" were evaporated to complete the tunnel junctions. Finally, solder pads were evaporated onto the ends of all the strips for electrical contacts. The *Al*, *Fe*, and solder were evaporated from tungsten boats. The *V* and Al_2O_3 were deposited using an electron-beam gun. It was difficult to obtain good tunnel junctions; most were either shorted or had an extremely high resistance. However, a few good ones were obtained and were used in this experiment.

Successful $Al/Al_2O_3/V$ junctions were readily made. First 5 Å of iron and then 300 Å of aluminum were deposited through a "long-strip" mask onto a glass substrate held at liquid nitrogen temperature. This was then warmed to room-temperature and glow-discharged in oxygen for $\sim$ 50 seconds. Finally, thin vanadium cross-strips were deposited to produce the junctions. These were coated with 50 Å of
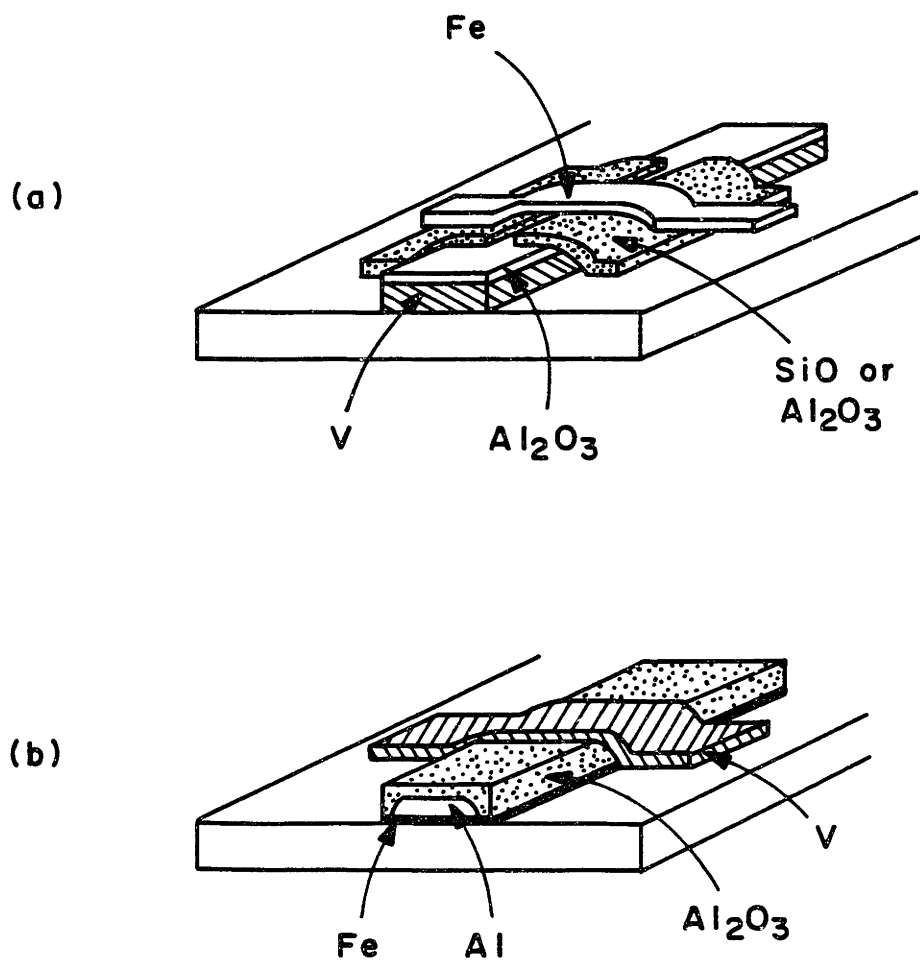
Figure 3.2: Schematic view of tunnel junctions used in tunneling studies on vanadium. (a) $V/Al_2O_3/Fe$ junctions. (b) $Al/Al_2O_3/V$ junctions.

Al_2O_3 to prevent oxidation. This is illustrated in Figure 3.2(b). The purpose of the iron was to drive the aluminum normal. This allowed for the observation of the vanadium quasiparticle density of states at low field, making it easy to determine the zero-field depairing.

A drawback to the latter preparation technique is that the vanadium must be deposited at room temperature so as not to destroy the barrier. We found that this did not significantly degrade the T_c for a given thickness over that obtained for films deposited at 700 °C (in this case sapphire substrates were used). The T_c's for films made at $\sim$ 80 K , however, were reduced significantly (see chapter 5). Attempts were made to produce junctions with the vanadium deposited first, onto a substrate held at $\sim$ 700 °C. The vanadium was deposited in an evaporator with a substrate holder which could be heated. It was then coated with a $\sim$ 10 − 20 Å of Al or Al_2O_3 to protect the surface of the vanadium from oxidation while transporting the sample to a second, similar, evaporator. Here a second layer of from 10 to 30 Å of one of the barrier materials mentioned above was deposited to complete the tunneling barrier. A larger pattern was used so as to cover the edges of the vanadium (see Figure 3.2(b)). Then aluminum was deposited to form the tunnel junction. Two evaporators were used because the first lacked a mask-changer and the second lacked the ability to heat the substrate. This failed to produce any

reasonable tunnel juntions. The morphology of thin vanadium films deposited at high temperature may not be conducive to producing successful barriers.

The junctions were mounted on a probe with a tiltable sample holder to align them with the field. This probe was inserted in a ^3He refrigerator which in turn was mounted in an 8 tesla superconducting magnet. The T_c's of the vanadium films were determined resistively while cooling. Critical field data were then taken in both the parallel and perpendicular directions. For junction resistances less than about $20k\Omega$ the dynamic resistance was measured as a function of voltage using the circuit shown in Figure 3.3(a). Here R_J represents the junction. The two X's are variable resistors which must be much larger than R_J so as to provide a constant current source. The voltage is ramped by a motor-driven pot connected to a battery (V_{DC}). R_1 and R_2 are varied inversely to control the amplitude of the AC signal across the junction. Note that this is a four terminal measurement. For greater resistances the dynamic conductance was determined using the circuit shown in Figure 3.3(b). This was necessary because of the difficulty in maintaining a constant, "dI" across a high resistance junction. In this circuit R_s is the resistor across which "dI" is measured and must be kept small compared to R_J. R_v can be used to vary the range of the DC bias voltage. The fact that the dI/dV mea-
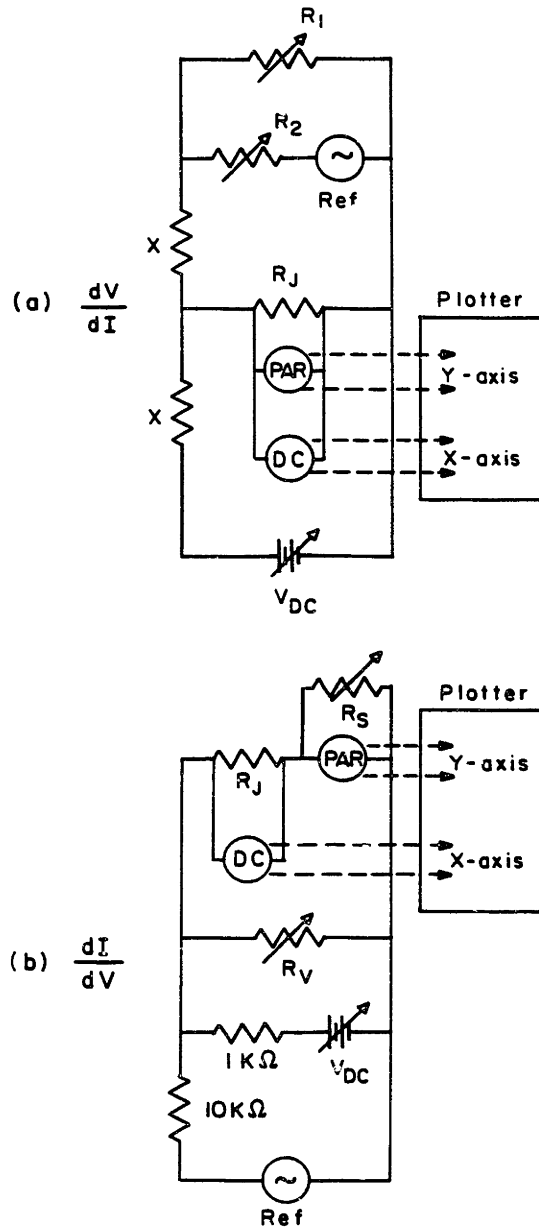
Figure 3.3: (a) Circuit used to measure dV/dI vs. V. Provides constant amplitude ac "dI" superimposed on dc bias current while monitoring "dV". (b) Circuit used to measure dI/dV. Provides constant "dV" while measuring "dI".

surement is two terminal is unimportant for high resistance junctions. The dynamic conductance (or resistance) was measured at a number of different fields at a temperature of $\sim 0.4K$. In both cases, a frequency of about 500 Hz was used. The amplitude of the modulation was kept at $20\mu V$ (0.23 K) so as to be below k_BT.

3.3 Description of Low Temperature Evaporator

The major experimental difficulty involved in working with amorphous gallium tunnel junctions is that they must be evaporated at liquid helium temperatures within a Bitter magnet and tested *in situ.* This is necessary both because amorphous gallium anneals to a more ordered phase at approximately 20K and because the extremely thin films which are required oxidize rapidly in air. A low temperature evaporator which can be operated within a 2" bore Bitter magnet was used. This device was originally constructed by Dr. Paul Tedrow and is shown schematically in Figure 3.4. The pumping system , vacuum monitoring equipment and thermometry were modified for the present experiment. The entire apparatus is mounted on a moveable stage which can be positioned around the Bitter magnet. A Janis cryogenic dewar is supported just above the magnet. The "tail" section of the dewar has been lengthened and is inserted through the bore of the

Low Temperature Evaporator
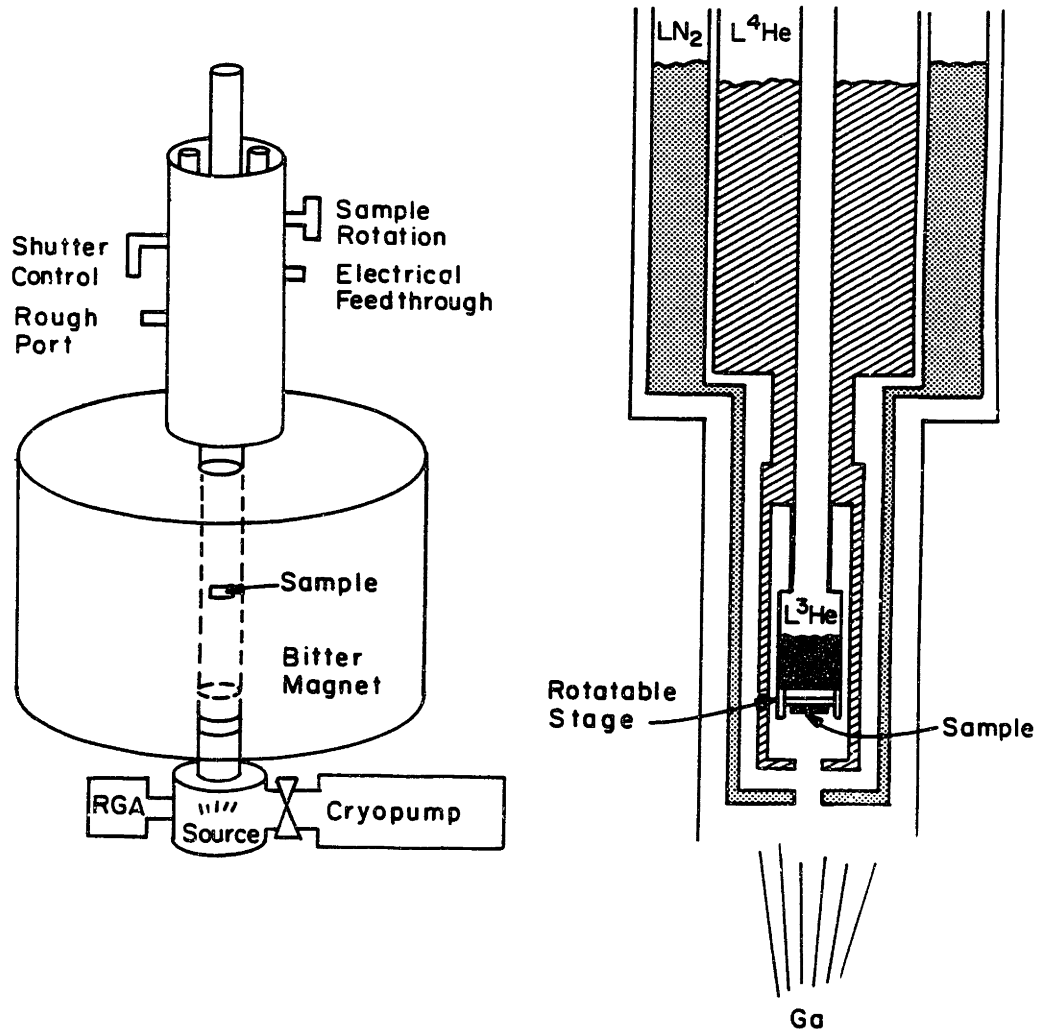
Figure 3.4: Schematic view of low-temperature evaporator used to make $Al/Al_2O_3/a\text{-}Ga$ tunnel junctions (left). Cross-sectional view of modified Janis dewar in which sample was mounted (right).

magnet. The end of the "tail" section is clamped to a metal bellows which is attached to a vacuum chamber which lies below the magnet. This facilitates removal of the system from the magnet. A four inch diameter flange with three water-cooled high-current feedthroughs is mounted on the bottom of the vacuum chamber. Either one metal boat or two with a common ground can be attached between the electrodes. We used tungsten boats for the evaporation of both Ga and Al. The evaporation boats are surrouded by a liquid nitrogen cooled shield with an opening at the top. A shutter is positioned above this opening and can be controlled from the outside via a rotary vacuum feedthrough. A water-cooled quartz crystal rate monitor views the source through a second hole in the liquid-nitrogen shield. The vacuum spaces between the liquid nitrogen and liquid helium are connected with each other as well as the vacuum chamber below the magnet. This single vacuum space is pumped by a CTI-8 cryopump which is mounted directly on the side of the vacuum chamber next to the evaporation sources through a 4.5" gate valve. The short distance and large aperture between the source and the cryopump maximize the pumping speed for the gases evolved during evaporation. There is also a port on the side of the Janis dewar which was used for rough pumping the system with a liquid nitrogen trapped rotary-vane pump. A Quadrupole mass spectrometer residual gas analyzer

and a triode ionization gauge were mounted on the vacuum chamber. When the system was fully cooled the pressure at the ion gauge was less than 10^{-7} torr. The pressure at the sample, which was completely surrounded by surfaces at $\sim$ 1K or less, was no doubt considerably lower. A ^3He pot is attached to a tube which runs up through the ^4He chamber (see Figure 3.4). The sample substrate is mounted on a rotatable stage which is thermally anchored to the ^3He pot. The sample stage can be oriented from the outside by means of cables which are connected to a rotary feedthrough. The sample is turned so as to face down toward the source during deposition and then, by rotating 90°, aligned parallel to the field for measurements. The sample is surrounded by a copper radiation shield which is mounted on the bottom of the pumped ^4He bath. This, in turn, is surrounded by an aluminum radiation shield which is thermally anchored to the bottom of the liquid nitrogen bath. There is a 3/8" opening at the bottom of each shield for the passage of the evaporants. This pathway can be blocked by a shutter which is thermally anchored to the ^3He pot. A mask can be attached to the sample holder so as to produce the desired pattern. The temperature is monitored by calibrated carbon-glass and Allen-Bradley resistors on both the sample holder and ^3He pot. By pumping on the ^3He bath temperatures as low as 0.7K could be achieved.
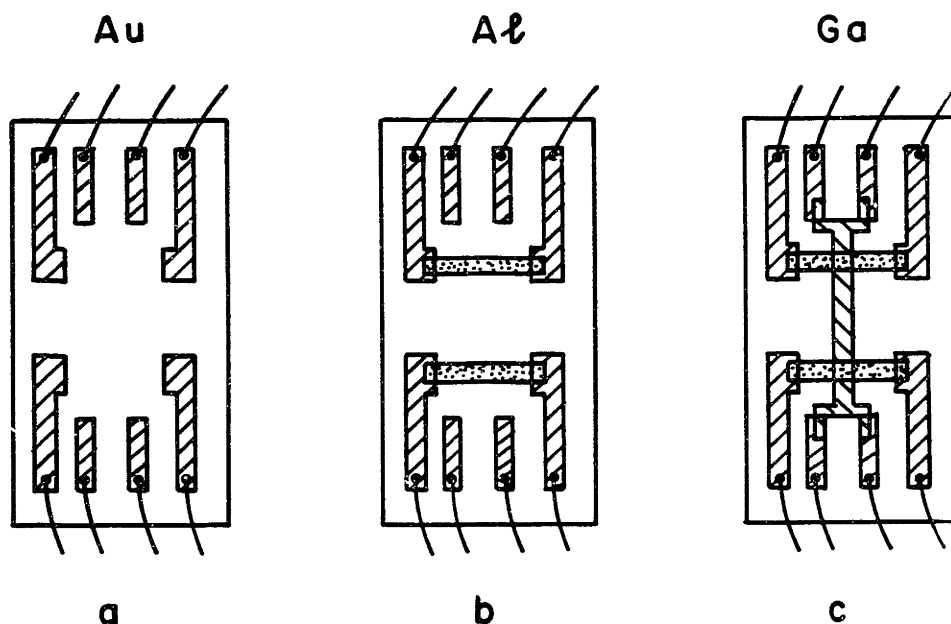
Figure 3.5: Three steps in the production of $Al/Al_2O_3/a$-Ga tunnel junctions. (a) Evaporation of gold contacts onto $1/4'' \times 1/2''$ glass substrates in separate evaporator. (b) Evaporation of Al "cross-strips" at 77K in low-temperature evaporator. (c) Completion of two tunnel junctions by evaporation of Ga "long-strip" at $\leq$ 2K.

3.4   Making and Testing $Al/Al_2O_3/a$-Ga Tunnel Junctions

Gold contacts between 150 and 300Å thick were evaporated onto liquid nitrogen cooled glass substrates in a separate evaporator (see Figure 3.5a). These were then mounted in the low-temperature evaporator and leads were attached to the gold contacts with pressed in-

dium. The sample was again cooled to liquid nitrogen temperature by putting liquid nitrogen in the ^3He compartment. Approximately 300Å of aluminum were evaporated in order to complete the 'cross-strips' (see Figure 3.5b). The system was then warmed to room temperature and the mask changed. In the process the aluminum was exposed to air for between fifteen minutes and one hour. This oxidized the top surface of the aluminum and formed a tunnel barrier. The system was then cooled to the lowest possible temperature ($\sim$ 0.7 K) and the gallium was evaporated, forming two tunnel junctions (see Figure 3.5c). Note that four-terminal measurements of the gallium 'long-strips' could also be made. The gallium films were made as thin as possible in order to minimize their orbital depairing in a field. This was accomplished by depositing about one third of an Å/sec while monitoring the electrical continuity of the film. The films generally became continuous at approximately 20Å but evaporation was continued until they reached about 30Å. Thinner films usually did not survive long and had unmanageably low critical currents. It was found that in order to obtain electrical continuity at low coverage it was essential not to outgas the source prior to deposition. When the source was outgassed before evaporating, electrical continuity was not achieved below 60Å mean coverage. It appears as though the "dirt" which is outgassed seeds the growth of a more uniform layer. It is

difficult to monitor the temperature of the surface of the glass substrate during the evaporation. However, we found that an aluminum film with a T_c of 2.3K remained superconducting during the gallium evaporation. A temperature of below 2.3K is more than sufficient to produce amorphous gallium.

The junctions were formed immediately before scheduled "magnet time"[1] . They were then aligned parallel to the field by maximizing the critical field of the aluminum strip. The aluminum was used because the parallel critical field of the gallium films was often greater than the available field of 20 tesla. The dynamic conductance of the tunnel junctions as a function of voltage was measured for various fields at a temperature of about 0.8K. If time permitted, the conductance was also measured at higher temperatures, although the temperature smearing became rapidly larger and limited us to at most 2.5K. The circuit of Figure 3.2 was used. dI/dV was measured rather than dV/dI because the junction resistance was typically $20 - 100$ $k\Omega$. An amplifier with an input impedance of 100 $M\Omega$ was used to read the DC bias so as not to short out the junction. Finally, the critical field was measured at as many points as possible. At temperatures over 2.5K this meant sweeping the temperature while holding the field constant. The temperature of the sample could not be stabilized when there was

---

[1]Experimenters are assigned three and one quarter hour sessions during which power is available for their magnet.

no liquid ^3He condensed in the ^3He pot.

Chapter 4

Analysis of Gallium Data

4.1 Properties of a-Ga Films

The ordinary gallium phase found at room temperature has a T_c of 1.07 K. Phases with higher transition temperatures have been produced by evaporating gallium onto cooled substrates (eg. Bückel and Hilsch, 1954). High T_c modifications have also been obtained in small gallium particles produced by evaporation in an oxygen atmosphere (eg. Cohen, et al., 1967) or ultrasonic dispersion of molten gallium (Feder, et al., 1966; Parr and Feder, 1973). The phases observed include amorphous gallium (Bückel and Hilsch, 1954; $T_c = 8.4$ K), γ gallium (Feder, et al., 1966; $T_c = 7.6$ K), and β gallium (Bosio, et al., 1965; $T_c = 6.2$ K). The critical fields of thin, amorphous gallium films have been measured by Bergmann (1973), and Crow, et al., (1974). Tunneling studies on amorphous gallium have also been performed (see references in Table 4.1). Zeeman splitting of the quasiparticle
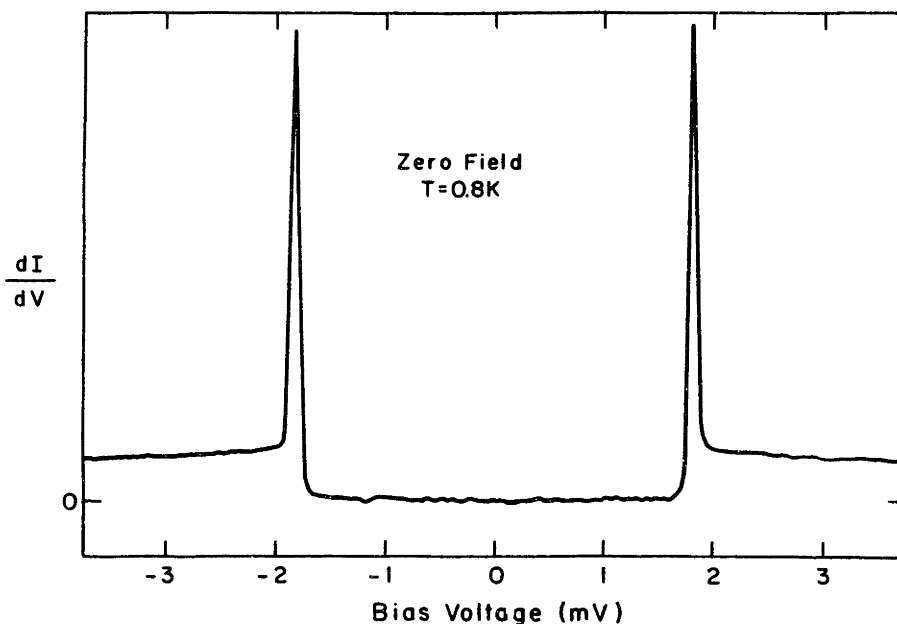
Figure 4.1: Dynamic conductance vs. bias voltage for a typical $Al/Al_2O_3/a$-Ga tunnel junction at $H = 0$, $T = 0.8$ K. At this low temperature only the "sum" peaks are observed.

density of states of thin, amorphous gallium films in a parallel magnetic field has been observed by Tedrow and Meservey (1975a) and Meservey, *et al.*, (1978). Additional amorphous gallium research is cited below.

Figure 4.1 shows the dynamic conductance versus bias voltage for one of our $Al/Al_2O_3/a$-Ga tunnel junctions at zero field and low temperature. The leakage current is negligible and the features are quite sharp, indicating that tunneling is the primary conduction process and that the films are uniform and of high quality. The peaks at
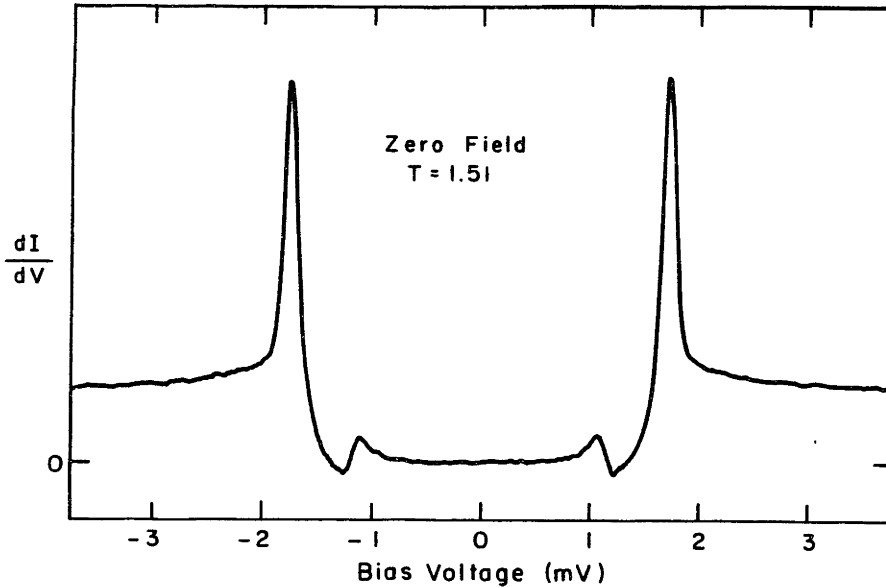
Figure 4.2: Dynamic conductance at $H = 0$, $T = 1.5$ K. At this temperature both the sum and difference peaks are observed.

the gap edge are particularly sharp here because at this low temperature and field the aluminum is also superconducting. Thus, what we are seeing are the conductance peaks at the sum of the half gaps $(\Delta_{Al} + \Delta_{a-Ga})$. The difference peaks are not observed because they are not thermally populated at low temperature. In Figure 4.2 we see a similar junction at a higher temperature where both the sum and difference peaks are observable. This gives an additional measure of the gap in both the aluminum and gallium. The normal state tunneling resistance of these junctions varied between 20 and 100 kΩ.

Source of Data	T_c	$2\Delta_0/k_BT_c$
Chen, *et al.* (1969)	8.56 ± 0.02	4.51 ± 0.04
Minnigerode and Rothenberg (1968)	8.47	$4.50 - 4.52$
Wühl, Jackson, and Briscoe (1968)	8.4 ± 0.1	4.5
Cohen, Abeles, and Weisbarth (1967)	8.4 ± 0.14	4.2
Present work	6.8-7.7	4.45

Table 4.1: Comparison of measured $2\Delta_0/k_BT_c$ values for amorphous gallium.

The transition temperature, measured resistively, of the gallium films varied from 6.8 to 7.7 K. The energy gaps varied with T_c such that $2\Delta_0/kT_c$ was always about 4.45 (see discussion in section 4.2). This is close to the value reported by others for amorphous gallium (see Table 4.1). The T_c's are somewhat lower than for bulk amorphous gallium. This is a common feature of superconducting thin films and has been observed previously in amorphous gallium. Naugle and Glover (1969) found a d^{-1} dependence of T_c on thickness consistent with the present result. The resistivities of the gallium films were in the range of 100 to 500 $\mu\Omega-cm$. There is an uncertainty of about a factor of two in these measurements due to the geometry of the films. The parallel critical fields of these films at low temperature were typically at the limit of the magnet, or just slightly more than 20 tesla. The perpendicular critical fields ranged from 11 to 13 tesla. One very thin film ($\sim 20\text{\AA}$) had a perpendicular critical field of 15 tesla. In both cases the resistive transitions were usually about one

tesla wide.

4.2 Analysis of Tunneling Data

The purpose of this section is to describe the fitting and analysis of the tunneling data. We used a program written by Rainer based on his extension of the theory of high-field superconductivity[1] to include Fermi-liquid interactions. The input parameters to the theory are T_{c0}, the spin-orbit scattering rate, the orbital-depairing parameter, and G_0. The spin-orbit scattering parameter that we will use, b_{so}, is given by

$$b_{so} = \frac{\hbar}{3\tau_{so}\Delta_0}$$

Here τ_{so} is the spin-orbit scattering time and $\Delta_0 = 1.764 \, k_B T_{c0}$. T_{c0} is the transition temperature in the absence of all pairbreaking. The orbital depairing has two terms. Theoretically, for a thin film in a parallel field the orbital depairing should be proportional to the square of the field. We find that in order to get the best fits to the data we must include a pairbreaking term, P_0, which is independent of field. This is commonly found to be the case for tunneling data. It may in part be due to overmodulation of the junction by either noise or the test signal itself. A further possibility, that of correlation effects, will be discussed in Appendix B.2. Thus, the total pairbreaking term, P,

---

[1] Werthamer, Helfand, and Hohenberg (1966). Maki (1966).

is

$$
\begin{aligned}
\Delta_0 P &= \left(\frac{k_B T_{c0}}{\Delta_0}\right) c_F \left(\frac{\mu_B H}{k_B T_{c0}}\right)^2 + P_0 \\
&= \frac{\alpha}{k_B T_{c0}} + P_0 \qquad\qquad\qquad (4.1)
\end{aligned}
$$

We will use c_F and P_0 to describe the total pairbreaking. c_F is given by

$$
c_F = \frac{D e^2 d^2 \Delta_0}{\mu^2 \hbar c^2}
$$

where $D = v_F l/3$ is the Fermi surface averaged diffusion constant (with v_F and l the corresponding Fermi velocity and mean free path) and d is the thickness. The alternate form given in the second line of Eq. 4.1 was included to show the relationship of c_F to the parameter α, which is often used in the literature. In de Gennes' interpretation (1966), 2α is the energy difference between time-reversed states.

The program, as written, does not explicitly include strong-coupling. We have, in the case of amorphous gallium, approximated its effect by simply multiplying the gap by $[2\Delta/kT_{c0}]/3.52$ wherever it appears, as suggested by Rainer. For all five of the junctions measured it was found that using $2\Delta/kT_{c0} = 4.45$ produced very good fits to the data. This value is very close to those reported by others (see table in Section 4.1).

After entering c_F, b_{so}, G_0, P_0, H and T/T_{c0}, the program generates the superconducting density of states as a function of energy. It

then convolves this with the Fermi-Dirac temperature dependence using Eq. 2.22 and plots the result[2]. These plots were compared by eye with the data. First, a conductance curve just above the critical field of the aluminum electrode was fitted. This was generally at about four tesla. At this low field the effects of the renormalization, spin-orbit scattering, and H^2 part of the orbital depairing were negligible. Thus, the only adjustable parameter was P_0. After determining P_0, higher field curves were used to determine c_F, b_{so}, and G_0. The following strategy was used in doing this. First, c_F was determined by roughly fitting the size of the gap at high fields. Then b_{so} and G_0 were determined by fitting the full shape of the curve. The effect of increasing the spin-orbit scattering rate or the renormalization is illustrated in Figure 4.3. It can be seen that while both decrease the apparent splitting, the overall change in the shape of the density of states is not exactly the same. For example, increases in b_{so} result in larger relative increases in the height of the "shoulder" at the positions of the inner peaks. Thus, by carefully fitting the full shape of the conductance curves it is possible to distinguish the effects of the renormalization from those of spin-orbit scattering and accurately determine both G_0 and b_{so}. This fact is further illustrated in Figures 4.4 and 4.5. Here, the solid curves are data taken on a single junction at two different

---

[2]The temperature convolution was added to Rainer's program by G. Hertel and J.A.X. Alexander.
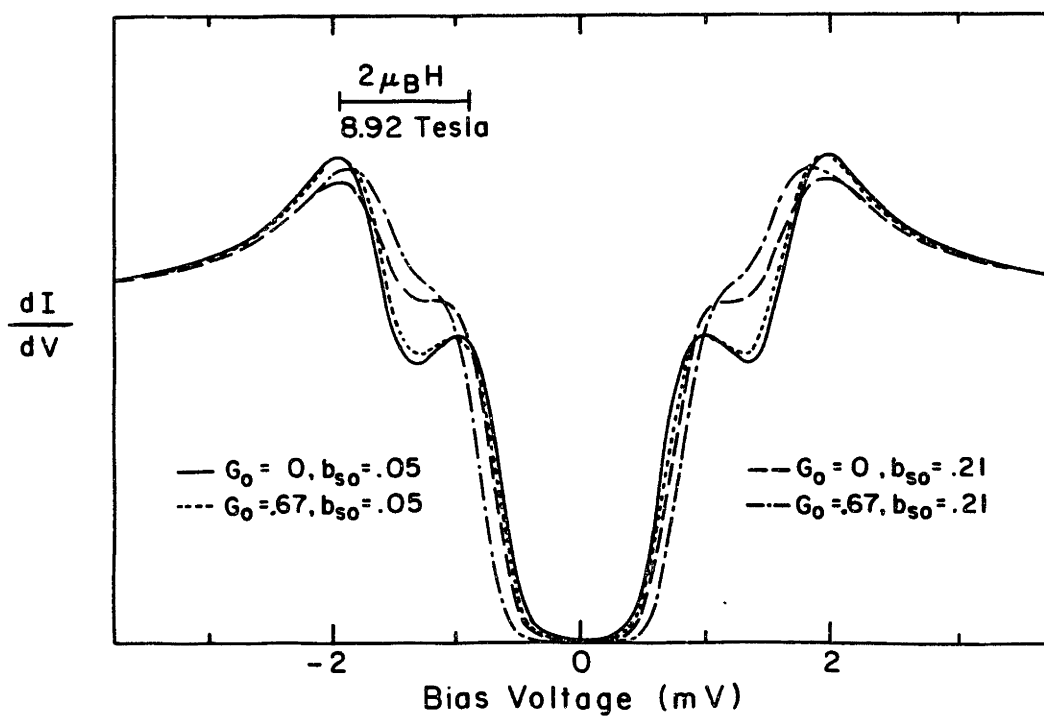
Figure 4.3: The solid curve is the prediction of Rainer's theory for $G_0 = 0$, $b_{so} = 0.05$. The dotted curve is that predicted for $G_0 = 0.67$, $b_{so} = 0.05$. The dashed curve corresponds to $G_0 = 0$, $b_{so} = 0.21$ and the dash-dot curve is for $G_0 = 0.67$, $b_{so} = 0.21$.

H= 8.92 Tesla
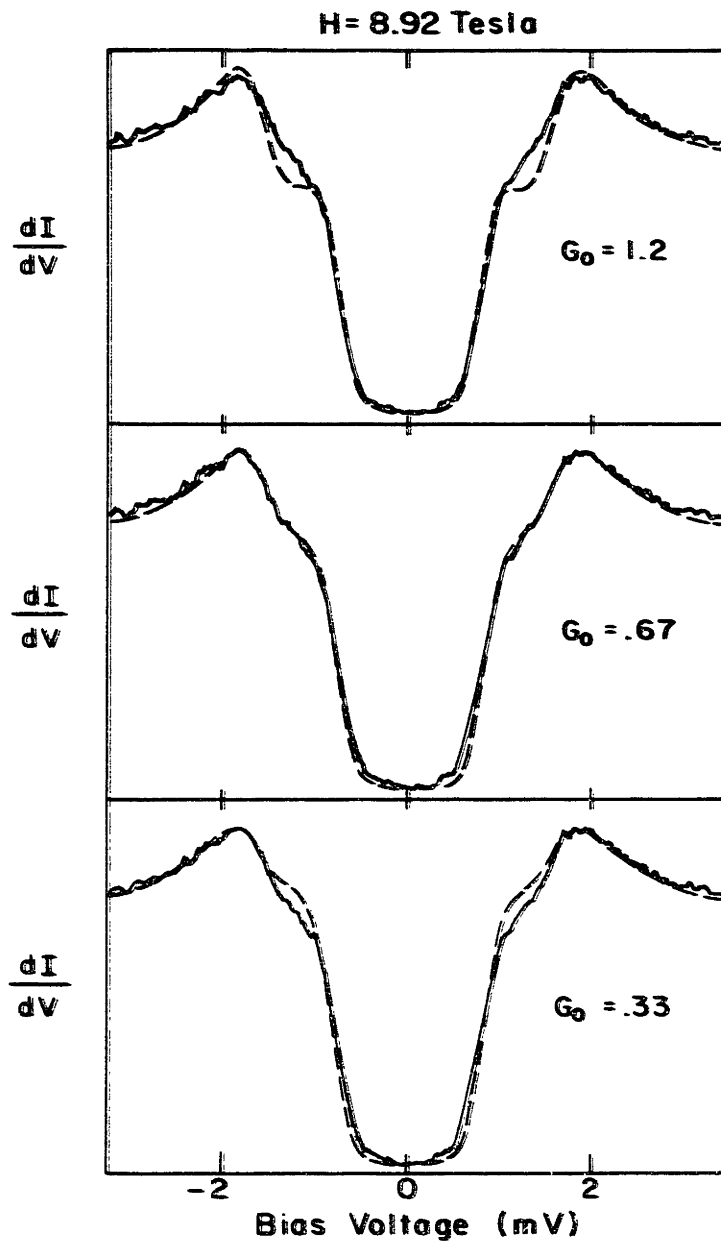
Figure 4.4: Solid curve in each part is experimental data taken at 8.92 T. Dashed curves are best fits obtained for these data while simultaneously fitting all the data taken on this junction at other fields and temperatures. In each of the three cases G_0 was held fixed at the indicated value while the other parameters were varied.
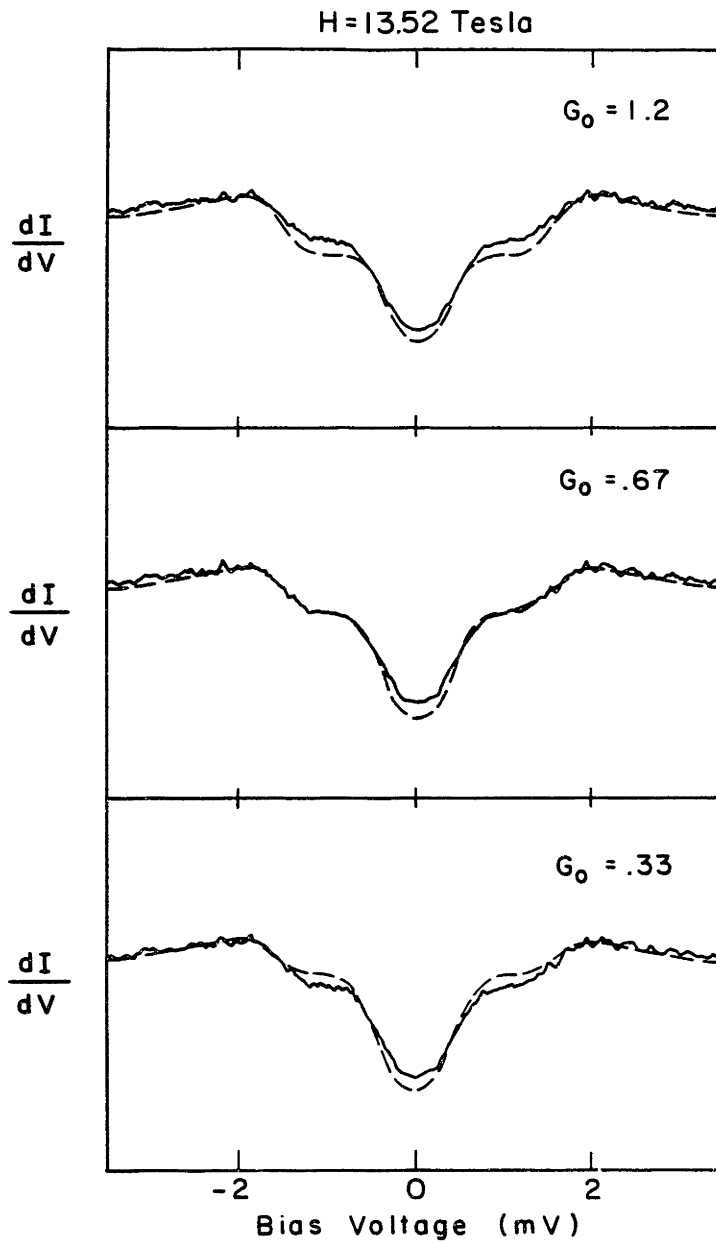
Figure 4.5: Same as Figure 4.4 for an experimental curve from the same junction taken at 13.52 T.

fields. The dashed lines are a fit to these data. The same parameters were used to fit both curves as well as others taken on the same junction at different fields and temperatures. The values $G_0 = 0.67$, $b_{so} = 0.21$, $c_F = 0.235$, and $P_0 = 0.055$, provide a very good fit to all the experimental curves (see middle plot in each figure). Now if we arbitrarily hold G_0 fixed at 0.33 and vary the other parameters to get the best fit simultaneously for all the curves, the best we can do is shown in the plots at the bottom. Similarly, if we fix G_0 at too large a value, say 1.2, the best fit we have managed is shown in the plots at the tops of the figures. This clearly shows that the effects of the renormalization and spin-orbit scattering can be distinguished. It also provides a measure of the accuracy with which we can determine G_0. With good data, such as that shown, careful fitting can determine G_0 to within about 10% (assuming the theory is accurate!).

Figure 4.6 shows conductance curves at a number of fields for a single junction. Again, the dashed curves are a fit to the theory of Rainer using a single set of parameters. A very good fit is obtained over the entire range of magnetic field. The increasing discrepancy near zero-bias is a common feature of tunneling conductance fits in high fields. This may in part be the result of flux penetration due to imperfect alignment of the sample in the field. It may also be partly due to lifetime broadening effects (see appendix B.2). A further pos-
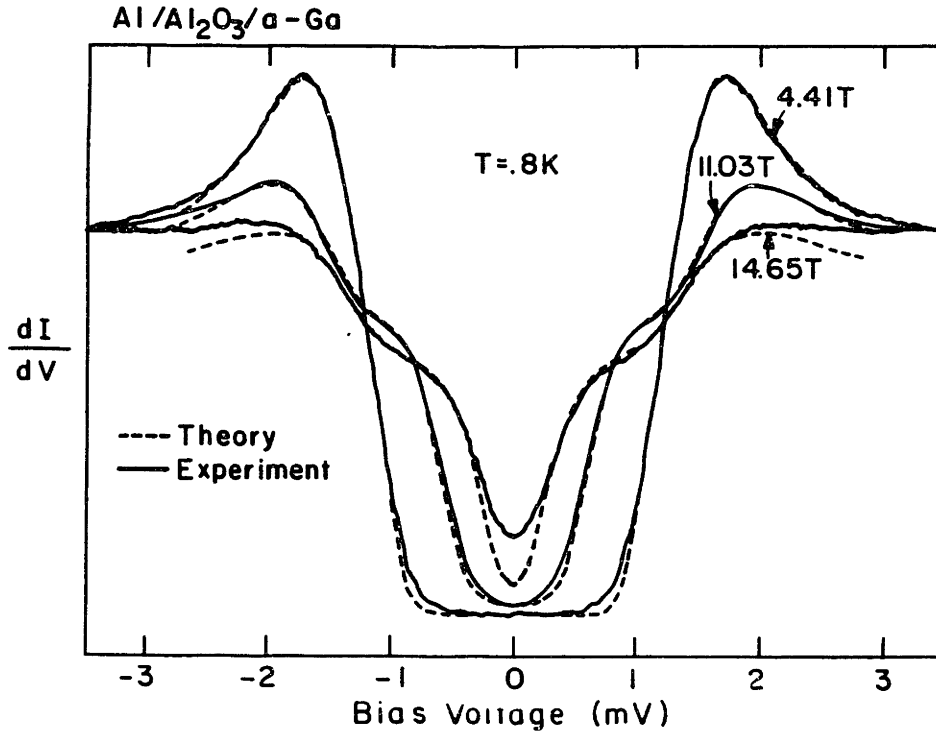
Figure 4.6: Conductance curves at three different fields for a single junction. Dashed curves are a fit to the theory of Rainer (using Eqs. 2.18) with $G_0 = 0.82$, $b_{so} = 0.16$, $c_F = 0.325$, and $P_0 = 0.11$. $T_{c0} = 8.4$.

sibility is overmodulation of the junction. Typically a $20\mu V$ ac signal
was used to determine the dynamic conductance. However, noise fluc-
tuations due to external sources may at times have been larger. Noise
due to oscillations in the magnet current is expected to increase with
field. Thus, noise could explain both the constant pairbreaking term
and the increasing discrepancy between theory and experiment with
increasing field. The values obtained for P_0 for various junctions rep-
resent pairbreaking energies of between 35 and 100 μeV. Although
this energy is not exactly equivalent to a noise amplitude, it does in-
dicate that overmodulation could be a significant component of P_0.
Note that it was difficult to find any correlation between P_0 and either
the resistivity or the thickness of the films. However, there did seem
to be some correlation with the noisiness of the measurements.

There is also an increasing difference between the experimental
curves and the theory at voltages above the gap. We believe this is
due to electron correlation effects. The gallium films are very thin
($\sim 20 - 30 \mathring{A}$) and highly disordered. Consequently, the electrons' mo-
tion is diffusive, screening is reduced, and the Coulomb interaction
is enhanced. Figure 4.7 shows the dynamic conductance of a rep-
resentative junction out to 50 meV both above and below the T_c of
the gallium. The background curvature cannot be attributed to an
increasing tunneling probability with increasing voltage. First of all,
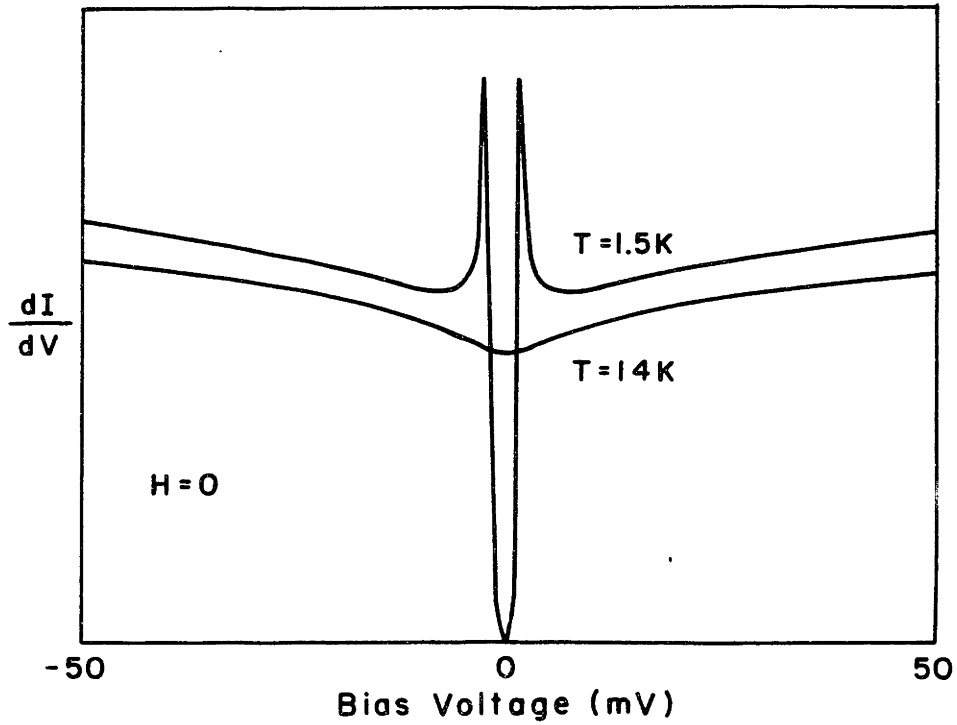
Figure 4.7: Dynamic conductance vs. bias voltage above and below the critical temperature of the gallium film.

the second derivative with respect to voltage of the background con-
ductance is of the wrong sign. Also, Al_2O_3 barriers are on the order
of 2 eV high and should not cause any curvature at these low biases.
The resistivity of the aluminum electrodes is low ($\sim 10\mu\Omega \cdot cm$) so that
we do not expect correlation effects in them. In fact, junctions with
similar aluminum electrodes used in other studies do not show this
background. However, the resistivity of the gallium films is typically
several hundred $\mu\Omega-cm$ (so that $k_F l$ is $\sim$ 5-20). In Appendix B.1 we
demonstrate that the background curvature observed is of the form
predicted for corrections to the normal state density of states due to
correlation effects. In any case, we can simply divide the measured
background conductance out of the data and compare the result with
the theory. The result of doing this for the data in Figure 4.6 is shown
in Figure 4.8. Note that dividing out the background makes negligible
difference in the value obtained for G_0 (Over the range of voltage ex-
amined the change in normal state conductance changed typically by
only 10 − 30%). As we do not have data on the background conduc-
tance at each field and temperature for this (or any other) junction,
the division was accomplished as follows: First a straight line was
fit to dI/dV versus $V^{1/2}$ at voltages well above the superconducting
energy-gap for $T = 0.9K$ and $H = 0$. This is the functional form pre-
dicted for sufficiently thick films at sufficiently large bias voltage (see
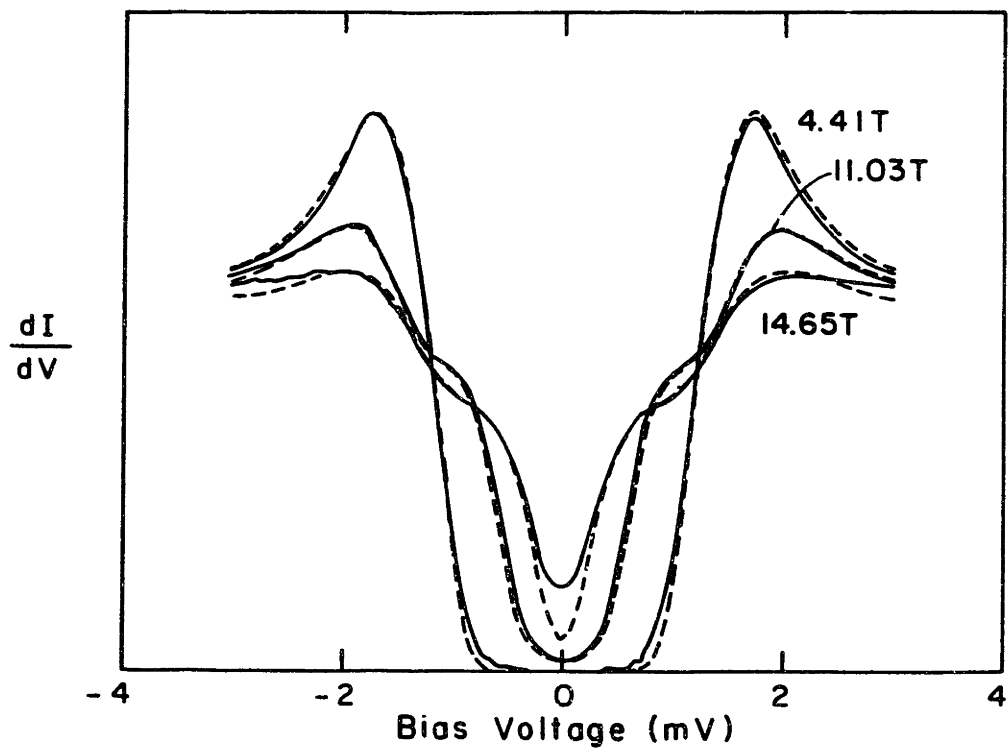
Figure 4.8: Data of Figure 4.6 with measured background conductance divided out.

Appendix B.1). Then this function was divided out of all the measured curves regardless of T and H. Above the gap there appeared to be negligible change in the background curvature in the range of field and temperature used in this experiment: $0-20$ tesla, $0.8-3.5$ K (see Appendix B.1). At voltages below the gap it is difficult to determine the effect of the field and temperature because of the superconducting energy-gap. For the present experiment it suffices to note that the value of G_0 obtained is insensitive to the removal of these small amounts of background curvature.

Figure 4.9 shows how at the highest fields the depairing becomes too large to observe the splitting. Here again the background observed at zero field has been removed. In most of the junctions the Zeeman splitting of the quasiparticle excitations became indiscernable at about 17 tesla. The highest field at which splitting was observed was 17.2 tesla. The parameters used to fit the curves in Figure 4.9 also gave an excellent fit to lower field curves taken on the same junction. Figure 4.10 shows the effect of holding the field constant while raising the temperature. The data here are from the same junction shown in Figures 4.6 and 4.8. A good fit to the data is obtained using the same set of parameters used in those figures.

In all, the data from five junctions were fitted to the theory of Rainer. The results are summarized in Table 4.2. The results are
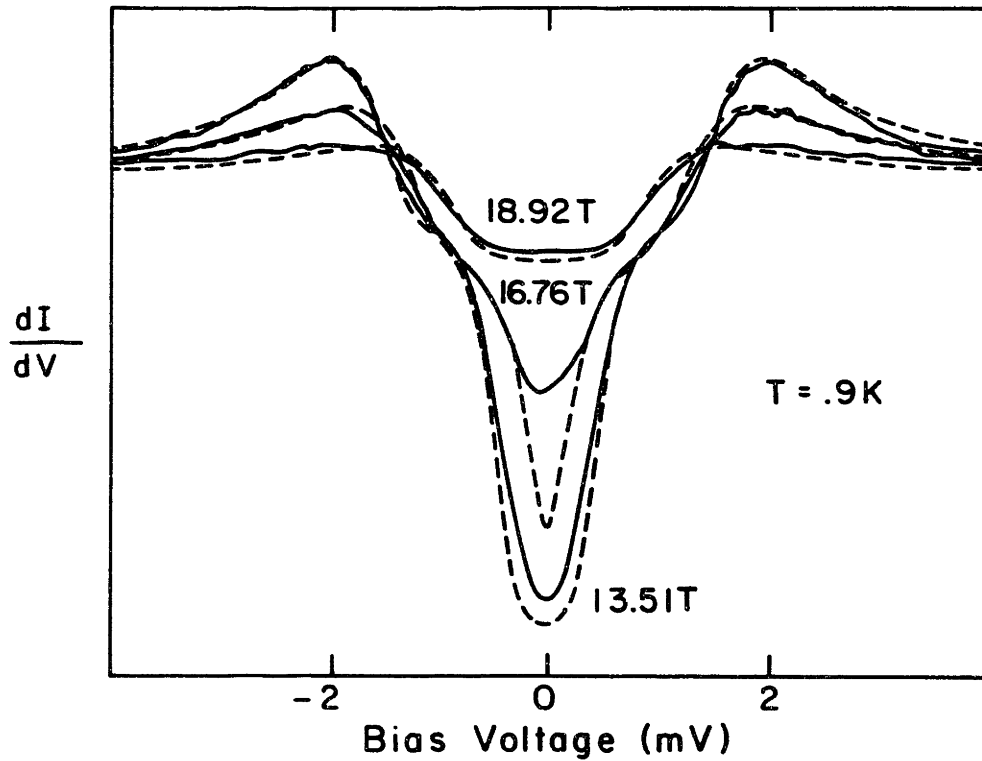
Figure 4.9: Dynamic conductance at high fields. Solid curves are experimental and dashed lines are a fit to Rainer's theory using $G_0 = 0.818$, $b_{so} = 0.19$, $c_F = 0.35$, and $P_0 = 0.04$. Above 17.2 tesla splitting could not be observed in any of the junctions studied due to the large depairing.
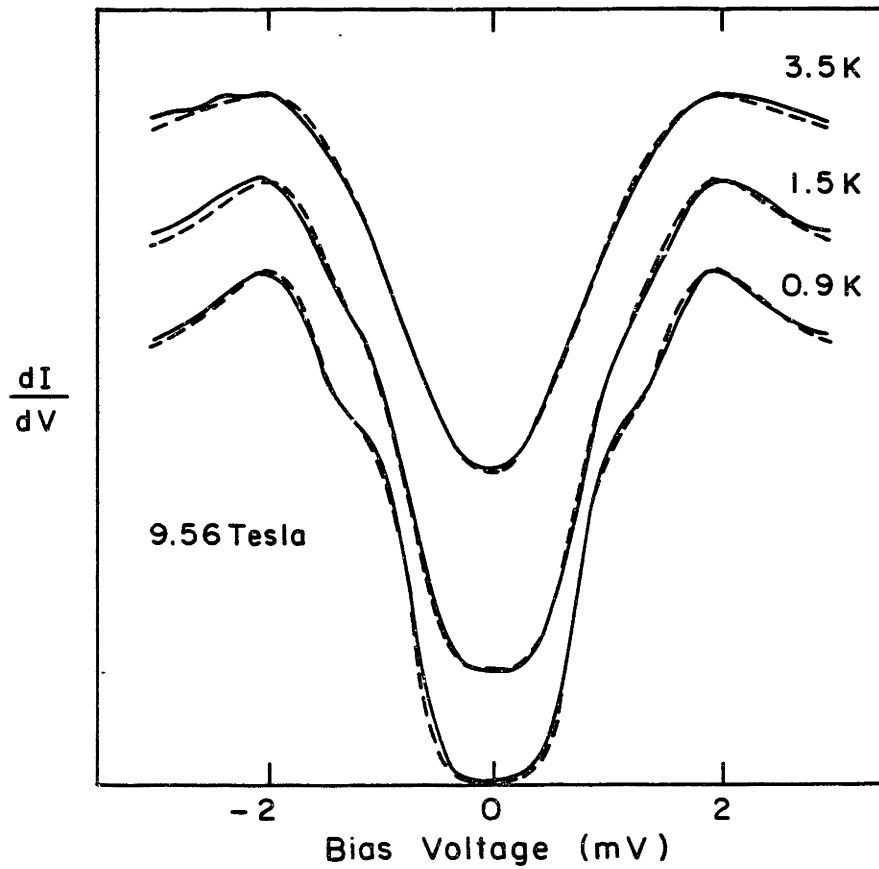
Figure 4.10: Temperature dependence of conductance. Solid curves are experimental data on the same junction shown in Figs. 4.6 and 4.8. Dashed lines are the prediction of Rainer's theory for the same parameters used in those figures.

Junction	G_0	b_{so}	c_F	P_0	T_c	T_{c0}
1	.724	.17	.17	.155	7.22	8.25
2	.667	.21	.235	.055	7.27	7.6
3	.818	.19	.35	.04	7.75	8
4	.818	.16	.325	.11	7.66	8.4
5	.95	.16	.13	.07	6.8	7.2

Table 4.2: Fitted parameters and measured T_c's for amorphous gallium junctions.

quite consistent from junction to junction. We obtain the values $G_0 = 0.81 \pm 0.14$ and $b_{so} = 0.18 \pm 0.03$.

4.3   Critical Fields of Gallium Films

Critical field data were also taken on some of the gallium films when time permitted. The data points shown in Figure 4.11 were taken on the gallium electrode of the junction used in Figures 4.6 and 4.8. The solid curve is the theoretical prediction for the critical field derived by using the values obtained from the tunneling data for c_F, P_0, b_{so}, and G_0. The agreement between the tunneling data and the critical field data is quite good. There is some uncertainty in the temperature of the data points taken above 4.5K because of the difficulty in stabilizing the temperature of the sample without ^3He condensed in the ^3He pot. Between 2 and 4.5 K there are no data points because of the extremely rapid fluctuations of the temperature in this range. The higher temperature points were taken by holding the field constant
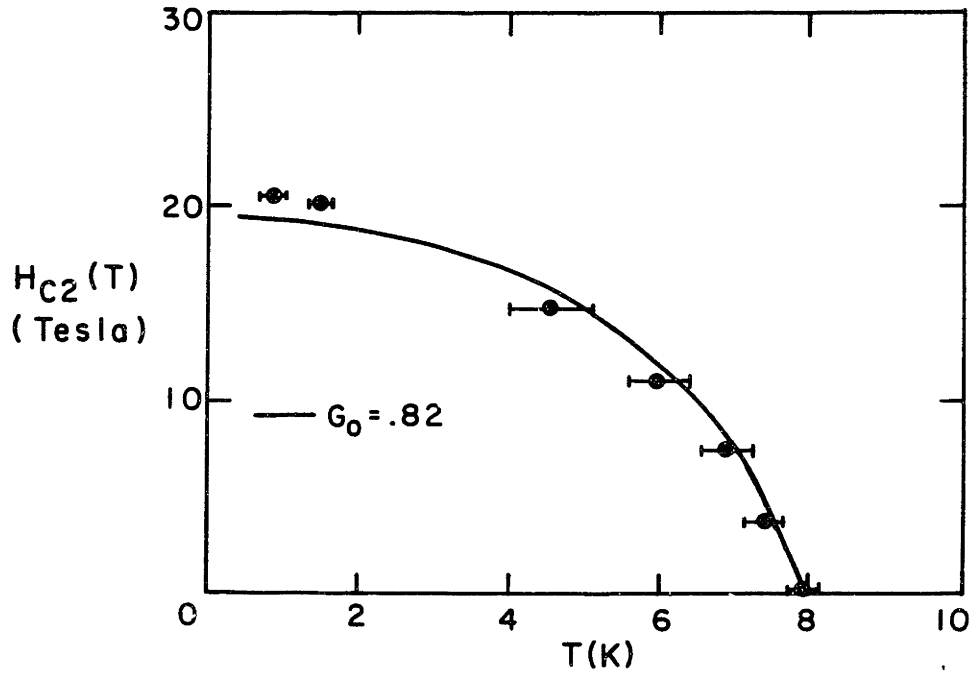
Figure 4.11: Critical field data for gallium film of junction used in Figures 4.6 and 4.8. The solid curve is the prediction of Eq. 2.19 using the parameters obtained from the tunneling data ($G_0 = 0.818$, $b_{so} = 0.16$, $c_F = 0.325$, and $P_0 = 0.11$).

and letting the temperature slowly drift through $T_c(H)$.

A caveat should be issued when comparing the data in Figure 4.11 with the theoretical curve. Recall that $2\Delta_0/k_B T_c \simeq 4.45$ for amorphous gallium and that this critical field curve is calculated using a weak-coupling theory. Rainer, *et al.* (1973), have calculated the critical field for $Pb_{.75}Bi_{.75}$ using the full $\alpha^2 F(w)$ dependence on frequency. They find that the bulk critical field is enhanced at low temperature by roughly 10% to 20% over the weak-coupling calculation (depending on the spin-orbit scattering rate). The phonon spectral density of $Pb_{.75}Bi_{.25}$ is very similar to that of amorphous gallium (Leslie, *et al.*, 1970). Because of the very short mean free path in the gallium films their perpendicular critical field should be a significant fraction of their parallel critical field. (This is, in fact, the case. Typically $H_{c2||} \sim 20$ tesla and $H_{c2\perp} \sim 13$ tesla.) Thus, we expect roughly the same change upon including strong-coupling in our parallel gallium films as for bulk $Pb_{.75}Bi_{.25}$. This is not a large correction and, if anything, should bring the prediction into closer agreement with the data at low temperature. Thus, it is fair to say that the critical field data is consistent with the tunneling data.

Chapter 5

Analysis of Vanadium Data

5.1 Properties of the Vanadium Films

As shown in Figure 5.1 the T_c of vanadium films electron-beam deposited onto sapphire substrates held at $\sim 700\ ^{\circ}C$ shows a rough $1/d$ dependence. This is typical of many transition metal superconductors. Teplov, et al. (1976), have observed almost exactly the same dependence of T_c on thickness for vanadium films from 2900 to 60 Å as that shown in Figure 5.1. The resistive transition of vanadium deposited on room-temperature glass substrates was similar for thicknesses around 100 Å $(3 - 3.5K)$. The critical fields were also virtually identical. However, T_c was significantly reduced when the deposition was done at liquid nitrogen temperature. For a 100 Å thick film this resulted in a T_c of less than $2K$. The room temperature films became electrically continuous at about 70 Å, the 700 $^{\circ}C$ films at about 90 Å. This fact limited us to studying relatively "thick" films (~ 100 Å),

Figure 5.1: Critical temperature vs. reciprocal thickness of vanadium films deposited at 700 °C on sapphire substrates.

for which the orbital depairing was significant. However, as we shall
see, the splitting of the spin conductances in a magnetic field was still
clearly observable.

The residual resistivity ratios of our films varied from 3 to 15.
They tended to be higher for thicker films. The variance could not be
correlated with changes in preparation conditions. The residual resis-
tivities of our vanadium films varied from 3.5 to 50 $\mu\Omega-cm$. There
was some correlation between the resistivity and thickness. This too
was observed by Teplov, *et al.* (1976), whose residual resistivites var-
ied from 4.5 to $20\mu\Omega-cm$. This may indicate that for thinner films
the mean free path is diminished by scattering at the surfaces. We
can estimate this length using the formula (Hake, 1966),

$$l_{tr} = 9 \times 10^{11}\hbar(3\pi^2)^{\frac{1}{3}}[e^2\rho_{\Omega-cm}(n^{\frac{2}{3}}S/S_F)]^{-1}cm$$

where S is the Fermi surface area and S_F is S for a free electron gas
with density n^1. We find that the transport mean free path, l_{tr}, is
$10 - 50$ Å for the 100 Å thick films and saturates at about 300 Å for
samples over 1000 Å thick. Here we have used the bulk value for n
and assumed $S \sim S_F$. Similarly, the effective coherence length can be
estimated using

$$H_{c2}^{\perp} = \frac{\Phi_0}{2\pi\xi_{eff}^2}.$$

---

[1]This is a crude estimate. We are ignoring the logarithmic correction to this
formula which is necessary for accurate results when $d \sim l_{tr}$.

This yields $\xi_{eff} \sim 115$ Å for the 100 Å films discussed in the following section. Thus, these films are in the dirty limit, for which the theory was derived. For the 1000 Å film used in the $V/Al_2O_3/Fe$ junction discussed in Section 5.3 we obtain $\xi_{eff} \sim 200$ Å. The transport mean free path for this same film is about 250 Å. It is therefore on the edge of being 'dirty'.

The parallel upper critical field of 100 Å films at zero temperature was about 4.5 tesla whereas the perpendicular critical field was 2−2.5 tesla. We will fit the full temperature dependence of these critical fields to the high-field theory, including the renormalization, in the following section. Critical field measurements on thin vanadium films have previously been made by Tedrow and Meservey (1975), Gibson, Meservey, and Tedrow (1985), and Gibson and Meservey (1986). Zeeman splitting of the quasiparticle density of states in thin vanadium films has been observed by Tedrow and Meservey (1978a).

We found that using the weak-coupling limit with $2\Delta/k_B T_c = 3.52$ worked quite well for all our tunneling data. This is consistent with the tunneling results of Vedeneev and Pogrebnyakov (1978) who obtained a value of 3.5 from V-oxide-Pb junctions.
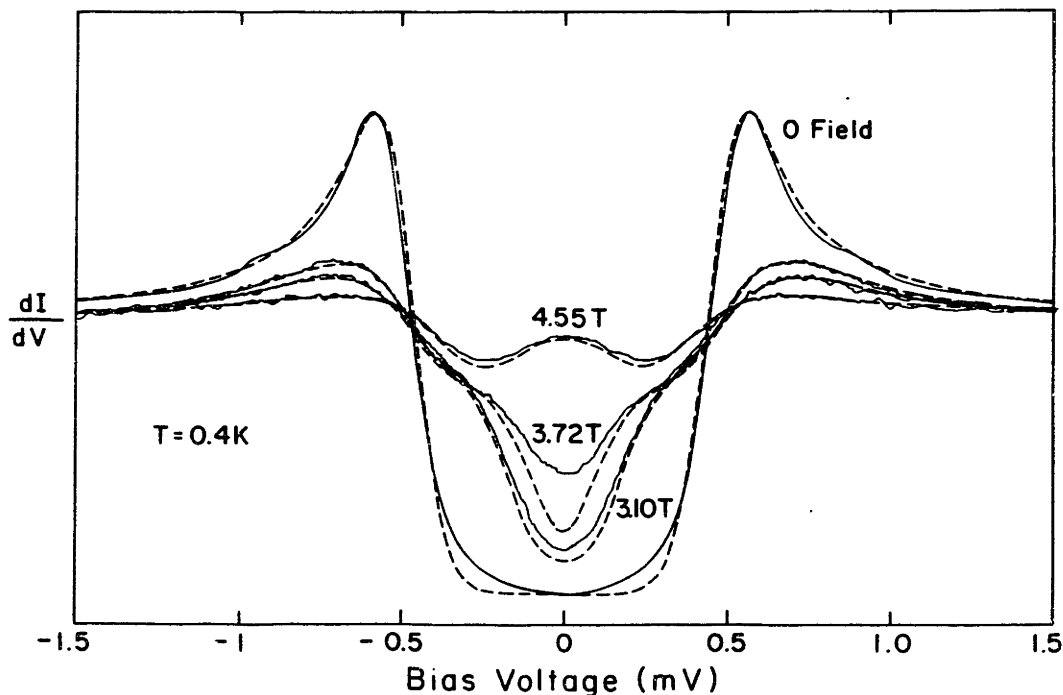
Figure 5.2: Dynamic conductance vs. bias voltage for an $Al/Al_2O_3/V$ tunnel junction at a number of fields. The dashed curves are a fit to the theory using Eqs. 2.18. Here we have used $G_0 = 0$, $c_F = 0.9$, $b_{so} = 0.09$, and $P_0 = 0.1$. The vanadium film is 100 Å thick.

5.2   Analysis of $Al/Al_2O_3/V$ Tunneling Data

We will begin by discussing the determination of G_0 in vanadium using $Al/Al_2O_3/V$ tunnel junctions. This was accomplished by fitting their dynamic conductance versus bias voltage to the theory of Rainer, as was done for amorphous gallium. A typical set of conductance curves, at low temperature, is shown in Figure 5.2. The dashed curves are

curves are a fit to theory using $G_0 = 0$. The most interesting feature of these curves is the peak at zero-bias which appears at high field. This peak is a consequence of the fact that in our thin vanadium films the gap remains large even very close to the phase boundary. It is the result of the overlap of the peaks of the two spin density of states when $\Delta(H) \sim \mu H$ (see Figure 5.6). Combined with knowledge of the critical fields it provides extremely useful information for determining the fitting parameters. In the case of amorphous gallium this peak is not observed for two reasons. First, the transition to the normal state is far from first order. Consequently, the ratio $\mu H/\Delta(H)$ is close to one only when $\Delta(H)/\Delta(0)$ is small. More importantly, the spin-orbit scattering rate is too large. As we shall see it is difficult to observe this peak for $b_{so} \geq 0.12$.[2] However, in amorphous gallium, because the critical field is so large, the splitting can be easily observed despite the large renormalization . In the case of vanadium, the critical temperature is a factor of two smaller whereas the critical field is almost a factor of five smaller. Therefore, the splitting is a smaller feature relative to the scale of the other features in the conductance curves. This problem is compounded by the fact that we cannot make extremely thin vanadium films that are electrically continuous without depositing them on very cold substrates, which severely degrades the

---

[2]This limit applies to the present data. If b_{so} is made larger than 0.12 and c_F and G_0 are adjusted so as best to fit the critical field data the peak is not observed.

transition temperature. Thus, the films we have used exhibit significant orbital depairing. Despite this, the splitting can still be observed at intermediate fields and provides useful information on the renormalization and spin-orbit scattering rate. The zero-bias peak which emerges in high fields is a fortunate development. It allows us an accurate look at what is going on near the phase boundary. As we shall see, much can be learned about the renormalization from this peak in conjunction with knowledge of the critical field curve.

Figure 5.3 shows a number of conductance curves at fields approaching the critical field. It is clear that the order parameter of the vanadium is large until quite close to the phase boundary. This indicates that we are approaching a first order transition or at least a second order transition which is close to being first order. The dashed lines are a fit to Rainer's theory (again using $G_0 = 0$) and will be discussed below. Figure 5.4 shows a typical phase diagram for a thin film in a parallel magnetic field, for which the transition is of first order below a critical temperature, T^*. In order to obtain a first order transition the spin-orbit scattering, renormalization and orbital depairing must all be sufficiently low. Increasing any of these changes the susceptibility of the superconductor such as to lower T^*. T^* can be calculated from the Ginzburg-Landau theory; for a review see Fulde (1973). We have used a program written by Tkaczyk (1988),
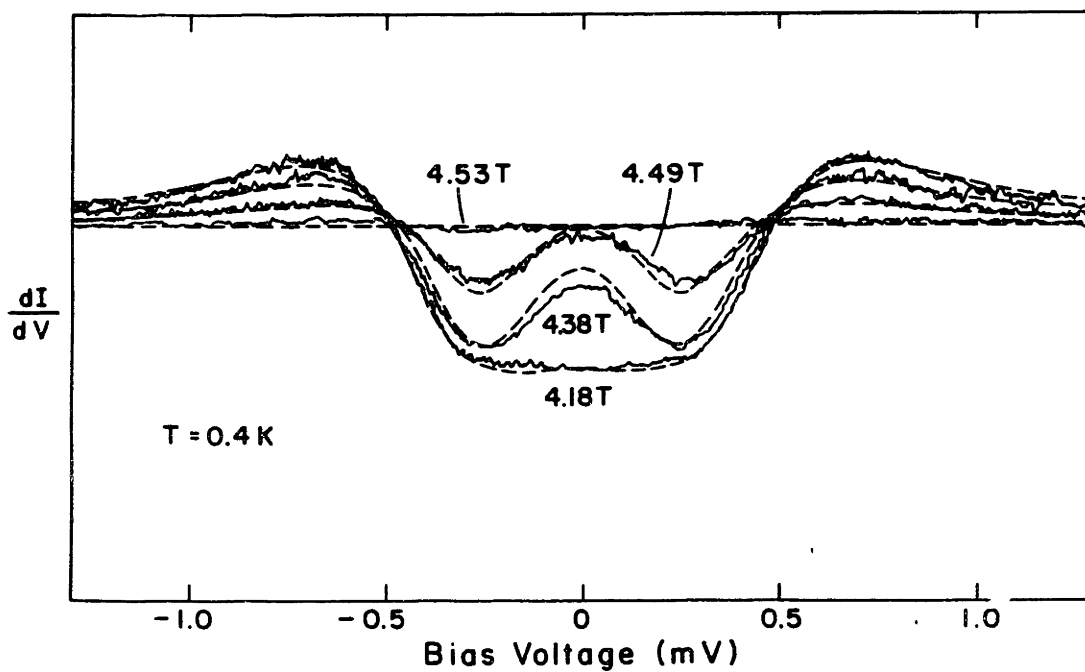
Figure 5.3: Dynamic conductance at a number of fields approaching the phase boundary. The vanadium gap remains large until very close to the transition. Dashed lines are a fit to the theory with $G_0 = 0$, $b_{so} = 0.05$, $c_F = 0.93$, and $P_0 = 0.1$. $T = 0.4K$.
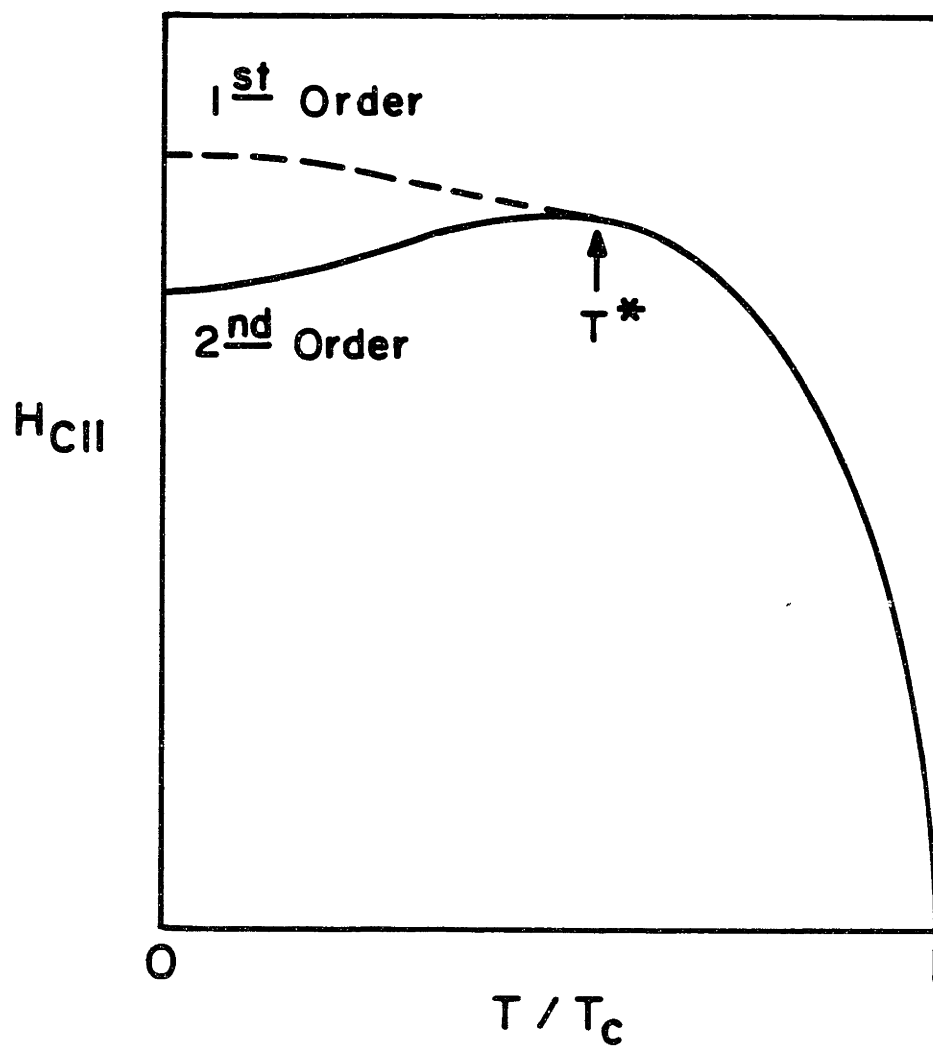
Figure 5.4: Phase diagram for thin superconductor parallel to magnetic field.

based on the approach outlined by Fulde, to calculate T^*. It turns out that if $c_F = b_{so} = G_0 = 0$ then $T^*/T_c = .567$. For $c_F \geq 1.66$ there is no first order transition even for $b_{so} = G_0 = 0$.

If we use the parameters obtained from fitting the curves in Figure 5.3 to calculate the order parameter as a function of applied field (again using Rainer's theory) we get the curve labelled '2' in Figure 5.5. Curve '1' is the result of fixing G_0 at -0.167 while varying the other parameters so as to best fit the parallel critical field curve (see Figure 5.7) for the same vanadium film. Here we have used $c_F = 0.63$, and $b_{so} = 0.065$ (with $P_0 = 0.1$, and $T_{c0} = 3.62$). The dashed part of the curve is the "unphysical" second solution for the gap in the region between the first and second order phase boundaries. Similarly, curve '3' is obtained by fixing G_0 at 0.5 (and using $c_F = 1.45$, and $b_{so} = 0.02$). All three curves are for $T = 0.4$ K. The vertical lines indicate the range of field over which the zero-bias peak was observed at this temperature. Clearly, the transition is close to being first order. For the parameters which provide the best fit (those of curve '2' in Figure 5.5), the calculated value for T^* is 0.28 K. Figure 5.5 can be used to demonstrate how definite limits may be placed on G_0. Roughly speaking, the zero-bias peak is only seen if $\mu_B H/\Delta(H) \geq 0.7$. The exact cutoff depends on the shape of the individual spin densities of states, which are determined by the renormalization, depairing and
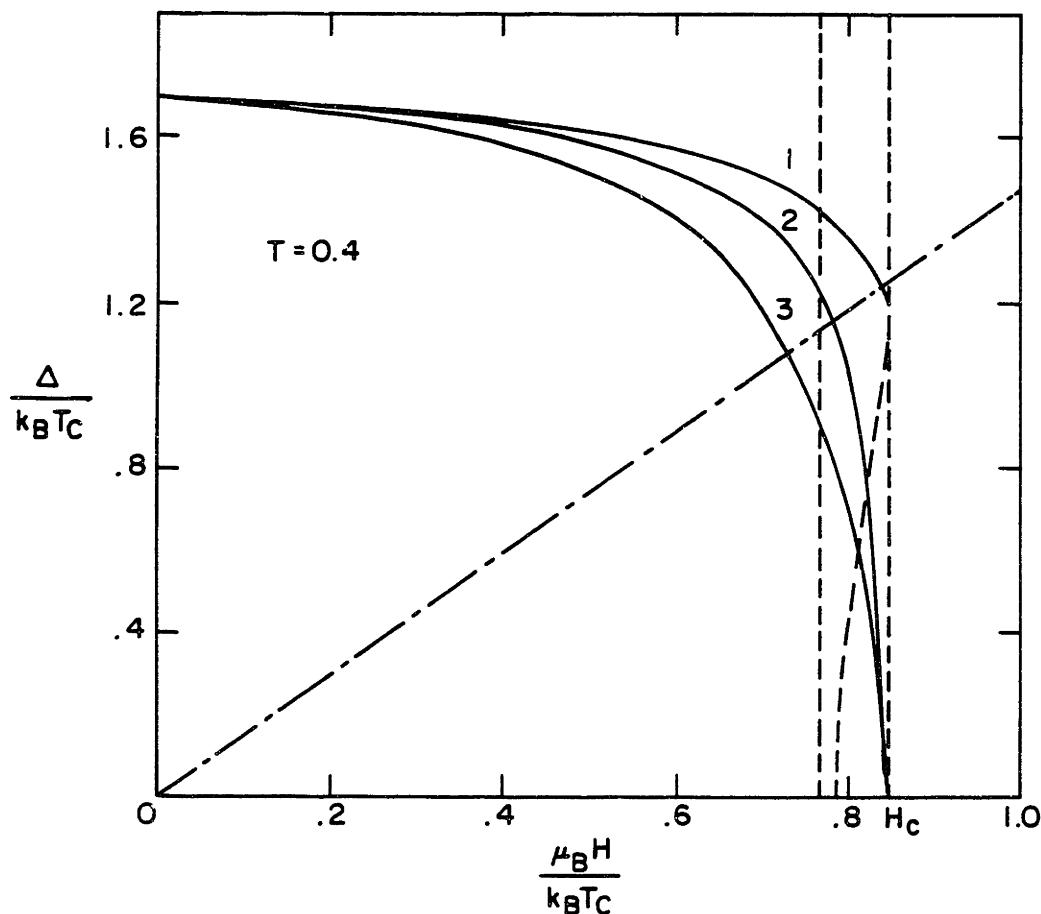
Figure 5.5: Gap vs. applied field in units of k_BT_c at $T = 0.4$ K. Curve '2' is that obtained using the fitting parameters from Figure 5.3. Curve '1' is the result of fixing G_0 at -0.167 while varying the other parameters so as best to fit the parallel critical field curve for the same vanadium film. Similarly, curve '3' is obtained by fixing G_0 at 0.5. The vertical lines indicate the range of field over which the zero-bias peak is observed. Usually, this peak can only be seen for values of Δ and H to the lower right of the dash-dot line.

spin-orbit scattering. Increasing the spin-orbit scattering, for exam-
ple, makes it more difficult to observe the peak in the sense that one
must be closer to the phase boundary. This is illustrated in Figure
5.6. Here we have shown the theoretical prediction for the dynamic
conductance and its spin components for two different values of the
spin-orbit scattering rate. The other parameters used are typical for
vanadium. Since the critical field is raised by increasing b_{so} we have
used a higher field for the dashed curves. $\mu_B H/\Delta$ is actually slightly
larger for the dashed curves (0.969) than for the solid ones (0.935).
This should actually make it easier to observe the peak for the higher
spin-orbit scattering case. However, as can be seen from the figure,
the change in shape of the individual spin conductances precludes
this. In general, it becomes difficult to observe the zero-bias peak for
values of b_{so} greater than about 0.12. This provides an interesting
way for determining an upper limit on this parameter.

Returning to Figure 5.5, we note that for $G_0 = -0.167$ the gap
is too large to observe a zero-bias peak. If we fix G_0 at -0.167, and
then vary the other parameters so as best to fit the critical field data,
we find that the transition is first order. The gap is much larger than
the splitting and we do not get a peak. T^* is a strong function of
G_0. If we decrease G_0 below zero it rapidly becomes impossible to
observe a peak (for a film with this critical field). An upper bound
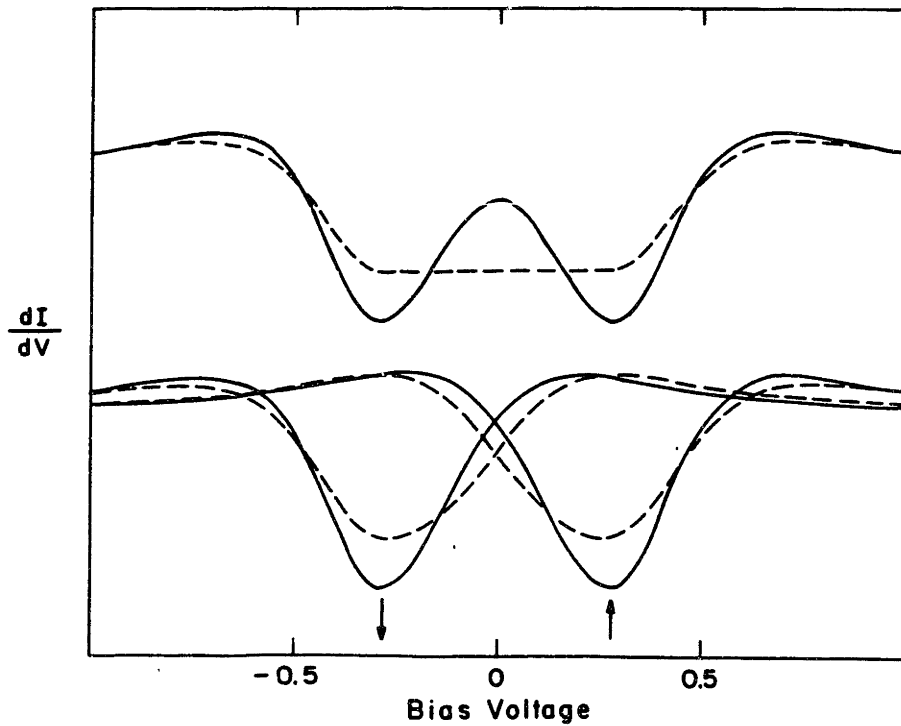
Figure 5.6: Dynamic conductance and its individual spin components for two different values of b_{so} at $T = 0.4$ K. Solid curves, $b_{so} = 0.05$; dashed curves $b_{so} = 0.15$. In both cases the other parameters were typical for 100 Å vanadium films: $G_0 = 0$, $c_F = 0.85$, $P_0 = 0.1$, and $T_c = 3.33$ K. $\mu_B H/\Delta(H)$ is 0.935 for the solid curves and 0.969 for the dashed ones. Zero-bias peak disappears for large values of b_{so}.

can also be placed on G_0, but not with quite the same accuracy. If G_0 is fixed at a value larger than zero, the resulting gap is too small, as in curve '3'. The predicted curves then look narrower than the data. The shape of these curves also changes more slowly than the data with increasing field near the phase boundary. In this way we can put an upper bound of about 0.2 on G_0.

A factor which slightly complicates this determination is the presence of some zero-field depairing. We determine this depairing, P_0, by fitting the zero-field conductance, as described in Section 4.2. This depairing lowers the predicted T_c so that we must raise T_{c0} to compensate. This leads to conductance curves which are effectively more depaired as we approach the phase transition. This depairing can actually make it easier to observe the zero-bias peak. However, in the present experiment we find $P_0 = 0.1$ and the effect is small.

We can fit the conductance curves near the phase boundary using a range of values for the spin-orbit scattering ($b_{so} \sim 0.03 - 0.10$). Values at the lower end of this range, such as the value $b_{so} = 0.05$ used in Figure 5.3, seem to work slightly better. The shape of the curves and the rate of change of this shape with increasing field matches the data more closely. The rate of change of the curves with field is influenced by the spin-orbit scattering mainly through the fact that changing b_{so} changes T^*, and therefore alters the slope of $\Delta(H)$ near H_c. On

the other hand, the apparent splitting of the conductance curves at intermediate fields is small, indicating a somewhat larger value for b_{so}. This is typified by the junction shown in Figure 5.2. Here the value $b_{so} = 0.09$ fits the splitting of the 3.10 and 3.72 tesla curves, as well as that of other curves at "intermediate" fields not shown.

As in the case of amorphous gallium, using smaller values for G_0 tends to push the theoretical prediction for the "shoulder" up the page (see Figure 4.7). The height of the shoulders in Figure 5.2 provides further evidence that G_0 must be low. The value $G_0 = 0$ fits all the curves quite well.

We can also limit the range of values for G_0 by simply fitting the parallel critical field as a function of temperature to the theory as given by Eq. 2.21. The critical fields of the three 100 Å films studied were very similar. As can be seen in Figure 5.7(a), the value $G_0 = 0$, along with $c_F = 0.9$ and $b_{so} = 0.07$, fits the data quite well. The variance of the twelve data points from the theory is only $0.11 \ [kG]^2$. If we try to use $G_0 = 0.5$, as in Figure 5.7(b), then the theoretical prediction is too high at low temperature, even with $b_{so} = 0$ (Variance equals $3.49 \ [kG]^2$). The only way to correct this is to increase the orbital depairing, c_F, considerably. This will cause the fit at lower temperatures to be even worse. Similarly, if we fix G_0 at -0.167 and try to fit the data we get results like that shown
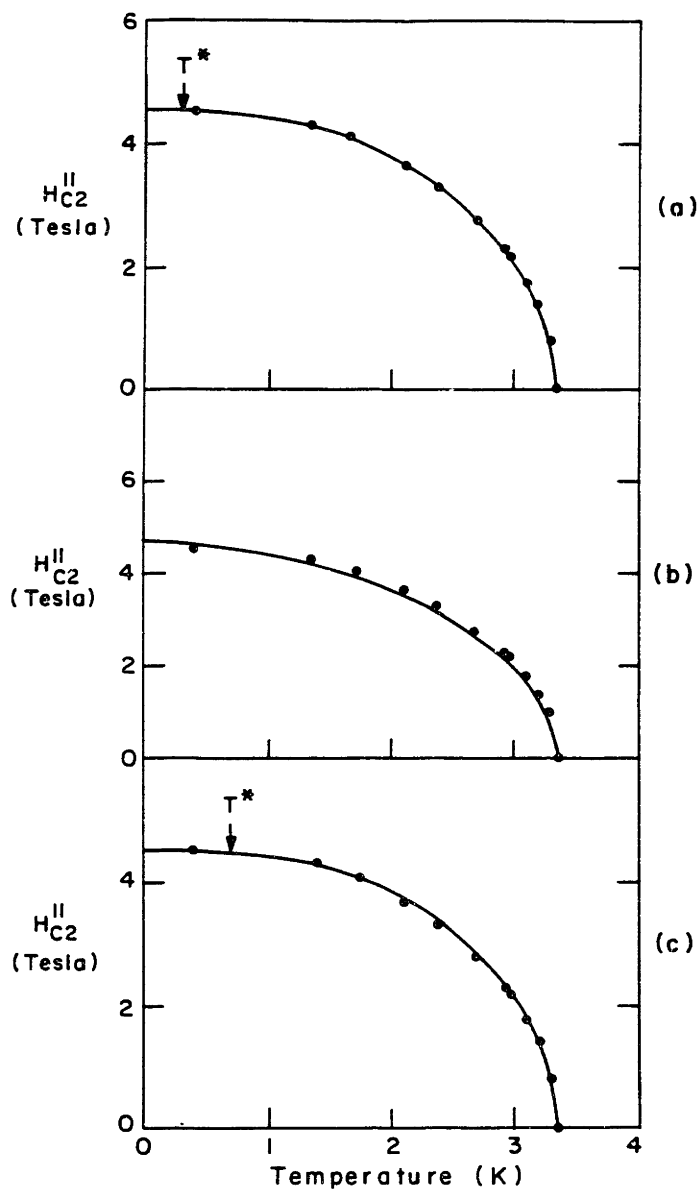
Figure 5.7: Points are parallel critical field data for a typical 100 Å vanadium film. Solid lines are prediction of high-field theory for the second order phase boundary as given by Eq. 2.19 using (a) $G_0 = 0$, $c_F = 0.90$, and $b_{so} = 0.07$; (b) $G_0 = 0.5$, $c_F = 1.32$, and $b_{so} = 0$; (c) $G_0 = -0.167$, $c_F = 0.65$, and $b_{so} = 0.14$. In all cases $P_0 = 0.1$, and $T_{c0} = 3.62$ so that $T_c = 3.33$. T^* is indicated in the figures. In (b) the transition is second order at all temperatures.

in Figure 5.7c (Variance equals 3.62 $[kG]^2$). Here, in order to make the critical field high enough at low temperature we must make the spin-orbit scattering rate at least 0.14. As we have seen, such a high value would preclude observation of the zero-bias peak. In order to make the fit better at intermediate temperatures we would have to increase c_F. We would then need an even larger value for b_{so} to fit the low temperature points.

In summary, the presence of a zero-bias peak in the dynamic conductance of $Al/Al_2O_3/V$ junctions with the observed critical fields indicates that G_0 must be positive (or at least greater than about -0.05). It also puts an upper limit on the spin-orbit scattering rate of about 0.12. The shape of the conductance curves near the phase boundary and the rate at which they change with field as this boundary is approached indicate that $G_0 \simeq 0$. This was the case for all four junctions studied, each of which had a 100 Å thick vanadium electrode. The shape of the conductance curves at intermediate fields, in particular the features associated with the splitting, indicate that $G_0 \simeq 0$ and that $b_{so} = 0.07 - 0.10$. Finally, the parallel critical field as a function of temperature is consistent with $G_0 = 0$ and a small value for b_{so} (0.03 − 0.10).

5.3   Analysis of $V/Al_2O_3/Fe$ Tunneling Data

In this section we will discuss our results from the $V/Al_2O_3/Fe$ junctions described in Section 3.2. A caveat must be issued before doing so. It was necessary to deposit a relatively thick aluminum layer $(45-50 \text{ Å})$ on the vanadium to form the tunneling barrier. It is doubtful that all of this aluminum was oxidized during the glow-discharge. The need for so much aluminum may be partly due to the surface diffusion and aggregation properties of aluminum on vanadium. It is also possible that there is some diffusion of either iron or vanadium into the barrier, even at room temperature. At any rate, it seems likely that there are pockets of unoxidized aluminum present on the side of the barrier next to the vanadium. This seems especially likely in view of the fact that in some junctions the vanadium gap obtained from tunneling curves indicated transition temperatures of about 2.8 K, even when the vanadium was thick (1000 Å) and had a resistive transition of over 4 K. Note that 2.8 K is still significantly higher than the transition temperature of aluminum films of the same thickness as those used to make the barrier $(\leq 2.3 \text{ K})$. We believe that we are tunneling into a combination of vanadium and aluminum which is proximity-effect coupled to vanadium. We present these results here both for completeness and because the measured values for G_0 and b_{so} should still be strongly influenced by the properties of vanadium.

The values we obtain are in close agreement with those obtained on pure vanadium from the $Al/Al_2O_3/V$ tunnel junctions.

Tunnel conductance data were taken at a number of fields and temperatures on three $V/Al_2O_3/Fe$ junctions. We present here the data on the best such tunnel junction. This junction was deemed best based solely on the fact that its tunneling characteristic indicated the highest transition temperature (2.79 K). Presumably this meant that its behaviour was most nearly that of pure vanadium.

Figure 5.8 shows the tunneling conductance for this junction at two representative fields. The characteristic asymmetry obtained with iron counterelectrodes is observed. The dashed lines are a fit to the theory using $G_0 = 0.177$, $c_F = 0.20$, $b_{so} = 0.03$, $P_0 = 0.05$, and $T_{c0} = 2.79$. A slight background curvature similar to that observed in amorphous gallium is present in these data. However, the vanadium film is thick (1000 Å) and has a low resistivity ($12\mu\Omega-cm$). Therefore the conductance data may indicate that the tunneling is into a disordered region at the interface. Note that no curvature was seen in any of the $Al/Al_2O_3/V$ tunnel junctions.

The curves in Figure 5.8 can be readily separated into their individual spin components using the algebra described in Section 3.1. The result of doing this for the 3.10 tesla curve of Figure 5.8 is shown in Figure 5.9. The dashed and solid curves represent the 'up' and
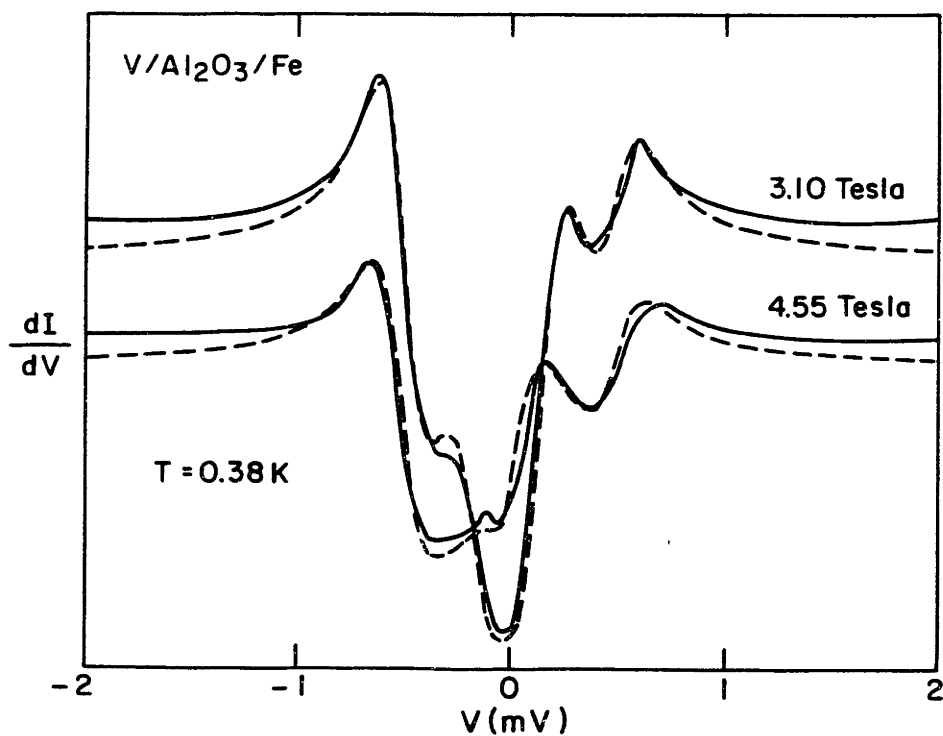
Figure 5.8: Dynamic conductance vs. bias voltage at two fields for a $V/Al_2O_3/Fe$ tunnel junction. Solid lines are experimental and dashed lines are the prediction of theory for $G_0 = 0.177$, $c_F = 0.20$, $b_{so} = 0.03$, $P_0 = 0.05$, and $T_{c0} = 2.79$.
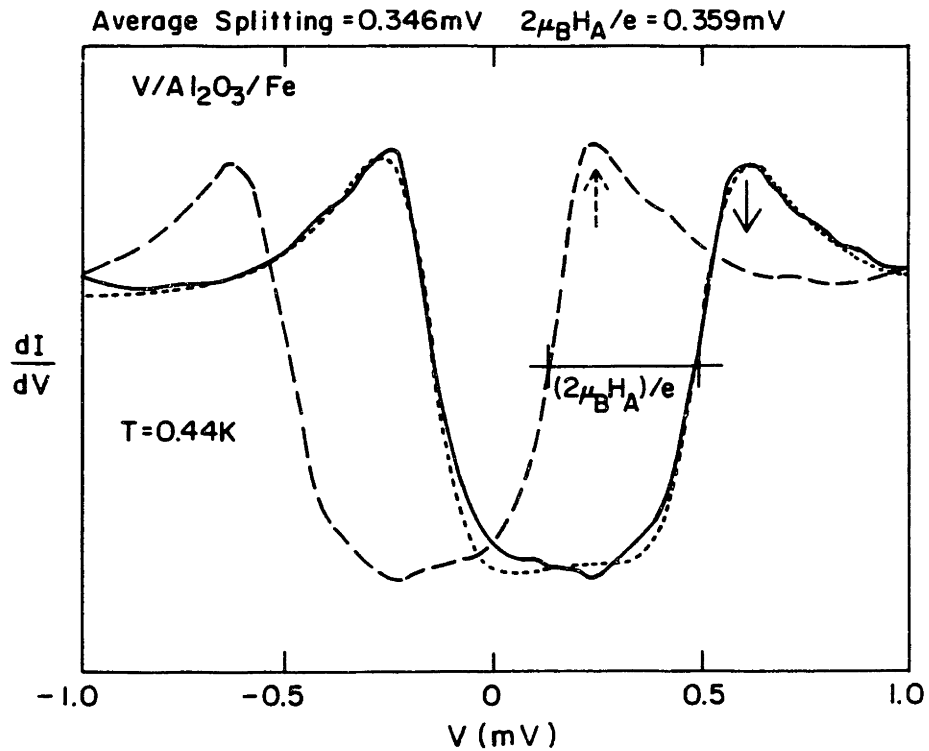
Figure 5.9: Individual spin conductances of the 3.10 tesla curve from Figure 5.8. The dotted line is the prediction of the theory using the same parameters used to fit the curves in that figure. Horizontal bar represents $2\mu_B H/e$ for the applied field.

'down' spin conductances, respectively. One curve is simply a reflection of the other about $V = 0$. The dotted line is the prediction of the theory using the same parameters as in Figure 5.8 ($G_0 = 0.177$, $c_F = 0.20$, $b_{so} = 0.03$, $P_0 = 0.05$, and $T_{c0} = 2.79$). Note that the bottom of the experimental curve does not exhibit the slight 'foot' due to spin-orbit scattering which can be seen in the theoretical curve (A more pronounced example of this foot can be seen in Figure 2.3a). This is a problem common to spin-separated data. The bottom portion of the curves, even of those produced from very clean data, is frequently distorted. Consequently, this part of these curves cannot be used to determine the spin-orbit scattering rate. We have used the difference in peak heights of the separated curves, as well as the overall fit of the total conductance, to determine b_{so}.

The two spin conductance curves are stored digitally in a computer. We have used a program written by Tkaczyk (1988) to average the splitting between the two curves. At this field the average splitting (0.346 meV) is just slightly less than the applied field (0.359 meV). The result of doing this at a number of different fields and at two different temperatures is shown in Figure 5.10. Here the apparent splitting, δ, as measured directly from curves such as those in Figure 5.9, is plotted as a function of applied field. The last data point for each temperature is just slightly below the critical field at that tem-
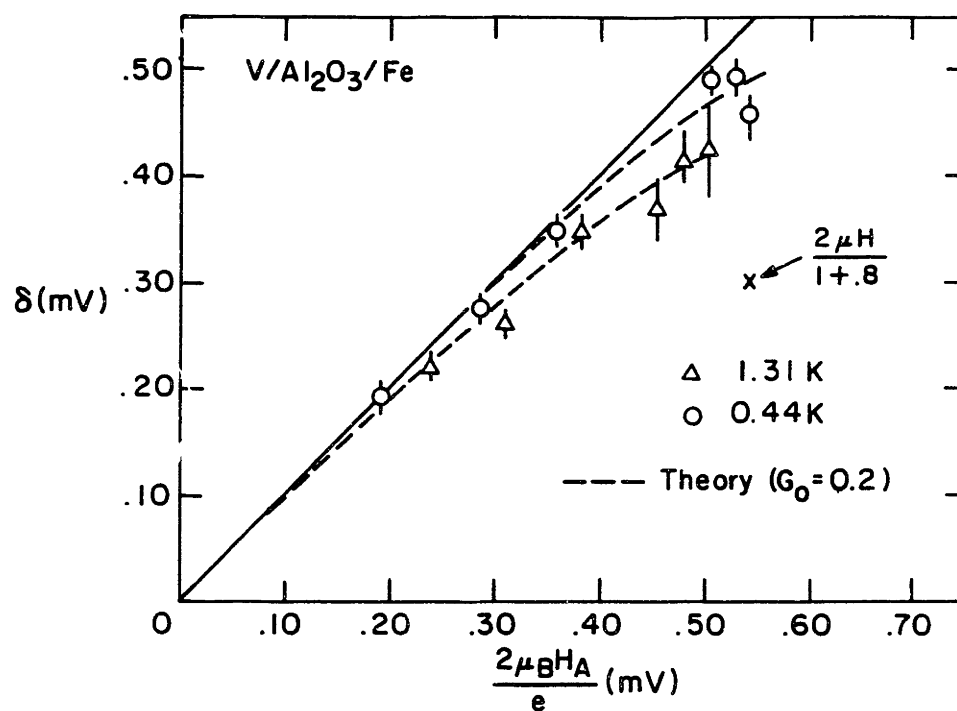
Figure 5.10: Apparent splitting, δ, as a function of field at two temperatures. Solid line represents $\delta = 2\mu_B H$, which is expected in the absence of Fermi-liquid effects. Vertical error bars are the variance in the splitting between curves such as those in Figure 5.9. Dashed lines are the prediction of the theory for $G_0 = 0.2$.

perature. The solid line represents $\delta = 2\mu_B H$. Thus, in the absence of Fermi-liquid effects all the data should fall on this line. The dashed curves are the prediction of the theory for $G_0 = 0.2$.

Despite some scatter in the data, it is clear that the deviation of δ from $2\mu_B H$ is not large. This is also the case for the other two $V/Al_2O_3/Fe$ tunnel junctions. This provides direct evidence that G_0 is small, and is consistent with a value of no more than 0.2. It is also consistent with the data taken on $Al/Al_2O_3/V$ tunnel junctions. At the phase boundary δ should approach $2\mu_B H/(1 + G_0)$ (see Eq. B.1). If the electron-phonon interaction were the only important many-body interaction then we would expect from Eq. 2.21 that $\delta \rightarrow 2\mu_B H/(1 + \lambda_{ep}) \sim 2\mu_B H/1.8$ at the transition. The 'x' shown in Figure 5.10 indicates this value for the lower temperature data. Clearly, the deviation from $2\mu_B H$ is not nearly this large. This is graphic evidence for the importance of spin fluctuations in vanadium. This point will be discussed further in Section 6.2.

Chapter 6

Discussion of Results

6.1 Discussion of Gallium Results

In this section we will discuss the validity of the theory and the reasonableness of our result for G_0. We will also compare this result to that predicted by Eq. 2.14.

The first area of concern is the extreme thinness of the gallium films. It was necessary to make the films ≤ 30 Å in order to minimize the orbital depairing. By comparing the tables in Sections 4.2 and 4.3 we see that our T_c's are somewhat reduced from the bulk values for amorphous gallium. This is a common feature of many superconductors. Naugle and Glover (1969) have found a linear dependence of T_c on the inverse of sample thickness for amorphous gallium. The thinnest samples they measured were 150 Å but extrapolation of their data shows it to be consistent with the T_c's we obtained. This fact, along with the fact that $2\Delta_0/k_B T_c = 4.45$ and the knowledge that the

film temperature does not exceed 2.3 K during evaporation, assures us that the gallium is amorphous.

We may now ask whether the value for G_0 obtained from these thin films is applicable to the bulk. The fact that the T_c's are somewhat reduced indicates that there is probably some change in the phonon spectral density and/or the density of states. However the reduction in T_c is only $10 - 20\%$ so we do not expect this to be a large effect. Aside from changes in such intrinsic properties, the two dimensionality of the films in regard to their superconductivity (and the effect of a magnetic field) is, of course, taken into account by the theory. The effective coherence length at $T = 0$ we get from the perpendicular critical field is $\xi_{eff} = \sqrt{\frac{\Phi_0}{2\pi H_{c2}^{\perp}}} \sim 35\text{Å} \geq d$, so we are justified in taking the thin film, parallel field limit of the theory. That we are in the $2D$ limit can also be seen from the fact that $H_{c\parallel}^0/H_{c\perp}^0 \sim 1.67$.[1]

Another point of concern is the presence of correlation (and presumably localization) effects in the gallium films. In the limit where these effects become very large, Fermi liquid theory will break down. This occurs when $\lambda_F > l$, where λ_F is the Fermi wavelength and l is the mean free path for momentum scattering. In this limit the momentum relaxation rate is so fast that the momentum is no longer well defined. Fermi liquid theory is predicated upon having a sharp

---

[1]The value 1.67 is coincidental. The parallel critical field has a square-root dependence on temperature near T_c; we are not observing surface sheath superconductivity.

Fermi surface and long-lived excited states which can be described as nearly free particles with a definite momentum. These requirements are clearly not satisfied when there is so much scattering that $\lambda_F > l$. As discussed in appendix A.2 the diffusion constants determined from the perpendicular critical field, the tunneling data (orbital depairing parameter) or the residual resistivity using the Drude model are all $\sim 0.3 - 0.4 \frac{cm^2}{sec}$. If we naively take the bulk value for the Fermi velocity this gives a mean free path of 0.6 Å. This is, of course, absurdly short as it is less than the interatomic spacing so that $\lambda_F \sim l$. It can be taken as evidence, however, that, as expected for amorphous gallium, the scattering length, l, is on the order of the atomic spacing. However, in most of the films used in this study the change in the normal state conductance was only $\sim 10 - 30\%$ over the range of voltage studied. If the scattering is causing only a small change in the normal state density of states at the Fermi surface we expect the Fermi-liquid theory to remain valid. Also, the presence of moderate scattering helps justify the assumption of a spherical Fermi surface and the use of just the $l = 0$ Fermi-liquid parameter.

To incorporate strong-coupling we simply multiplied the gap by a constant factor wherever it appeared in the theory, as described in Section 4.2. A full strong-coupling calculation, including the energy dependence of the interaction, would be considerably more complicated.

To include higher order terms in T_c/Θ_D would require defining "higher order" Fermi liquid parameters as the mean-field potentials would no longer be linear functionals of the propagator, $\hat{g}$ (see Eq.2.16). We can view our result as an effective, first order (in T_c/Θ_D) Fermi-liquid parameter. Again, this is not a large effect.

The "bottom line" in considering all the above caveats is that the Fermi-liquid theory, as used here, seems to explain quite well the renormalization of the density of states in amorphous gallium, as both a function of temperature and field. Also, the parameters obtained from this theory are consistent from sample to sample.

We will now compare our result for G_0 with that predicted by Eq.2.14. The value obtained for G_0, 0.81 ± 0.14, is somewhat less than one would naively expect for an electron-phonon coupling constant $\lambda_{ep} = 2.25$. To our knowledge, the Stoner factor and the electon-electron mass enhancement, λ_s, have not been determined for amorphous gallium. However, we can make the following crude estimate. Chen, *et al.* (1969), have measured $\alpha^2 F(\omega)$ and inverted it to obtain $\lambda_{ep} = 2.25 \pm 0.2$ and $\mu^* = 0.17 \pm 0.02$, where μ^* is the Coulomb pseudopotential. This is an unusually large value for μ^*. One would expect a value more like 0.1 (Allen and Dynes, 1975), which is what they obtained for quenched-condensed bismuth. They found, however, that 0.17 gave a very good fit while 0.1 yielded a poor fit. The high value

may be the result of the renormalization described in Eq. 2.15. This
would indicate a value for $\lambda_s \sim 0.07$. The exact value of λ_s makes lit-
tle difference in Eq. 2.14 as it is small in any case. The large value of
μ^* is interesting in that it indicates that electron-electron interactions
may be strong. Jensen and Andres (1968) have shown that a crude
approximation for the Coulomb exchange potential is that it is three
times the Coulomb pseudopotential. Thus,

$$\bar{I} \sim N(0)\bar{V_c} \sim 3\mu^* \sim 0.5 \qquad (6.1)$$

If we plug these numbers into Eq. 2.14 we get,

$$1 + G_0 \sim (1 + 2.25 + 0.07)(1 - 0.5) = 1.66$$

This is very close to the measured result. As mentioned in Section 2.1,
Leavens and MacDonald (1983) argue that Eq. 2.14 is only good when
the exchange enhancement factor is large. The large measured value
for μ^* and our relatively small value for G_0 indicate that this may be
the case. Rainer (private communication) has also warned that it is
not conceptually correct to try to separate the net renormalization
into its constituent interactions. However, for both amorphous gal-
lium and, as we shall see, vanadium Eq. 2.14 seems to predict values
for G_0 consistent with our data.

As a final note, we consider our measured value for the spin-orbit
scattering rate, $b_{so} = 0.18 \pm 0.03$. We can make a rough estimate

for b_{so} using the formula derived by Gallagher (1978) using Fermi's Golden Rule

$$\hbar/\tau_{so} \sim 2\pi c \left(\Omega N(E_F)\right) |M_{so}|^2. \tag{6.2}$$

Here c is the fractional concentration of spin-orbit scattering centers (defects, impurities, etc.). $N(E_F)$ is the density of states at the Fermi level; and Ω is the volume of the unit cell. M_{so} is the matrix element for spin-orbit scattering. Note that Landau and Lifshitz (1971) have shown that $M_{so} \sim Z^2$ so that Eq. 6.2 leads to the Z^4 dependence mentioned in Section 2.3. For M_{so}^{Ga} we will use the value 0.102 meV obtained by Yafet (1963). If we make the assumption that all the spin-orbit scattering in these thin films occurs at the surface and that every surface atom causes scattering[2] then $c \sim 1/d$, where d is measured in lattice constants. Using the bulk values for crystalline gallium for the lattice constant (2.69 Å), and k_F $(1.65 \times 10^8 cm^{-1})$, we can calculate Ω (19.6 Å^3), c (0.067), and $N(E_F) = \frac{mk_F}{2\pi^2\hbar^2} \simeq 1.35 \times 10^{22} states/eV \cdot cm^3$ (using the free-electron model and the bare electron mass). From this we get $\hbar/\tau_{so} \sim 1.1$ meV. Thus, $b_{so} = \hbar/3\tau_{so}\Delta_0 \sim 0.25$. This is close to the measured value of 0.18. A similar analysis for thin aluminum films yields a value of $b_{so} \sim 0.12$. This is also somewhat more than the value (~ 0.05) obtained from tunneling (see, for example, Tedrow and Meservey, 1979; Alexander, 1986). In short, our measured spin-orbit

---

[2]Tedrow and Meservey (1978b) have shown that in thin films τ_{so}^{-1} is dominated by surface scattering.

scattering rate is consistent with a simple calculation and with mea-
surements on other superconductors. For a more complete discussion
of spin-orbit scattering in superconductors the reader is referred to
the theses of Gallagher (1978) and Tkaczyk (1988).

6.2   Discussion of Vanadium Results

We will begin by discussing the validity of the high-field theory, as
described in Chapter 2, for our vanadium samples.

First, we note that for the 100 $Å$ films used in the $Al/Al_2O_3/V$
junctions, as pointed out in Section 5.1, the mean free path is signifi-
cantly less than the coherence length. Thus, we are in the dirty limit
for which the equations in Section 2.2 were derived. In the case of the
1000 $Å$ vanadium electrode discussed in Section 5.3 we are still close
to being in the dirty limit.

Another point of concern is the fact that vanadium is a border-
line type II material. In the dirty limit κ becomes even larger. The
effective penetration depth at zero temperature for a 1000 $Å$ film has
been determined by Moodera (1986). He obtained a value of 900 $Å$
by observing the inductance of a meander line made from this film
(Moodera, *et al.*, 1985). This is significantly larger than the effective
coherence length of 250 $Å$ calculated from the perpendicular critical
field. We therefore expect vortices to be present above H_{c1} in the

1000 Å vanadium film of the junction discussed in Section 5.3. One could argue that these act like normal regions so that we have the equivalent of [normal metal/Fe] junctions in parallel with a [super-conductor/Fe] junction. In reality, however, the order parameter falls off continuously as we approach a vortex so that we would have tunneling from a continuum of regions with different effective depairing. On the other hand Tedrow and Meservey (1978) have procured a good fit to the quasiparticle density of states in the high κ alloy V-Ti. They used the theory of Bruno and Schwartz (1973)[3] to fit $Al/Al_2O_3/V$-Ti junctions both parallel and perpendicular to the field. Thus, leaving Fermi-liquid effects aside, the theory can be effective in the presence of vortices. In the case of the 100 Å films used in the $Al/Al_2O_3/V$ junctions

$$\lambda_{eff}^{100\overset{\circ}{A}} \sim \lambda_{eff}^{1000\overset{\circ}{A}} \frac{\left(\xi_0/l^{100\overset{\circ}{A}}\right)^{1/2}}{\left(\xi_0/l^{1000\overset{\circ}{A}}\right)^{1/2}} \sim 2000 \text{ Å}.$$

Thus, $d < \lambda, \xi$ and no vortices will form.

The existence of a first order portion of the phase boundary is not a problem. The theory as described in Chapter 2 predicts the density of states just as accurately near a first order transition as it does near one which is second order. However, care must be taken when considering the apparent splitting near a first order transition.

---

[3]This is essentially the same as the theory used here without the Fermi-liquid renormalization

Here the density of quasiparticles is not as high as the normal state density of electrons and the renormalization is less than the factor $(1 + G_0)^{-1}$ at the boundary. Thus, for example, in a figure such as Figure 5.9 if the data is below the tricritical point, T^*, then it will not be a strong function of G_0. For the parameters used to fit the data in Section 5.3, $T^* = 1.28$ K. Consequently, the low temperature data in Figure 5.9 is not strongly effected by the renormalization[4]. However, the higher temperature data is renormalized by the factor $(1 + G_0)^{-1}$ at the phase boundary and therefore indicates that G_0 is no more than 0.2.

Because the mean free path is fairly short, at least in the case of the 100 Å vanadium films, we expect the assumption that the interaction is isotropic to be fairly good.

In light of the previous discussion, it appears that the theory is applicable to the $Al/Al_2O_3/V$ data and that these data are representative of the properties of vanadium. In the case of the $V/Al_2O_3/Fe$ junctions this is not as clear because of the type II behaviour of the thicker film and because these samples are barely in the dirty limit. It is also unlikely that in the $V/Al_2O_3/Fe$ junctions the tunneling is into pure vanadium. However, as mentioned previously, the T_c measured

---

[4]Plugging the numbers into the theory indicates that for $G_0 = 0.2$, δ should be $0.95(2\mu_B H)$ at the phase boundary. On the other hand, T^* drops rapidly with increasing G_0. If we keep the other parameters the same and increase G_0 to 0.4 then T^* drops below 0.4 K and we see the full effect on δ.

for these junctions from tunneling (2.79 K) is significantly higher than that of aluminum films of the same thickness as the aluminum films oxidized to make their barriers ($\sim$ 2.3 K). Also, the value for G_0 determined from these junctions (≤ 0.2) is appreciably less than the value of $0.3 - 0.4$ obtained for aluminum (Tedrow, *et al.*, 1984; Alexander, 1986). We will take the values obtained from the $Al/Al_2O_3/V$ junctions as our result and treat the $V/Al_2O_3/Fe$ data as being consistent with it.

We will now consider the implications of our measured value for G_0 and whether it can be understood in terms of Eq. 2.14.

The electron-phonon coupling constant, λ_{ep}, and the Coulomb pseudopotential, μ^*, have been determined for vanadium from inversion of the phonon spectrum, $\alpha^2 F(\omega)$, by Zasadzinski, *et al.*, (1982). They find $\lambda_{ep} = 0.82$ and $\mu^* = 0.15$. This value for λ_{ep} is in reasonable agreement with the value of 1.04 calculated by Rietschel and Winter (1979). Allen and Dynes (1975) have shown that a large number of s-p superconductors fall along a well defined trajectory if plotted in the T_c/ω_{log} vs. λ_{ep} plane. Here $\omega_{log} = exp < \ln \omega >$ and $< \ln \omega >$ is the expectation value of the log of the phonon energy, weighted by the phonon spectral density

$$< \ln \omega >= \frac{2}{\lambda_{ep}} \int_0^\infty d\omega \alpha^2 F(\omega) \ln \omega \omega^{-1}.$$

This trajectory is predicted quite well by the Allen-Dynes T_c formula

(Allen and Dynes, 1975),

$$T_c \simeq \frac{\omega_{log}}{1.2} exp \left[-\frac{1.04(1 + \lambda_{ep})}{\lambda_{ep} - \mu^*(1 + 0.62\lambda_{ep})} \right]$$

with a value for μ^* of 0.1. Transition metals such as vanadium and niobium do not fall on this plot. Burnell, *et al.* (1982), have shown that if one assumes this is due to spin fluctuations these elements can be brought into agreement with the s-p superconductors. They do this by rescaling the values for λ_{ep} and μ^* using Eqs. 2.17 with $\lambda_s = 0.07$. This yields $\lambda_{ep} = 0.88$ and $\mu^* = 0.206$. If we make the same crude approximations we made in the case of gallium we can use this value for μ^* to estimate $\bar{I}$.

$$\bar{I} \sim N(0)\bar{V}_c \sim 3\mu^* \sim 0.6$$

Orlando and Beasley (1979) have estimated $\bar{I}$ for vanadium using the T_c equation of Jensen and Andres (1968)

$$T_c = \frac{\omega_{log}}{1.2} exp \left[-\frac{1 + \lambda_{ep} + \lambda_s}{\lambda_{ep} - \lambda_s - \mu^*} \right].$$

For $\lambda_s = 0$ this is approximately the Dynes-Allen formula. They did this by using measured values for T_c/ω_{log} and $N^\gamma/N^\chi = 1 + \lambda_{ep} + \lambda_s(1 - \bar{I})$ in this equation and obtained $\bar{I} = 0.4 - 0.5$.[5] We will average the results of these two methods and use $\bar{I} \simeq 0.5$. We can now estimate

---

[5]Recall from Section 2.1 that the ratio of the density of states determined from heat capacity to that obtained from the susceptibility is $1 + G_0$.

G_0 using Eq. 2.14

$$
\begin{aligned}
1 + G_0 &= (1 + \lambda_{ep} + \lambda_s)(1 - \bar{I}) \\
&= (1 + 0.88 + 0.07)(1 - 0.5) \\
&= 0.975
\end{aligned}
$$

This is in very good agreement with our experimental result, $G_0 = 0$. Note that Leavens and MacDonald (1983) have argued that the rescaling analysis of Daams, Mitrović, and Carbotte (1981) given in Eqs. 2.17 yields a value for λ_s which is a factor of two too small for vanadium. If this is true then the value for G_0 predicted by Eq.2.14 would be just above zero rather than just below it.

Spin fluctuations are believed to be instrumental in decreasing the transition temperature in a number of technologically important transition metals and $A15$ and $B1$ transition metal compounds (Gladstone, et al. 1969; Rietschel and Winter 1979; Rietschel, Winter, and Reichardt 1980; Orlando and Beasley 1981). In vanadium this decrease may be 12 K (Rietschel and Winter 1979) and in vanadium nitride as much as 20 K (Rietschel, Winter, and Reichardt 1980). Our small measured value for G_0 is strong new evidence for the importance of spin fluctuations in vanadium. It can be seen to be the result of the cancellation of the Fermi-liquid enhancement due to the electron-phonon interaction by an electron-electron interaction enhanced by spin fluctuations.

Finally, we can estimate b_{so} for vanadium as was done for gallium and compare the result to our measured value. The spin-orbit scattering matrix element has been determined in a band-structure calculation by Mackintosh and Anderson (1980). They get $M_{so} = 4.08 \times 10^{-2}$ eV. Using the bulk values for the lattice constant (2.44 Å) and K_F (1.2×10^8 cm^{-1}), we can calculate Ω (14.6 $Å^3$), c (2.44×10^{-2}), and $N(E_F) = 9.77 \times 10^{21} \frac{states}{eV \cdot cm^3}$. Plugging these numbers into Eq. 6.2 yields

$$b_{so} = \hbar/3\tau_{so}\Delta_0 \sim 0.023.$$

This is roughly within a factor of three of our measured value. This simple calculation seems to yield a reasonable result for both vanadium and amorphous gallium.

Chapter 7

Summary

We have found excellent agreement between Rainer's theory, which incorporates Fermi-liquid effects into the high-field theory of superconductivity, and our tunneling data on vanadium and amorphous gallium. This demonstrates the accuracy of the theory both when the net renormalization is large and when the electron-electron interaction is strong. In amorphous gallium we observed a large Fermi-liquid renormalization of the quasiparticle density of states. The change in this density of states as a function of both temperature and magnetic field could be fitted with a single set of values for the depairing, spin-orbit scattering and Fermi-liquid renormalization. The results for five different $Al/Al_2O_3/a\text{-}Ga$ junctions were consistent and yielded a value for the Fermi-liquid parameter, G_0, of 0.81 $\pm$ 0.14. This corresponds to an decrease in the apparent Zeeman splitting near the phase boundary of 45% and graphically demonstrates the need to include

Fermi-liquid effects in explaining the behaviour of superconductors. In the course of this work we found that the normal-state density of states in the gallium was altered due to correlation effects. These effects were qualitatively those predicted by Al'tshuler and Aronov (1979), McMillan (1981), and Al'tshuler, Aronov, and Lee (1980).

We found the Fermi-liquid parameter in vanadium to be close to zero. This was determined by fitting the conductance of $Al/Al_2O_3/V$ tunnel junctions to Rainer's theory as was done for amorphous gallium. This result was corroborated by directly observing the apparent Zeeman splitting of the spin components of the quasiparticle density of states in $V/Al_2O_3/Fe$ tunnel junctions. The low value for G_0 constitutes new evidence for the importance of spin fluctuations in vanadium. Spin fluctuations are of interest because of their role in lowering the transition temperature of a number of materials.

These results demonstrate the efficacy of determining the intrinsic Fermi-liquid parameters of a material from its superconducting properties. It was also found that the magnitude of the Fermi-liquid parameter G_0 could be accurately predicted from knowledge of its constituent interactions using the simple relation

$$1 + G_0 = (1 + \lambda_{ep} + \lambda_s)(1 - \bar{I}).$$

Finally, these techniques were found to yield values for the spin-orbit scattering parameter, $b_{so}^{a-Ga} = 0.18 \pm 0.03$ and $b_{so}^{V} = 0.06 \pm 0.03$,

which are fairly close to those predicted by a simple calculation.

Appendix A

Attempt to Make $Fe/Al_2O_3/a\text{-}Ga$ Junctions

The purpose of this appendix is to describe our attempts to make amorphous gallium tunnel junctions with a ferromagnetic counterelectrode. The goal in attempting this was to do spin-polarized tunneling on the gallium as described in Section 3.1. As we have seen, this is not necessary in order to determine G_0. However, by fitting the spin-resolved density of states we could have independently checked our values for G_0 and b_{so}.

We have on several occasions successfully made $Fe/Al_2O_3/a\text{-}Ga$ tunnel junctions. The iron films were typically $150 - 450\text{Å}$. The barriers were produced by evaporating $10 - 20\text{Å}$ of Al_2O_3 from sapphire pieces in an electron gun. These junctions showed very good tunneling characteristics at zero field. However, they never showed any signs of polarization or Zeeman splitting in a field (see Figure A.1). We obtain
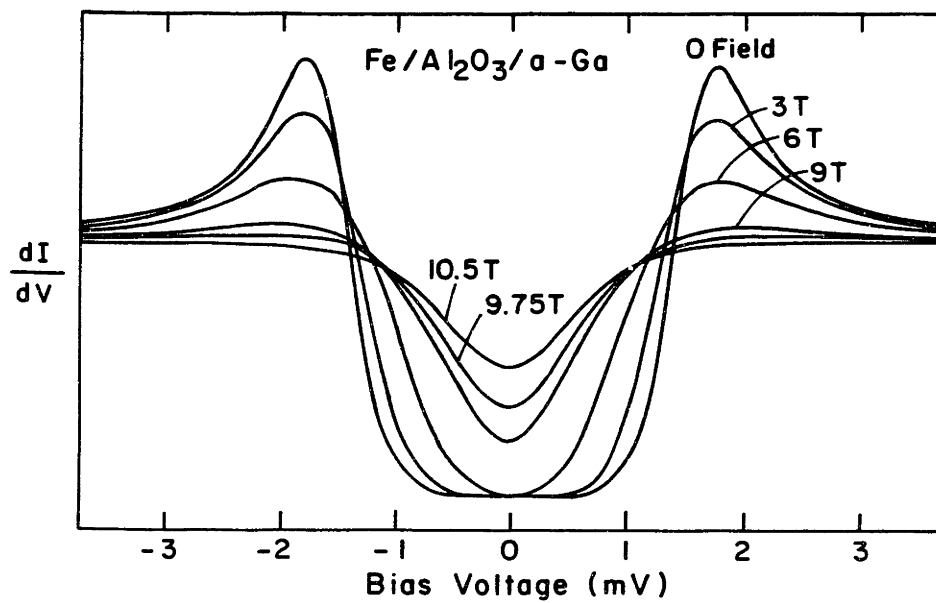
Figure A.1: Dynamic conductance for a single $Fe/Al_2O_3/a$-Ga tunnel junction at a number of fields.

the same mysterious result when using cobalt or an iron-cobalt alloy. Clearly, there are three possible sources of trouble: the ferromagnet, the barrier, and the amorphous gallium. We will now examine each of these possibilities.

We can quickly eliminate any intrinsic problems with the amorphous gallium, such as too high a spin-orbit scattering rate, in light of our success with $Al/Al_2O_3/a$-Ga junctions. It is possible to see the splitting in amorphous gallium. Also we have made these junctions with gallium films as thin as those in our successful $Al/Al_2O_3/a$-Ga junctions; orbital depairing is not the problem.

A likely source of trouble is the fact that the samples are exposed to air after the barriers are evaporated. Because the low temperature evaporator has no mask changer we must evaporate the ferromagnet and barrier in a separate system. In transporting the sample from one evaporator to the other water vapor, hydrocarbons, and other organics will adsorb on the surface of the barrier. These contaminants may be causing spin-flip or inelastic scattering during the tunneling process. The surface of the ferromagnet may even oxidize due to diffusion of contaminants through the extremely thin barrier. Some oxides of Fe are antiferromagnetic and therefore not conducive to spin-polarized tunneling. To test this we performed the following experiment. Iron electrodes with Al_2O_3 barriers were prepared in the

usual way. They were then allowed to sit in air for four hours, after which a counterelectrode of aluminum was deposited. Representative tunneling curves for one such junction which had a barrier of only $10\mathring{A}$ is shown in Figure A.2. The polarization and splitting are clearly evident. Does this indicate that the ferromagnetism is not destroyed at the surface of the iron and that spin-flipping is not a problem at the interfaces or in the barrier? It is possible that the aluminum is actually "curing" the sample by reacting with the adsorbed contaminants or by penetrating the adsorbed layer on the barrier's surface. Geiger, *et al.* (1969) have shown that inelastic electron tunneling spectroscopy (IETS) peaks such as that associated with the free OH stretching mode do not appear in junctions with aluminum electrodes on oxidized aluminum barriers. These peaks do appear, however, in junctions where elements such as gold or lead are substituted for the aluminum top electrodes. Geiger, *et al.* postulate that the aluminum diffuses through the contaminant layer upon deposition so that the tunneling bypasses the adsorbants. Sleigh, *et al.* (to be published) have correlated the presence of organic IETS peaks in oxidized aluminum barriers with various properties of the electrodes used. They find aluminum to be a 'good actor' in the sense that it minimizes inelastic scattering in the tunnel barrier. Gallium has not been studied in this manner but it seems unlikely that it will readily penetrate the
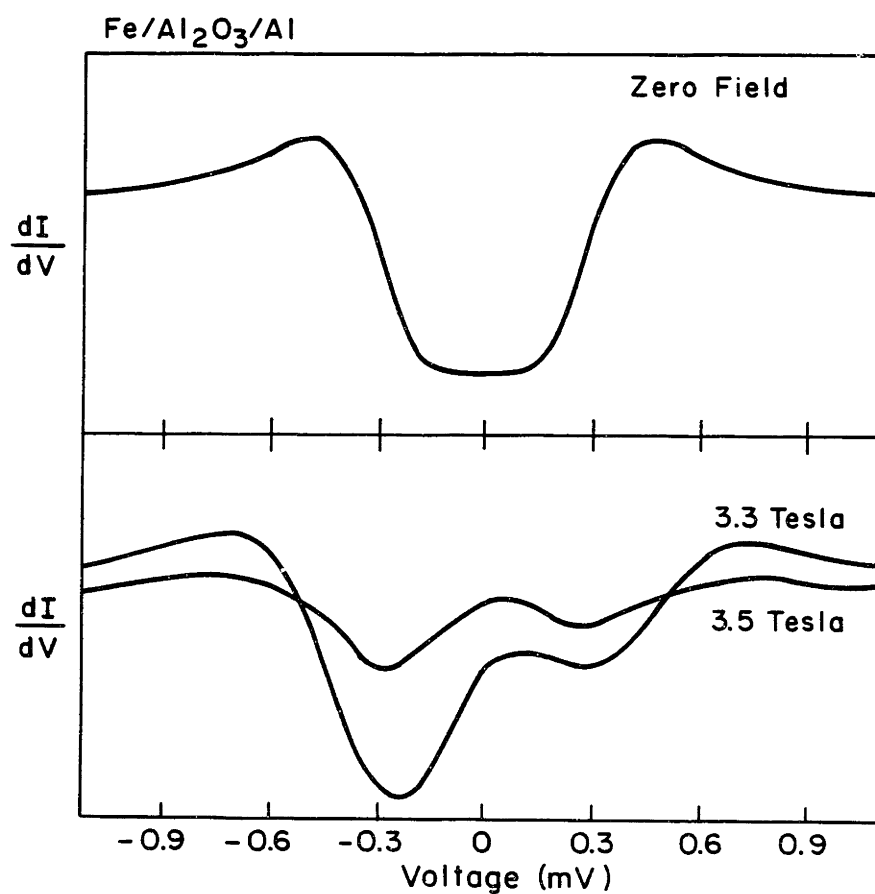
Figure A.2: (a) Zero-field curve for an $Fe/Al_2O_3/Al$ tunnel junction which was exposed to air for four hours prior to depositing the final aluminum layer. (b) Conductance curves for the same junction in a field. The asymmetry due to the polarization of the iron is clearly apparent.

adsorbed layer when deposited at less than 2.3 K.

The electrochemical potential of aluminum is larger than that of both iron and cobalt (see Table A), so it may be able to pull oxygen away from them in regions where the junction is almost shorted.

Element	Electrochemical Potential (volts)
Fe	−0.44
Co	−0.28
Al	−1.6
Mg	−2.4
Ga	−0.56

This could have the added benefit of adding some Al_2O_3 to the barrier. Gallium, on the other hand is not as fond of oxygen and water. Furthermore, the gallium samples are not warmed to room temperature after depositing the gallium. The aluminum sample may have reacted with the contaminants when it was warmed to room temperature after deposition of the aluminum. As a further test we made $Fe/Pd(15\text{Å})/Al_2O_3/a\text{-}Ga$ junctions. Moodera (1987) has observed 23% polarization in $Fe/Pd(15\text{Å})/Al_2O_3/Al$ junctions. It was hoped that the palladium would protect the iron surface during exposure to air. Again no polarization or splitting were observed. Our tentative conclusion is that there is nothing wrong with the ferromagnetism at the surface of the ferromagnetic electrode.

This leaves the barrier as the most likely source of trouble. Again, there could be something adsorbing onto the barrier during its expo-

sure to air. Alternatively, something may be cryocondensing onto the sample while it is cooled to low temperature. Note that the gallium samples were cooled to ~ 0.8K before the gallium was deposited. The *Fe/Al$_2$O$_3$/Al* samples which were exposed to air were only cooled to ~ 80K before the aluminum was deposited. Thus, the gallium samples may have had gasses such as oxygen and hydrogen condensed on them which were not present in the *Fe/Al$_2$O$_3$/Al* samples. Some phases of solid oxygen have a very large susceptibilty (The γ phase has a susceptibility of 10^{-2} in cgs units). Atomic hydrogen could also be detrimental. To minimize these contaminants the ionization gauge and residual gas analyzer were usually left turned off. Hot filaments tend to disassociate the residual gases, such as water vapor, in a vacuum chamber. The sample was kept warmer than the surrounding radiation shields until just before the evaporation. Most of the residual gases should have been prevented from reaching the sample. The residual gas analyzer indicated that the partial pressures of hydrogen and oxygen were less than 10^{-11} torr when the system was cooled. At the sample, the pressure should have been even lower. On several occasions we tried heating the junction just prior to the gallium evaporation by passing a current through the aluminum strip. It was hoped that this would drive off the condensates. It is difficult to know exactly how warm the junction got. By calibrating the resistance of

the aluminum as a function of temperature during the cooldown, and then watching its resistance as we did the heating, we estimate that in some instances the junction was heated to about room temperature. After turning off the current, it cooled back down within 20 seconds. The evaporation was then immediately begun. This procedure did not improve the results. However, Bowser and Weinberg (1976,1977) have shown that a temperature of 150 °C is necessary to dehydroxylate oxidized aluminum barriers. We also tried evaporating a thin layer (1–5Å) of Mg just prior to heating. It was hoped that the magnesium would react with the condensates and "neutralize" them. This also did not help.

This brings us to the possibilty that the contamination occurs during the actual evaporation. A large volume of gas is evolved when the source is first heated. Unfortunately, as was mentioned in Section 3.4, we cannot outgas the source prior to the evaporation. The "dirt" which is deposited on the sample during the initial stages of the evaporation seems necessary for growing thin, electrically continuous gallium films. Without thin films the orbital depairing is too large to perform the experiment. We tried both glass and sapphire substrates. We also tried depositing a thin layer (1–2Å) of Pt to cut down the surface mobility of the gallium atoms. Nothing seemed to work as well as the "dirt" in producing thin films.

Our conclusion is that the most likely source of trouble is the presence of contamination in the barrier. This contamination could be due to outgassing of the source during evaporation. It could also consist of gasses which are adsorbed during the exposure to air or are cryocondensed during cooling and are hard to drive off. The contamination may be causing spin-flip and/or inelastic scattering in the tunneling process. The presence of spin-flipping could explain the lack of polarization. However, it seems some amount of inelastic scattering is necessary because spin-flip alone could not explain the lack of observed splitting[1]. On the other hand, although the tunneling curves are somewhat depaired (rounded; see, for example Figure A.1), their features look well enough resolved to observe the splitting. This is reminiscent of the behaviour of amorphous silicon (Meservey, Tedrow, and Brooks, 1982), and amorphous germanium (Gibson and Meservey, 1985) tunnel barriers.

The source of all this trouble is the fact that the gallium must be kept cold. Several attempts were made to circumvent this problem. Chief among these was an attempt to stabilize a high temperature phase of gallium at room temperature. It was found that gallium evaporated on amorphous SiN with a protective Al_2O_3 overlayer had

---

[1]Note that contamination of the barrier during evaporation can explain the lack of polarization but not the lack of splitting. This is because splitting is easily observed in the $Al/Al_2O_3/a$-Ga junctions, which are exposed to the same contamination.

a T_c of about 6.7 K even after thermal cycling. Unfortunately, we could not make good quality thin films in this way. Moodera (1987b) has also found that a stable phase of gallium with a T_c of $\simeq$ 6.5 K can be grown on nickel. We were unable to make good junctions on such films. It is uncertain whether these phases would have as interestingly large an electron-phonon coupling constant as the amorphous phase.

Appendix B

Correlation Effects

B.1 Correlation Effects in the Normal State

In disordered materials the motion of electrons is diffusive, screening is reduced, and the Coulomb interaction is enhanced. There are two channels for this interaction: the diffusive channel, where electrons with similar energy and a small combined momentum interact, and the Cooper channel, where the interaction is between an electron and a hole of similar energy and small combined momentum. It has been shown by Al'tshuler and Aronov (1979) and McMillan (1981) that in three dimensions this leads to a cusp in the normal state density of states,

$$N(E) = N(0) \left(1 + \left(\frac{E}{\Delta} \right)^{1/2} \right) \tag{B.1}$$

where E is the energy measured from the Fermi level and Δ is the correlation gap. In two dimensions the singularity becomes logarithmic in the energy (Al'tshuler, Aronov, and Lee 1980). The crossover

137

from two to three dimensional behavior should occur at a length scale
given by (Imry and Ovadyahu (1982), Lutskii, *et al.* (1985)).

$$L_V = (\hbar D/eV)^{1/2} \tag{B.2}$$

In order to observe two dimensional behaviour the film must also be
thinner than a temperature length scale given by,

$$L_T = (\hbar D/kT)^{1/2} \tag{B.3}$$

Here D is the usual diffusion constant. In Figure B.1 we have plot-
ted the higher temperature conductance curve shown in Figure 4.7
vs. $V^{1/2}$. It suggests that the normal state density of states in the
gallium is of the form of Eq. B.1. Note that this implies that the gal-
lium behaves three dimensionally, at this temperature, down to low
energy. The deviation from linearity at the low voltage end of this
plot is expected because of temperature smearing and also because the
junction may have been somewhat overmodulated when taking this
data. Most of the junctions showed this $E^{1/2}$ dependence at energies
above the gap. Over most of the range of temperatures and fields used
in this experiment it is difficult to observe the normal state density
of states at low energy because of the superconducting energy gap.
Figure B.2 shows the dynamic conductance as a function of field at
$T = 0.9$ K. Here the field is oriented perpendicular to the sample.
This junction had the thinnest gallium film $(\simeq 20\text{Å})$ obtained in any
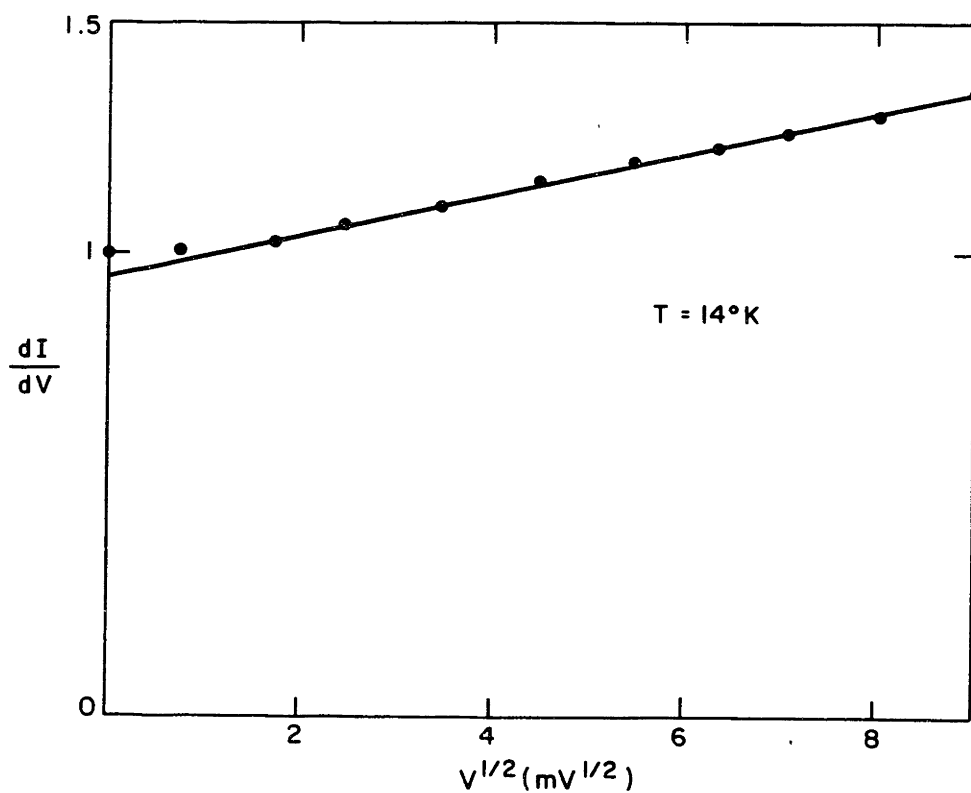
Figure B.1: Dynamic conductance of junction with gallium normal. Shows $V^{1/2}$ dependence as in Eq.B.1.
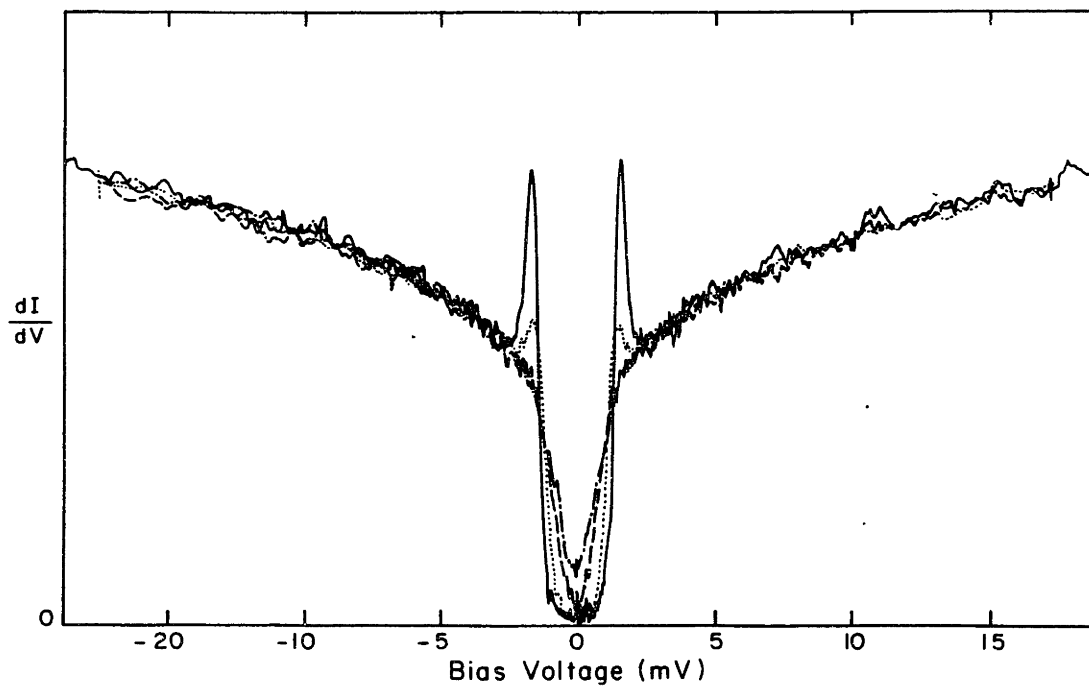
Figure B.2: Dynamic conductance at low temperature and a number of fields for a thin ($\simeq 20\text{Å}$) film oriented perpendicular to the field.

sample. It also had the highest resistivity ($\sim 800\mu\Omega \cdot cm$) and the largest background curvature. In Figure B.3 the 10.91 tesla curve is plotted versus $\ln V$. At this field the superconductor is almost completely depaired so that the remaining structure is due principally to the correlation effects. The energy dependence of the quasiparticle density of states appears to be two dimensional at this temperature. If we naively calculate the diffusion constant from the resistivity using the Drude model and bulk values for n, v_F, and m we get $D \sim 0.4\frac{cm^2}{sec}$. Interestingly, if we determine D from the perpendicular critical field using the weak-coupling theory we get $0.3 - 0.4\frac{cm^2}{sec}$. Finally, from the tunneling data we have

$$c_F = \frac{De^2 d^2 \Delta_0}{\mu_B^2 \hbar c^2} \sim 0.2 - 0.3$$

This yields $D \sim 0.2 - 0.3$. Thus, at the temperature used in Figures B.2 and B.3 (0.9 K), the temperature length scale , L_T, should be an order of magnitude larger than the thickness. Similarly, the energy length scale is approximately

$$L_V = \frac{50}{V^{1/2}} \; (\mathring{A}) \tag{B.4}$$

where V is measured in mV and we have used $D = 0.4$. This indicates that it is reasonable to see a $\ln V$ dependence for this junction over the entire range of voltage measured. A crossover from two to three dimensional behaviour has been observed previously in granular aluminum, indium oxide, and bismuth by Gershenzon *et al.* (1986), Imry
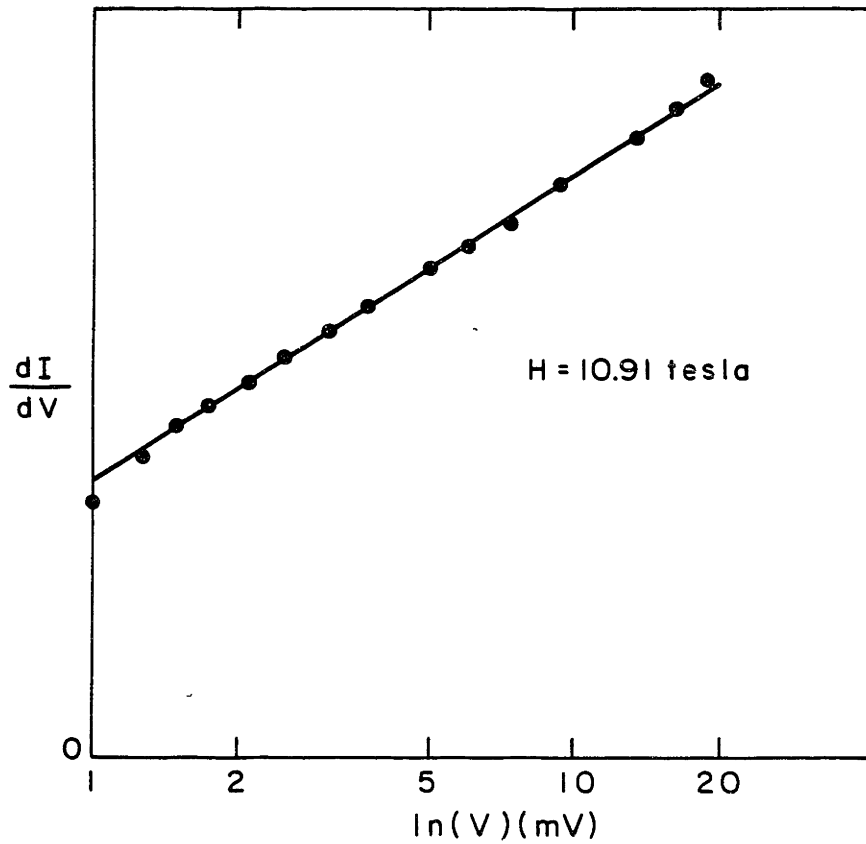
Figure B.3: Dynamic conductance of junction in Figure B.2 at 10.91 tesla vs. $\ln V$.

and Ovadyahu (1982), and Lutskii *et al.* (1985), respectively. The fact that we see a $V^{1/2}$ dependence above the gap in most of our junctions may be because they had a lower resistivity and were thicker than the film of Figures B.2 and B.3. They may have switched over to a *lnV* dependence at an energy below the superconducting gap. There may also be a difference between the two cases because the films used in the Fermi liquid study were oriented parallel to the field. The curve shown in Figure B.1 was taken at a higher temperature where L_T is on the order of the thickness. In any event, it seems likely that correlation effects are the source of the background curvature observed in these experiments.

The same background was divided out of all the curves for a given junction as described in Chapter 4. In most cases the zero field background was used and was extrapolated to low voltage using a $V^{1/2}$ dependence. This should work because of the observed independence of the effect on field. The interaction in the Cooper channel for a $3D$ film should be suppressed at a field given by

$$H_C = \pi c k T / e D \qquad (B.5)$$

This is about 2 tesla at 0.9 K for the junctions used in this study. The lack of change from 0 to 20 tesla indicates that the diffusion channel is dominant. The effect of the magnetic field on this channel is determined by spin effects. Al'tshuler and Aronov (1983) and Millis

and Lee (1984) have shown that if the total spin relaxation time, $\hbar/\tau_s \ll g\mu_B H$, then the contribution from the interaction between electrons with a total spin $j = 1$ is split into two spin subbands which are shifted in energy by $\pm g\mu_B H$. This splitting would be difficult to observe in our data because of the superconductivity and may not be present due to spin scattering.

In regard to the present study dividing the same background out of all the curves for a given junction is a simple, reasonable method for bringing the theory into closer agreement with the data. For the junctions used in this study the correlation effects changed the conductance only by $10 - 20\%$ over the voltage range examined and the fitted value for G_0 was insensitive to their removal.

B.2 Correlation Effects in the Superconducting State

In addition to changing the normal state density of states near the Fermi level, correlation can also affect the superconducting excitation spectrum. In this section we will discuss the possibility that the latter effect is in part responsible for the need to include a field-independent pairbreaking term when fitting our data. Other possible sources for this term, such as overmodulation, were discussed in Section 4.2. Alexander (1986) also found it necessary to incorporate such

a term when fitting her data on thin films of aluminum deposited at liquid nitrogen temperature. Similarly, Dynes, *et al.* (1984), proposed a simple, one parameter pairbreaking correction to the density of states of their granular aluminum samples. They added an imaginary lifetime broadening term, $i\Gamma$, to the quasiparticle energy in the BCS density of states

$$N_s(E, \Gamma) = Re\left(\frac{E - i\Gamma}{[(E - i\Gamma)^2 - \Delta^2]^{1/2}}\right). \qquad (B.6)$$

They attributed this lifetime broadening to inelastic electron-electron scattering and found that the lifetime, $\hbar/\Gamma$, correlated well with resistivity. The same correction to the density of states was earlier proposed by Dynes, *et al.* (1978), to account for lifetime broadening in PbBi. In this case the broadening is due to enhanced quasiparticle recombination in the presence of strong coupling. This phonon-induced broadening increases with temperature as more quasiparticles become available for recombination. Note that amorphous gallium is as strongly coupled as PbBi. Lifetime broadening due to disorder and strong-coupling enhanced recombination may be important in our samples. These may also explain the increasing discrepancy in the conductance near zero-bias with increasing field. The number of particles available for recombination and inelastic scattering will increase as the phase boundary is approached.

A simple way to see how lifetime broadening mimics pairbreaking

is to look at the small gap (large depairing) limit.

$$N_s(E) \xrightarrow{\ \Delta \ll E\ } 1 + \frac{\Delta^2}{2} \frac{E^2 - \Gamma^2}{E^2 + \Gamma^2} \qquad (B.7)$$

$$N_s(E) \xrightarrow{\ \Delta \ll \alpha\ } 1 + \frac{\Delta^2}{2} \frac{E^2 - \alpha^2}{E^2 + \alpha^2} \qquad (B.8)$$

The first equation is derived from Eq. B.6. The second relation is derived by Tinkham (1975). α is the pairbreaking energy, or the energy difference between time reversed states. We see that in this limit $\alpha \sim \Gamma$. Note that we determine P_0 by fitting the tunneling conductance near the gap edge where these relations are approximately correct and the effects of lifetime broadening are qualitatively like those of pairbreaking. At lower bias voltage pairbreaking and lifetime broadening have qualitatively different effects (Dynes, *et al.* (1978); Dynes, *et al.* (1984)).

Recently, Browne, *et al.* (1987), have explicitly calculated the effects of disorder-enhanced Coulomb interactions on the superconducting density of states by using the Eliashberg approach. They find that it leads to gaplessness qualitatively like that of the simple pairbreaking model. For the same scattering lifetime their numerical calculation shows somewhat more apparent "pairbreaking" than Eq. B.6.

It seems likely that diffusion-enhanced Coulomb interactions play a role in the need for a field-independent pairbreaker in fitting our data. This is especially likely in view of the fact that we observe

correlation effects in the normal state density of states of our gallium films. Lifetime broadening due to quasi-particle recombination may become more significant with increasing field (or temperature) and help to explain the discrepancy between theory and experiment at low voltage and high field.

Appendix C

Publications

Abstract Submitted
for the General Meeting
26-30 March 1984

Amorphous Ge Tunnel Barriers.[*]   G.A. GIBSON and
R. MESERVEY, Francis Bitter National Magnet Laboratory
M.I.T.--We have studied the properties of amorphous Ge
(a-Ge) tunnel barriers deposited on substrates cooled
to liquid nitrogen temperature. Measurements of the
tunnel current and tunnel conductance were made as a
function of voltage, temperature, Ge thickness and mag-
netic field. Barrier heights and thicknesses are esti-
mated by applying the W.K.B. approximation to a trape-
zoidal barrier. The thickness is compared to that
obtained from quartz oscillator mass measurements and
capacitance measurements. The current and conductance
of superconductor-superconductor tunnel junctions were
measured. Results will be compared to similar results
obtained with a-Si barriers.

Prefer Standard Session

Gary Gibson
MIT National Magnet Lab
170 Albany Street
NW14-3211
Cambridge, MA   02139

Critical Field and Tunneling Measurements of Thin
Vanadium Films,* G.A. GIBSON, R. MESERVEY, and P.M. TEDROW,
Francis Bitter National Magnet Laboratory,+ MIT.--We
have measured $H_{c\parallel}(T)$, $H_{c\perp}(T)$ and T_c for vanadium films
ranging from 200 nm to less than 7 nm whose surfaces were
protected by an ultra-thin Al film. Tunneling measure-
ments as a function of temperature and magnetic field
were made on low leakage junctions fabricated with Al_2O_3
barriers. By fitting the tunneling conductance and criti-
cal field measurements to theory,[1-4] values for the spin-
orbit scattering and orbital depairing parameters, and
Fermi liquid renormalization effects can be obtained.
The influence of the proximity effect and fluctuations on
these results will be discussed.
*Supported by the AFOSR contract No. F49620-82-K-0028.
+Supported by the NSF.

1. K. Maki, Phys. Rev. 143, 362 (1966).
2. N.R. Werthamer, E. Helfand, and P.C. Hohenberg, Phys.
   Rev. 147, 295 (1966).
3. P. Fulde, Adv. Phys. 22, 667 (1973).
4. P.M. Tedrow, J.T. Kucera, D. Rainer, and T.P. Orlando,
   Phys. Rev. Lett. 52, 1637 (1984).

Prefer Standard Session

Gary A. Gibson

MIT
NW14-2524
Cambridge, MA 02139
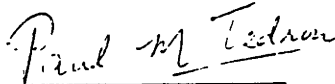
Magnetic Field Studies of Superconducting NbN
and VN Thin Films,* J.S. MOODERA, P.M. TEDROW, G.A.
GIBSON, J.E. TKACZYK, and R. MESERVEY, Francis Bitter
National Magnet Laboratory,** MIT.--We have measured
the parallel and perpendicular critical magnetic
fields of thin superconducting films of NbN and VN.
The films were made either by reactive sputtering or
by heating evaporated pure metal films in a nitrogen
atmosphere. Films of thickness from 10 nm to 500 nm
were studied. Thick sputtered films had $H_{c2\perp} > H_{c2//}$,
a characteristic attributed to columnar grains. For
the evaporated films heated in nitrogen $H_{c2//} > H_{c2\perp}$ im-
plying the absence of columnar structure. On the other
hand thinner films ($< \sim 50$ nm) showed $H_{c2//} > H_{c2\perp}$ irres-
pective of the method of film formation. The critical
field data have been fitted to the theory.
*Supported by AFOSR contract F49620-82-K-0028.
**Supported by the National Science Foundation.

Prefered Standard Session

Paul M. Tedrow
MIT
NW14-3107
Cambridge, MA 02139

Sorting Category

22b

Spin-Orbit and Fermi Liquid Effects in Super-
conducting Vanadium Films.* G.A. GIBSON and R. MESERVEY,
Francis Bitter National Magnet Laboratory,+ MIT.---We
have made spin-polarized tunneling and critical field
measurements on V films approximately 300 Å thick.
Tunneling conductance of $V/Al_2O_3/Fe$ junctions was mea-
sured at 0.5 K and a number of magnetic fields approach-
ing the second order phase transition at $H_{c2\parallel}$. The
conductances of the two spin densities of states were
resolved and used to obtain the Zeeman splitting energy
δ. Preliminary results show a definite decrease of δ
from $2\mu_B H$ near $H_{c2\parallel}$ which implies a Fermi liquid renor-
malization parameter of about 20% and is consistent with
critical field measurements. This is similar to the
renormalization seen by Tedrow et al.[1] in Al. We have
measured the critical field of the V films with and
without a Pt overlayer. Little change in the spin-orbit
parameter was observed because of the Pt overlayer.

G.A. Gibson

NW14-2524
MIT
Cambridge, MA 02139

Prefer Standard Session

Sorting Catagory

22a

_____

Study of Superconducting Layered and Coevaporated
(V/Mo)N Films.* G.A.Gibson, J.S.Moodera, P.M.Tedrow and
R.Meservey, MIT Francis Bitter National Magnet Laboratory[+].
Layered films of V/Mo with layer thicknesses from 10 to
400Å were made by e-beam evaporation and subsequently
nitrided at ≈700 C. The parallel and perpendicular criti-
cal fields were measured as a function of temperature and
compared with the theory of Takahashi and Tachiki.[1]
Coevaporated V(Mo)N films with various Mo concentrations
were also made. Their critical fields and spin-orbit
scattering rates were compared with the layered (V/Mo)N
films. The effect of Mo concentration on the T_c of V(Mo)N
was also studied. In no case was a T_c greater than that
of pure VN obtained. This is of interest because of the
close lattice match of VN with the postulated high T_c
phase of MoN.

1. S.Takahashi and M.Tachiki, Phys.Rev.B33,4620(1986);
    ibid 34,3162(1986).

Prefer Standard Session

G. A. Gibson

MIT, NW14-2524
Cambridge,Ma.02139

Upper Critical Field Anisotropy in $YBa_2Cu_3O_7$
Single Crystals,* J.S. MOODERA, R. MESERVEY, J.E.
TKACZYK, G.A. GIBSON, C.Y. HAO, and P.M. TEDROW, Francis
Bitter National Magnet Laboratory, MIT -- Upper critical
fields, H_{c2}, of $YBa_2Cu_3O_7$ single crystals have been
measured with applied fields parallel to the a-b plane
$\left(H_{c2\parallel}\right)$ and perpendicular to the a-b plane $\left(H_{c2\perp}\right)$. The
slope $-dH_{c2}/dT$, obtained from the measurements of H_{c2} as
a function of temperature up to a field of 19 tesla, is
about a factor of four greater when the applied field is
along the a-b plane than when it is perpendicular to the
plane. The estimated coherence lengths, ξ_0, from these
measurements are 23 A and 6.3 A in the plane and perpen-
dicular to the plane, respectively.

Paul M. Tedrow

MIT Francis Bitter National
  Magnet Laboratory
170 Albany Street, NW14-3107
Cambridge, MA 02139

Prefer Standard Session

Fermi-Liquid Renormalization of the Zeeman Splitting of the Superconducting Density of States in Amorphous Gallium Films.*

G.A. GIBSON, R. MESERVEY and P.M. TEDROW, NML,† M.I.T.

-- Cryogenically condensed gallium has a very large electron-phonon coupling constant (λ_{ep} ~2) which should make the many-body interactions between quasi-particles strong and easily observable. We have condensed Ga on substrates held at ~1.8 K in an evaporator capable of being operated within a 2" bore Bitter magnet and obtained the high T_c, amorphous phase. This material was deposited onto oxidized Aℓ electrodes and high-quality Aℓ/Aℓ$_2$O$_3$/a-Ga tunnel junctions were produced. The conductance vs. bias voltage for these junctions has been measured as a function of H and T. A significant decrease in the Zeeman splitting from $2\mu_B H$ was observed. The conductance curves can be fitted quite well by a single set of parameters to the theory of high-field superconductivity as extended by Rainer to include the Fermi-liquid renormalization. These parameters are consistent with critical field data taken on the same films. However, the value obtained for the Fermi-liquid parameter, G_0, (~0.8) is less than one would naively expect for such strong electron-phonon coupling.

G.A. Gibson

MIT Francis Bitter National
    Magnet Laboratory
170 Albany Street, NW14-2524
Cambridge, MA 02139

Prefer Standard Session

Electron-Spin Polarization in Tunnel Junctions
with Ferromagnetic EuS Barriers

J.S. Moodera, X. Hao, G.A. Gibson, and R. Meservey

Francis Bitter National Magnet Laboratory
Massachusetts Institute of Technology
Cambridge, MA 02139

The discovery of Zeeman splitting of the quasiparticle density of states of superconducting Aℓ [1] immediately led to the ability to determine the electron spin polarization P of tunnel current. Using this technique the value of P for electrons tunneling in Aℓ/Aℓ$_2$O$_3$/FM, where FM = Ni, Co, Fe, and 3d alloys, was extensively studied [2,3]. The spin polarization has been attributed to the difference in the spin densities of states of the itinerant electrons in the ferromagnet at the Fermi energy [4]. In contrast, the present experiments show polarization of the tunneling currents from nonferromagnetic electrodes which may be explained by the different barrier heights for the two spin directions of the ferromagnetic insulator (EuS) in the MIM structure. This effect is known as the spin-filter effect. Internal field emission study on junctions having EuS and EuSe as barriers by Esaki et al. [5], Schottky barrier tunnel junction studies between In and doped EuS by Thompson et al. [6], electron field emission from W through EuS layer by Müller et al. [7] and Kisker et al. [8] are closely related to the present observation.

In the present study, tunnel junctions of Aℓ/EuS/Aℓ, Fe/EuS/Aℓ and Au/EuS/Aℓ were prepared by vacuum deposition on glass substrates. Tunneling conductance was measured as a function of temperature and at 0.4 K as a function of magnetic field (H) applied parallel to the film surface. In field H the junction conductance peaks are each Zeeman split in energy and show asymmetry due to spin polarization. In a conventional tunnel junction such as Aℓ/Aℓ$_2$O$_3$/Ag where the barrier is nonmagnetic, the Zeeman splitting is equal to $2 \mu_B H_a$, where μ_B is the Bohr magneton. However, in the present junctions we observed much greater splitting than those corresponding to the applied field. This is similar to the enhanced Zeeman splitting found by Tedrow et al. [9] when Aℓ films were in contact with various rare-earth oxides. Thus the internal field B experienced by Aℓ in contact with EuS is much higher than H, as implied by the Zeeman splitting. For H = 0.35 tesla, B turns out to be 3.9 tesla and when H was reduced to zero, Zeeman splitting persisted corresponding to a value of 1.5 tesla for B. In fact, in several cases, Zeeman splitting and polarization were observed even <u>before</u> any external field was applied (other than the ambient field of about 1 gauss). This effect had never been observed previously with spin-polarized tunneling studies.

The asymmetry in the Zeeman-split conductance curves implies electron-spin polarization of the tunneling current. From the asymmetry, the value of electron-spin polarization P was calculated using the complete theory including spin-orbit scattering. For Fe/EuS/Aℓ junctions P ≈ 65%, for Aℓ/EuS/Aℓ junctions P ≈ 18%, and for Au/EuS/Aℓ junctions P ≈ 80%. In the case of the Fe counterelectrode, it is unclear to what extent Fe

contributes to P since for an $A\ell/A\ell_2O_3/Fe$ junction $P \approx 44\%$. In $A\ell/A\ell_2O_3/A\ell$ and $A\ell/A\ell_2O_3/Au$, $P = 0$ since all elements are nonmagnetic. Below the Curie temperature $T_c = 16.7$ K of EuS, its conduction band is exchange split and the tunnel barrier is different for the two spin directions giving rise to the observed polarization. For the Au junctions, with the estimated barrier height and known exchange splitting, the calculated tunnel current using Simmon's theory [10] for the two spin directions yields a value of P in reasonable agreement with the measured value.

References

[1] R. Meservey, P.M. Tedrow, and P. Fulde, Phys. Rev. Lett. 25, 1270 (1970).

[2] P.M. Tedrow and R. Meservey, Phys. Rev. Lett. 26, 192 (1971).

[3] R. Meservey, D. Paraskevopoulos, and P.M. Tedrow, Phys. Rev. Lett. 37, 858 (1976); Phys. Rev. B16, 4907 (1977).

[4] M.B. Stearns, J. Magn. Magn. Mat. 8, 167 (1977).

[5] L. Esaki, P.J. Stiles, and S. von Molnar, Phys. Rev. Lett. 19, 852 (1967).

[6] W.A. Thompson, F. Holtzberg, T.R. McGuire, and G. Petrich, AIP Conf. Proc. No. 5, 827 (1971).

[7] N. Müller, W. Eckstein, W. Heiland, and W. Zinn, Phys. Rev. Lett. 29, 1651 (1972).

[8] E. Kisker, G. Baum, A.H. Mahan, W. Raith, and B. Reihl, Phys. Rev. B18, 2256 (1978).

[9] P.M. Tedrow, J.E. Tkaczyk, and A. Kumar, Phys. Rev. Lett. 56, 1746 (1986).

[10] J.G. Simmons, J. Appl. Phys. 35, 2472 (1964).

Properties of amorphous germanium tunnel barriers

G. A. Gibson[a] and R. Meservey

Francis Bitter National Magnet Laboratory, Massachusetts Institute of Technology, Cambridge, Massachusetts 02139

The properties of tunnel barriers made with amorphous Ge (a-Ge) deposited at approximately 80 K were studied in Al/a-Ge/Al tunnel junctions and also in junctions where one electrode was Ni or Fe. The conduction process was shown to be tunneling for barriers less than about 100 A at liquid He temperature and consistent with Mott variable-range hopping for higher temperatures and thicknesses. Measurements were made of current density J and dynamic conductance dJ/dV as a function of voltage V, thickness s, and temperature T. The measurements were compared with available theoretical expressions for rectangular tunnel barriers based on the WKB approximation. The applicability of these expressions for barrier heights less than 100 meV was examined and a modified equation for $J(V)$ was derived which eliminated assumptions which are inaccurate for such low barriers. The measurements were also compared to this modified equation and to numerical solutions. Values for the effective tunnel barrier height ranging from 20 to 80 meV were obtained. Theoretical expressions for $J(V)$ could be fitted to the measurements fairly well, but not perfectly; for $J(T)$ the fit was poor. Values of s obtained using the modified expression for $J(V)$ tended to be 10%-20% less than those measured by a quartz-crystal thickness gauge using the bulk crystal density. The conductance peaks corresponding to the peaks in the superconducting density of states were considerably broadened over Al/Al$_2$O$_3$/Al junctions either because of depairing of the Al films in contact with a-Ge or from an inelastic process in the barrier. No spin polarization of the tunnel currents was observed when one of the electrodes was Ni or Fe. Some measurements were made of a-Ge barriers treated with glow discharges in N$_2$, O$_2$, and H$_2$. The properties of a-Ge were very similar to those previously found for a-Si. Evidently the basic conduction process in these junctions is tunneling, but the simple tunneling model cannot entirely explain the results. Various proposals to account for these divergences from the simple tunneling model are discussed.

I. INTRODUCTION

A study of the properties of amorphous Si (a-Si) when used as a tunnel barrier in metal/semiconductor/metal tunnel junctions was published recently.[1] The present research is a similar study of the properties of amorphous Ge (a-Ge). This work was undertaken to provide more information on the systematics of the conduction process in such amorphous semiconducting tunnel barriers. It was also hoped that a-Ge might have a lower effective barrier than a-Si and allow thicker and therefore more reproducible artificial tunnel barriers to be made. Much of the previous work on artificial barriers was cited in Ref. 1 and in a more recent publication describing artificial Al$_2$O$_3$ barriers.[2] Barriers using a-Ge have been tried previously by a number of workers, but with somewhat limited success.[3-6] These barriers, which were deposited near room temperature, were typically hundreds of angstroms thick and needed a native oxide on the counterelectrode to suppress leakage currents. In related work, Seto and Van Duzer[7] obtained good Josephson properties with amorphous Te using Pb electrodes; however, these junctions relied on PbO to reduce leakage currents. Smith and co-workers[8] have made Nb/a-Si/Nb junctions of high quality by magnetron sputtering. Kroger *et al.*[9] have reported excellent Josephson junctions made by chemical vapor deposition of polycrystalline Ge barriers.

In the present research we have measured the properties of a-Ge barriers deposited on liquid nitrogen cooled substrates. These barriers are much thinner and more uniform than barriers deposited at room temperature and do not rely on forming a native oxide on one electrode. We compare the tunneling properties of cryogenically deposited a-Ge with those obtained previously with a-Si. We have also more closely examined the applicability of various approximate theoretical expressions used to analyze tunneling results, compared them to each other, to numerical solutions of the WKB approximation, and to the experimental data.

II. THEORY

Tunneling conductance measurements have traditionally been compared with theoretical results based on the WKB approximation applied to a rectangular or trapezoidal barrier. The use of this approximation is warranted because the image force and the diffuseness of the interface between the metal and the barrier material smooths the discontinuities in the effective potential.[10] We will use this approach and compare our data with approximate analytic solutions and numerical calculations both based on the WKB approximation. The adequacy of this simple tunneling model will be considered in the discussion but it appears to be the best theoretical framework presently available with which to compare the data.

[a] Also Physics Department, Massachusetts Institute of Technology, Cambridge, MA.

159

A. Calculated tunnel current

Metal/insulator/metal junctions and metal/semiconductor/metal junctions at low temperature are often compared with an expression for the current density J as a function of applied voltage V which was derived by Simmons[11] using the WKB approximation in the zero temperature limit. For a general barrier shape this expression for J is given by

$$J = J_0\{\phi \exp(-A\phi^{1/2}) - (\phi + eV)$$
$$\times \exp[-A(\phi + eV)^{1/2}]\}, \qquad (1)$$

where

$$\phi = \left(\frac{1}{\Delta s}\right)\int_{s_1}^{s_2} \phi(x)dx$$

is the mean barrier height above the Fermi energy of the negatively biased electrode and

$$J_0 = (e/2\pi h)(\beta\Delta s)^{-2},$$

$$A = (4\pi\beta\Delta s/h)(2m)^{1/2},$$

$$\beta \approx 1 - \frac{1}{8\phi^2\Delta s}\int_{s_1}^{s_2} [\phi(x) - \phi]^2 dx.$$

It is unclear what dispersion relation is appropriate for the mobility gap of amorphous Ge. In giving numerical values we shall assume that m is the free electron mass. In some equations where m appears only in the forms $m\phi_0$ or ϕ_0/m, ϕ_0 can be considered as an effective barrier height. The question of effective mass will be taken up in the discussion and in the Appendix, where we list the relevant equations with the effective mass written explicitly. β is a factor introduced to approximate a barrier of general shape with a rectangular barrier so that the integral arising in the tunneling probability can be evaluated analytically. For rectangular barriers of height ϕ_0, Simmons uses the approximate value $\beta = 1$ for $eV < \phi_0$ and the exact result $\beta = 23/24$ for $eV > \phi_0$. $\Delta s = s_2 - s_1$, where s_1 and s_2 are the classical turning points for the motion of an electron at the Fermi energy of the negatively biased electrode.

For a trapezoidal barrier (see Fig. 1) when $eV < \phi_2$ and $\phi = (\phi_1 + \phi_2 - eV)/2$, Eq. (1) can be written in the form

$$J = J_0\left\{\left(\phi_0 - \frac{eV}{2}\right)\exp\left[-A\left(\phi_0 - \frac{eV}{2}\right)^{1/2}\right]\right.$$
$$\left. - \left(\phi_0 + \frac{eV}{2}\right)\exp\left[-A\left(\phi_0 + \frac{eV}{2}\right)^{1/2}\right]\right\}, \qquad (1a)$$

where $\phi_0 = (\phi_1 + \phi_2)/2$ is the average barrier height for $V = 0$, $\Delta s = s$, and $\beta = 1$. Simmons[12] derived from Eq. (1a) an approximate expression for J,

$$J = \alpha(V + \gamma V^3), \qquad (2)$$

where

$$\alpha = [(2m\phi_0)^{1/2}e^2/sh^2]\exp(-D\phi_0^{1/2}),$$

$$\gamma = [(De)^2/96\phi_0] - (De^2/32\phi_0^{3/2}),$$

$$D = (4\pi s/h)(2m)^{1/2}.$$
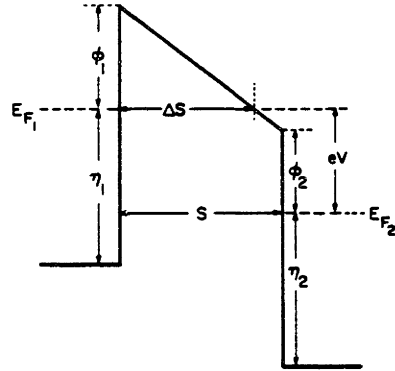
FIG. 1. Trapezoidal barrier for an insulating film between two metal electrodes.

Assuming the free electron mass for m, numerical values of α and γ are given by

$$\alpha = \frac{3.16 \times 10^{10}\phi_0^{1/2}}{s}\exp(-1.025s\phi_0^{1/2}), \qquad (3a)$$

$$\gamma = \frac{0.0109}{\phi_0}s^2 - \frac{0.032}{\phi_0^{3/2}}s, \qquad (3b)$$

where ϕ_0 is measured in electron volts, s is measured in angstroms, and J in A/cm^2. If we neglect the second term in Eq. (3b) we can write s and ϕ_0 explicitly in terms of α and γ.

$$s = \{-9.33(\gamma)^{1/2}\ln[3.03 \times 10^{-10}\alpha(\gamma)^{1/2}]\}^{1/2}, \qquad (4a)$$

$$\phi_0 = (0.01094/\gamma)s^2. \qquad (4b)$$

The values of α and γ can be determined from the slope and intercept of a plot of J/V vs V^2 as was done for a-Si barriers in Ref. 1.

Equations (1)–(4) are based on Simmons' results in Eqs. (20), (24), and (27) of Ref. 11. The numerical coefficients given in Eqs. (2)–(4) have been corrected from those given in the previous publication[1] on a-Si. This discrepancy arose from using the early paper of Simmons[12] which started with a result of Holm[13] which was slightly in error, but which Simmons corrected later.[11]

In deriving Eq. (1) Simmons had a mind, barrier heights on the order of 1 eV and discarded several terms which are not small for barrier heights less than 100 meV. Actually, for $V \gg \phi$ Eq. (1) yields negative values for J and the approximations made in Eq. (1) are compounded in going to Eq. (2). A low barrier height also increases the error in using the approximation $\beta = 1$ for $eV < \phi_0$ in deriving Eq. (2). We have generalized Simmon's expression [Eq. (1)] for use with low barriers by retaining the discarded terms (see Ref. 11, p. 1795). This leads to the following equations for a rectangular barrier.

1585   J. Appl. Phys., Vol. 58, No. 4, 15 August 1985

G. A. Gibson and R. Meservey   1585

160

$$J(V) = 6.16 \times 10^{10}/s^2 \left\{ \left[\phi_0 - \frac{eV}{2} + \frac{2.93}{s}\left(\phi_0 - \frac{eV}{2}\right)^{1/2} + \frac{2.86}{s^2} \right] \exp\left[-1.025s\left(\phi_0 - \frac{eV}{2}\right)^{1/2} \right] \right.$$
$$\left. - \left[\phi_0 + \frac{eV}{2} + \frac{2.93}{s}\left(\phi_0 + \frac{eV}{2}\right)^{1/2} + \frac{2.86}{s^2} \right] \exp\left[-1.025s\left(\phi_0 + \frac{eV}{2}\right)^{1/2} \right] \right\}, \quad \text{for } eV < \phi_0, \quad (5a)$$

$$J(V) = 3.36 \times 10^{10}\frac{F^2}{\phi_0} \left\{ \left(1 + 4.32\frac{F}{\phi_0^{3/2}} + 6.23\frac{F^2}{\phi_0^3} \right) \exp\left(-0.694\frac{\phi_0^{3/2}}{F} \right) \right.$$
$$\left. - \left[\left(1 + \frac{2eV}{\phi_0}\right) + 4.32\frac{F}{\phi_0^{3/2}}\left(1 + \frac{2eV}{\phi_0}\right)^{1/2} + 6.23\frac{F^2}{\phi_0^3} \right] \exp\left[-0.694\frac{\phi_0}{F}\left(1 + \frac{2eV}{\phi_0}\right)^{1/2} \right] \right\}, \quad \text{for } eV > \phi_0. \quad (5b)$$

Here s is the barrier thickness in Å, $F = V/s$ is the field strength in V/Å, ϕ_0 is the barrier height in eV, and J is measured in A/cm^2. In Fig. 2 we have compared Simmons' prediction, Eq. (1a), with the generalized version, Eq. (5), for $eV < \phi_0$ when $\phi_0 = 60$ meV and $s = 72$ Å. We have also included the results of numerically integrating the "exact" WKB expression for the current.[14] We have used a J/V vs V^2 plot to facilitate comparison with the straight line prediction of Eq. (2). For smaller values of ϕ_0 the discrepancy between Simmons' approximate Eq. (1a) and the numerical integration becomes larger and Eq. (5) remains significantly closer to the numerical solution than Eq. (1a).

B. Temperature dependence

For metal/insulator/metal junctions Stratton[15] has obtained for the temperature dependence of the tunnel current J

$$J(V, T) = J(V, 0)[\pi BkT/\sin(\pi BkT)], \quad (6)$$
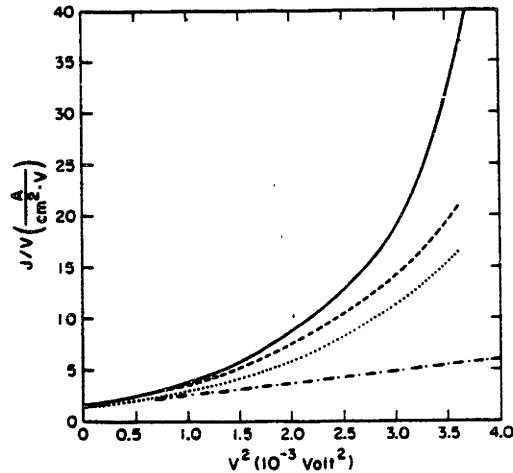
where

$$B = A/2\phi^{1/2}.$$

FIG. 2. Comparison of various theoretical calculations of the conductance J/V as a function of V^2 for a barrier height of 60 meV and a thickness of 72 Å. Simmons' expression [Eq. (1a)] is shown as a dotted curve; the low voltage approximation of this expression [Eq. (2)] is shown as the straight dash-dot line. The modified version of Simmons' result retaining terms important for low barrier heights [Eqs. (5)] is shown as a dashed line. Numerical integration of the WKB expression is given by the solid line.

and A is the constant in Eq. (1). This equation was derived from the same WKB expression as was Eq. (1), the difference being that the temperature dependence of the Fermi function was included. It should be accurate even for low barriers. In the limit where $\pi BkT \to 0$

$$J(V, T) = J(V, 0)[1 + (\pi BkT)^2/6 + \cdots]. \quad (7)$$

Simmons[16] has shown that for symmetric junctions the change in J with temperature goes as

$$\hat{J} \equiv [J(V, T) - J(V, 0)]/J(V, 0)$$
$$= \begin{cases} 3 \times 10^{-11}(sT)^2/(\phi_0 - eV/2), & eV < \phi_0, \\ 6 \times 10^{-11}\phi_0(sT/eV)^2, & eV > \phi_0, \end{cases} \quad (8)$$

where again s is in angstroms, ϕ_0 in electron volts, and T is in kelvins. According to Eq. (8) one should see a peak in $\hat{J}$ at $eV = \phi_0$.

C. Mott variable-range hopping

At higher temperatures one expects the variable-range hopping model of Mott[17,18] to dominate the conductance since there are a large number of localized states associated with dangling bonds in a-Ge.[19] In this model one assumes that there is a high density of localized states $N(E_F)$ in the vicinity of E_F, which is located near the center of the mobility gap of a-Ge. If, on average, there is one state within a sphere of radius L and within an energy E, then

$$1 = \Delta E \tfrac{4}{3}\pi L^3 N(E_F).$$

The conduction takes place by phonon-assisted tunneling between nearby localized states and the tunneling probability is given by

$$P = \nu_{ph} \exp(-2\alpha L)\exp(-\Delta E/kT).$$

Here ν_{ph} is the characteristic phonon frequency and α is the spatial decay constant of the localized state wave function [not to be confused with the coefficient in Eq. (2)]. Maximizing the tunneling probability with respect to L yields the most probable tunneling distance,

$$L = [\tfrac{1}{3}\pi\alpha N(E_F)kT]^{-1/4}, \quad (9)$$

from which the conductivity follows

$$\sigma = \sigma_0 \exp\{-2.1[\alpha^3/kN(E_F)T]^{1/4}\}, \quad (10)$$

where $\sigma_0 = (1/6)e^2L^2\nu_{ph}N(E_F)$. The above equations are those given in Ref. 1 corrected for typographical errors.

In Mott's derivation σ_0 has a $1/\sqrt{T}$ dependence owing to the L^2 term. By assuming a reasonable value for ν_{ph} and plotting $\ln(\sigma\sqrt{T})$ vs $T^{-1/4}$ and using Eq. (10) one can obtain

161

values for L, α, and $N(E_F)$. Other authors[20-23] have obtained for a-Ge values in the range $L \cong 80 - 150$ Å (at 77 K), $\alpha^{-1} \cong 5 - 10$ Å, and $N(E_F) \cong 10^{17}-10^{20}$ cm^{-3} eV^{-1}. How-ever, it has been pointed out[15] that this procedure is unrelia-ble and often leads to values of $N(E_F)$ which are unreason-ably large. The "constant" σ_0 is difficult to evaluate and involves a frequency term which has not been determined. In particular, Mott assumed energy independence of the den-sity of states at E_F in deriving the form for σ_0 used in Eq. (10). However several authors[24] have demonstrated that the ener-gy distribution of the density of states can be of major impor-tance.

III. EXPERIMENTAL METHODS

The tunnel junctions used in this study were made simi-larly to those used to study amorphous Si barriers.[1] The junctions were mainly Al/a-Ge/Al, although Al/a-Ge/Fe and Al/a-Ge/Ni junctions were also examined. All the junc-tions were made by evaporation onto glass substrates cooled to near 77 K. Al strips about 2.3×10^{-2} cm wide were depos-ited from a thermally heated Al$_2$O$_3$-coated tungsten wire basket. Very pure Ge was then evaporated by an electron beam to cover an area somewhat larger than that of the junc-tions. Finally, Al strips 2.3×10^{-2} cm wide were deposited perpendicular to the first Al strip to complete the junctions. The Ge barriers in some of the Al/a-Ge/Al junctions were treated with a glow discharge in O$_2$, N$_2$, or H$_2$. The Al films were usually made 42–45 Å thick so that the junctions could be measured in the superconducting state in parallel magnet-ic fields up to 3.5 T. Also, features in the conductance curves became sharper owing to the higher transition temperature ($T_c = 2.4$ K) of the thin Al films. For investigation of the high voltage region or with low resistance junctions, the Al films were made thicker so that the required voltage across the tunnel junction could be reached before the Al films ex-ceeded their critical current. Pressure during the evapora-tion was about 1×10^{-7} Torr. Film thickness was measured with a quartz-crystal gauge which was calibrated by optical interferometry. To increase the accuracy of the thickness measurement of the Ge, the junctions were made with a ro-tating sector disk.[25] Using the disk, a total deposit on the thickness gauge of, for instance, 300 Å would give Ge film thicknesses of 100, 81, 72, and 63 Å deposited on different portions of the substrate as determined by the openings in the sector disk. The density of a-Ge was assumed to be 5.35 g/cm^3. The known uncertainty in the Ge film thickness as determined by the quartz-crystal thickness gauge was about 5%. The Ge films covered a larger area than the junctions formed by the Al films and one might think that the current could travel directly through the Ge film and bypass the junction area. However, the sheet resistance of the Ge films was so high ($> 10^9$ Ω/unit area) that this effect is negligible even at room temperature.

Capacitance measurements were also made on several junctions; the results are plotted in Fig. 3. Taking the thick-ness to be that given by the quartz gauge we get a value for the dielectric constant $K = 16$, in agreement with the value for crystalline Ge,[26] but the value of K for our a-Ge film is not exactly known. It should be pointed out that if the bar-
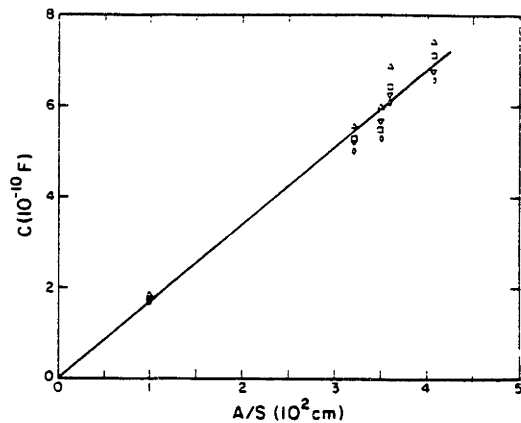

FIG. 3. Capacitance vs area/thickness for a number of junctions. $\triangle$ at $f \leqslant 2$ kHz, $T = 4.2$ K; ∇ at 10 kHz, 4.2 K; ▓ at < 2 kHz, 1.2 K; $\lozenge$ at 10 kHz, 1.2 K.

riers are nonuniform in thickness, the effective thickness de-duced from junction capacitance, which varies inversely as the thickness, may not agree with the thickness deduced from the tunneling resistance, which varies exponentially with thickness. Also Gundlach and Heldman[27] have found discrepancies between thickness deduced from the tunneling conductance and the capacitance of Al$_2$O$_3$ barriers depend-ing on the oxidation process and even the electrode material. Because of the above uncertainties, the capacitance cannot be relied upon for an accurate absolute thickness measure-ment, but for the thicknesses measured here and using $K = 16$ the value of the capacitance is consistent with the tunneling data and implies that the barriers are reasonably uniform.

It was also found that the optical transmission of the Ge films is a rather well-defined function of quartz monitor thickness and could be used as a consistency check on the thickness of the barrier at the position of each tunnel junc-tion measured. This was useful because some junctions lay in a transition region between Ge layers of different thickness. For these measurements white light was passed through the Ge films and the signal measured by a photocell mounted on one eyepiece of a dual eyepiece research microscope. A small aperture in the eyepiece defined the area being measured which could be selected by eye using the other eyepiece. Fig-ure 4 shows the measured transmission as a function of mea-sured Ge film thickness for all of the junctions used. The results form a fairly consistent pattern which is useful for comparing junctions of a given evaporation. The dashed line is a theoretical curve[28] for the transmissivity at normal inci-dence of light of 450 nm wavelength for a layer with an index of refraction of 4.5 and of absorption coefficient of 0.21 on a glass slide.[29] This theoretical curve is given only to show that the measured results are roughly what one expects and is not a measurement of the optical constants of the Ge film be-cause of the use of white light and converging illumination of the microscope. Both the method used here and the reflec-

162
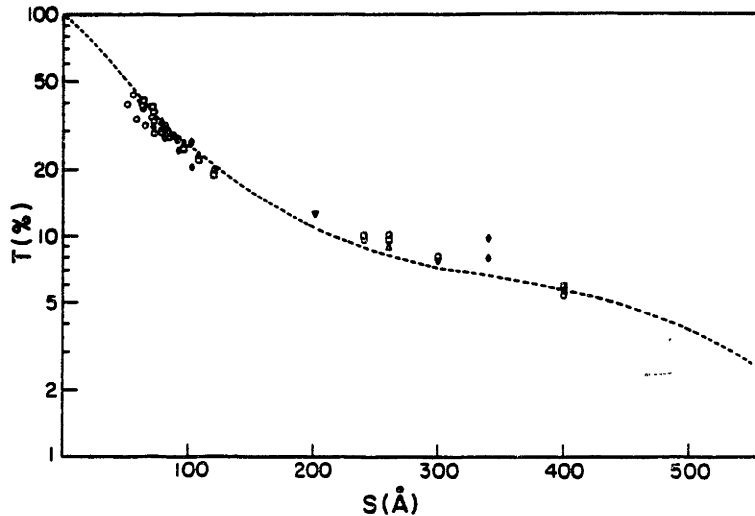
FIG. 4. Transmissivity of white light as a function of barrier thickness. Dashed line is theoretical curve described in text. Different symbols used for data points represent different sets of junctions.

tance technique used by Smith et al.[8] to measure the thickness of their a-Si films during deposition, illustrate the usefulness and sensitivity of optical methods for monitoring the thickness of amorphous semiconductors.

Four terminal current–voltage measurements were made from 300–4.2 K with the junctions enclosed in a brass container with He gas. The temperature was measured using a strain-gauge thermometer and a carbon–glass resistor. From 4.2–1.2 K the junctions were immersed in liquid He. Some junctions were measured down to 0.45 K in a ³He cryostat. Measurements of dI/dV and dV/dI were also made

at low temperature to investigate the effect of superconductivity on the tunnel conductance.

IV. EXPERIMENTAL RESULTS

A. Low temperature measurements

I vs V, dI/dV vs V, and dV/dI vs V measurements were made at about 1.2 K. The electrodes were typically 45 Å thick Al and became superconducting at $T_c \simeq 2.4$ K. The tunneling characteristic below T_c provided a means for checking the quality of our junctions. Current I as a function of voltage V at 1.1 K is shown in fig. 5 for two junctions made in the same deposition. Figure 6 shows dI/dV vs V at 1.2 K
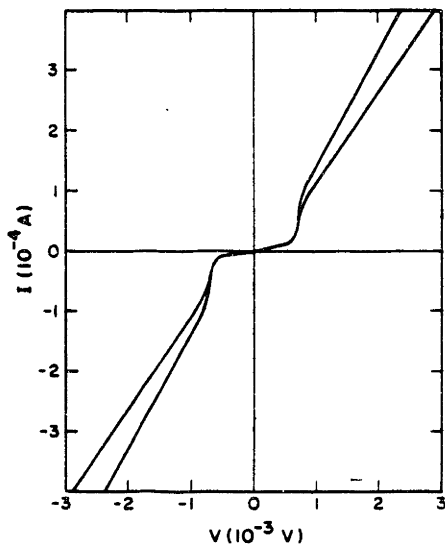
FIG. 5. I as a function of V for two typical Al/a-Ge/Al junctions made in the same deposition at $T = 1.2$ K.
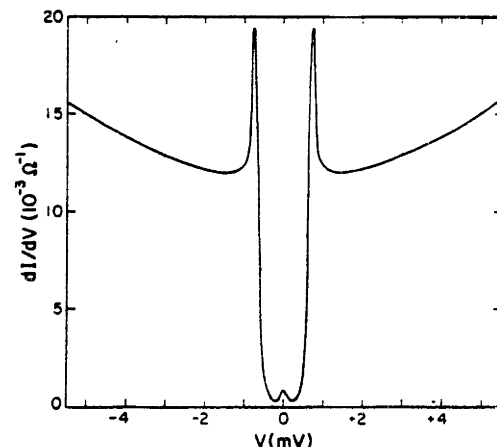
FIG. 6. dI/dV vs V for an Al/a-Ge/Al junction at 1.2 K, when the thin aluminum is superconducting. The superconducting energy gap is clearly visible. The large near-parabolic background is the result of the small effective barrier height. The small peak at zero voltage is characteristic of tunneling between identical superconductors at finite temperature.

163
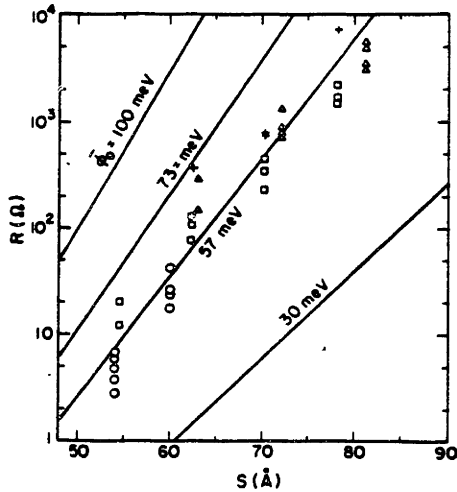
FIG. 7. R vs Ge barrier thickness s at 1.2 K. The nearly straight lines on the semilog scale are the predictions of Eq. (11) for four different mean barrier heights.

for another typical junction. Only junctions showing superconducting energy gaps were considered.

In the limit that T and V approach zero, the expression for the current density in Eq. (2) or (5) becomes $J = \alpha V$ and the resistance per unit area R_1 is

$$R_1 = a(s/\phi_0^{1/2})\exp(bs\phi_0^{1/2}),\tag{11}$$

where
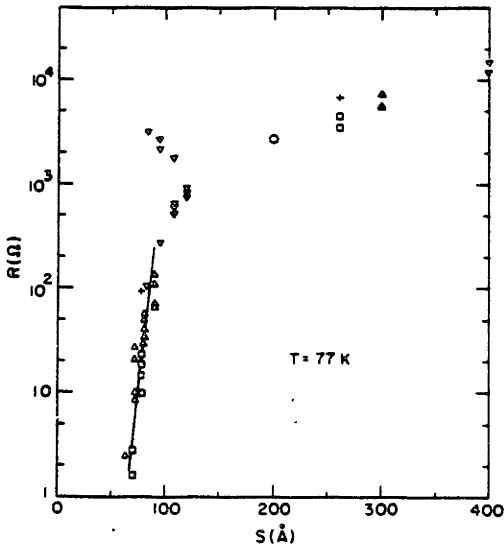
FIG. 8. R vs Ge barrier thickness at 77 K. The resistance is exponential in the thickness s for thin barriers, but levels off above 100 Å. The resistivity approaches a constant for large thicknesses.
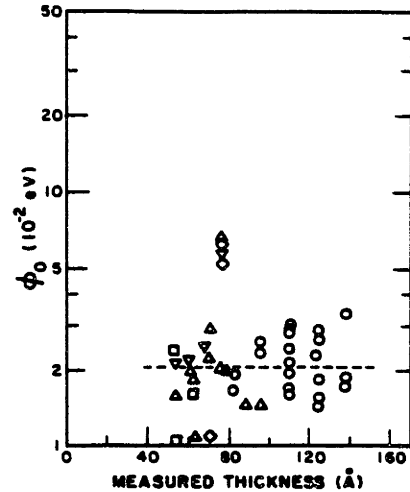
FIG. 9. Ge barrier heights ϕ_0 as calculated from Simmons' equation for low voltage [Eq. (4b)] vs thickness as measured by a quartz-crystal thickness gauge. Also included are the results for Si (calculated in the same way) from an earlier paper (see Ref. 1). O = Si, $\triangle$ = Ge. $\triangledown$ = Ge glow discharged in O_2, $\square$ = Ge glow discharged in N_2, and $\Diamond$ = Ge glow discharged in H_2.

$$a = h^2/e^2\sqrt{2m}, \quad b = 4\pi\sqrt{2m}/h.$$

Because of the large value of the argument of the exponential, the prefactor, which is linear in s, is not important in determining the thickness dependence of R_1. Therefore we expect R_1 to vary exponentially with s in the thickness range of interest. By extrapolating $R_1(V)$ from voltages greater than $4\Delta/e$ to $V = 0$, the zero-bias resistance for normal electrodes was obtained at 1.2 K, when the Al was superconducting. We plotted this zero-bias resistance at $T = 1.2$ K for thicknesses between 48 and 90 Å, and found that it was indeed exponential over at least four orders of magnitude (see Fig. 7). The results at 4.2 K are virtually identical. In Fig. 8 we see that at 77 K the resistivity levels off above a critical thickness. Included in Fig. 7 are theoretical predictions of Eq. (11) for several values of ϕ_0. The best fit is obtained with a barrier height of 57 meV.

As mentioned above, the application of Eq. (2) to junctions with low barriers is questionable. Curiously, we found that for many junctions a plot of J/V vs V^2 yielded a straight line out to about 40 meV (straighter than the prediction of the numerical solution of the WKB approximation). Figures 9 and 10 show the result of using Eqs. (4a) and (4b) to calculate the barrier height and thickness. The calculated thicknesses are generally higher than the measured values. Most of the ϕ_0 values cluster around $\phi_0 = 20$ meV. This is low compared to the value of 57 meV obtained from plotting ln R vs thickness. For comparison, data for a-Si from the previous paper[1] are also shown in Figs. 9 and 10. These values were also calculated using Eqs. (4a) and (4b).

It is difficult to determine how best to fit the data to the more accurate Eqs. (5). In Fig. 11 we have plotted the prediction of Eqs. (5) for 70 meV barriers of various thicknesses
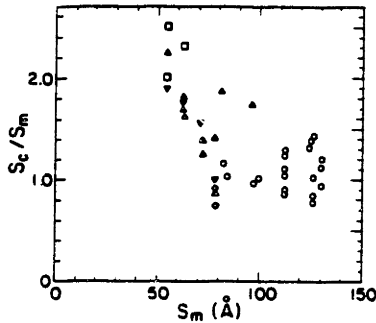
164

FIG. 10. Ratio of Ge barrier thickness s_c as calculated from Eq. (4a) to thickness s_m as measured by a quartz-crystal thickness gauge plotted as a function of measured thickness s_m. Included are the results for Si from Ref. 1. O = Si, △ = Ge, ▽ = Ge glow discharged in O_2. □ = Ge glow discharged in N_2, ◊ = Ge glow discharged in H_2.

(solid curves) and 72 Å thick barriers with different heights (dashed curves). Also plotted are a few data points for four junctions with different thicknesses. Clearly, the functional form of the current vs voltage characteristics obtained for our junctions does not exactly match that predicted for rectangular barriers. The thicker barriers can be more easily fit to the theory than the thinner ones. As can be seen from Fig. 11, it is not possible to closely fit both the low voltage (< 40 meV) and high voltage (> 40 meV) data by adjusting the values for the thickness and barrier height. This fit is also complicated by the fact that the measured conductance for these very thin Al films even in the normal state is often slightly depressed below the linear dependence of V^2 for V
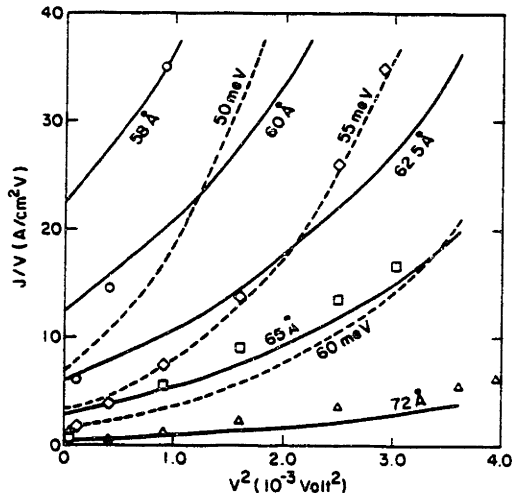
FIG. 11. Plots of $J//V$ vs V^2 as predicted by Eq. (5a). The solid curves are for 70 meV barriers of various thickness. The dashed curves are for 72 Å thick barriers with different heights. Also shown are a few experimental points taken from the I vs V curves of four junctions. O = 70.2 Å, ◊ = 78 Å, □ = 81 Å, and △ = 90 Å.
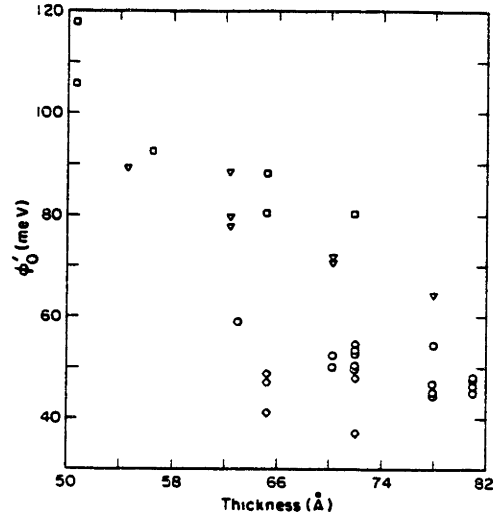
FIG. 12. Ge barrier height determined by matching current to prediction of Eq. (5) vs measured thickness. ▽ = Ge glow discharged in O_2. □ = Ge glow discharged in N_2, ◊ = Ge glow discharged in H.. and O = Ge not treated in glow discharge.

very close to zero. The same effect has been observed with ultrathin Al films with Si and Al_2O_3 barriers and is perhaps caused by a decrease in the density of states near $V = 0$ associated with localization and superconducting fluctuations in the extremely thin Al films. To avoid this complication the current was fitted at voltages higher than 10 meV. The best overall fits were obtained by using thicknesses $\simeq 10\%$–20% less than the value obtained from the quartz gauge and barrier heights in the range of 50–70 meV. To establish a consistent method for comparing the data with Eq. (5), we simply matched the absolute value of the current at 30 meV while assuming the thickness was that given by the quartz gauge. This is in the middle of the voltage range in which the functional form of the data tended to fit Eq. (5) the best. In Fig. 12 we have plotted the barrier heights calculated in this way (labeled ϕ'_0) as a function of thickness. The range of calculated barrier heights, 45–59 meV, is consistent with the value of 57 meV obtained from the change in zero-bias resistance as a function of thickness. Note that, in both of these methods of determining the barrier height, the absolute value of resistance as well as the change in resistance with voltage or thickness are consistent with the theory.

A few junctions with Ge barriers treated with a glow discharge in O_2, N_2, or H_2 were also studied. Plots of their zero-bias resistance as a function of thickness are shown in Fig. 13. The lines drawn through the data in this figure do not fit the theory as can be seen by comparing them with the dashed theoretical lines derived from Eq. (5). If we calculate the barrier height from the slope of the lines we obtain a value of $\phi_0 = 38$ meV for the nitrogen-treated barriers and $\phi_0 = 34$–46 meV for the oxygen-treated ones. Barrier heights can also be obtained by fitting Eq. (5) to the absolute values of the current at a given thickness. These values of

1590   J. Appl. Phys., Vol. 58, No. 4, 15 August 1985

G. A. Gibson and R. Meservey   1590

165
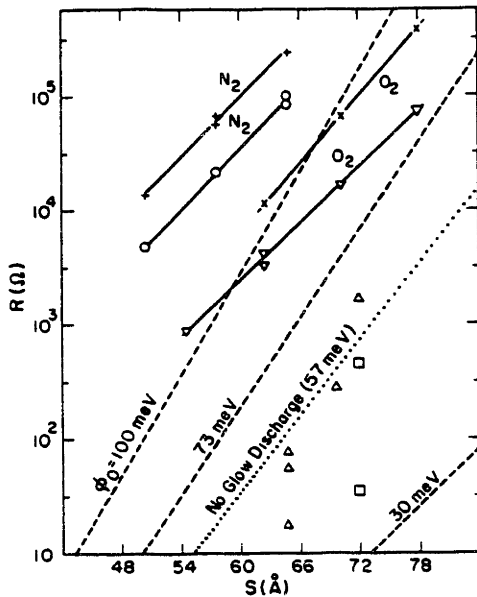
FIG. 13. Zero-bias resistance as a function of thickness for Ge barriers treated in a glow discharge. Two sets of junctions were glow discharged in O_2 (marked by X and ∇), two in N_2 (+ and O) and two in H_2 (△ and □). The dashed lines are the same as the theoretical lines shown in Fig. 7. The dotted line is that which best fits the data in Fig. 7. All data were taken at $T = 1.2$ K.

FIG. 14. Zero-bias conductance times $T^{1/2}$ vs $T^{-1/4}$ on a semilog scale for T from 150–4.2 K (bottom scale) for three junctions of different thickness. Part of the curve for the 340 Å thick junction is expanded (+) using the scale at the top of the figure. This junction shows the straight line behavior predicted by Mott for variable-range hopping.

barrier height ϕ_0' are shown in Fig. 12. The values of ϕ_0' obtained thus decrease with thickness and fall in the range of 118–64 meV, somewhat higher than those obtained from the resistance at $V = 0$.

B. Temperature dependence

The temperature dependence of the zero-bias conductance was measured for a number of relatively thick junctions from 170–4.2 K. Figure 14 shows the results for three junctions on a ln $(\sigma\sqrt{T})$ vs $T^{-1/4}$ plot. For the 340 Å thick barrier the plot is expanded in Fig. 14 (using the scale at the top of the figure) to show that from 140–70 K this plot is a straight line. It should be pointed out that it is, in general, quite easy to fit points to the functional form $\ln(\sigma\sqrt{T}) \sim T^{-1/4}$ over a limited range. The data do not, however, have a $\ln(\sigma) \sim T^{-1}$ dependence; conduction in this region does not seem to be a simple temperature-activated process. If we try to calculate α and $N(E_F)$ independently using the slope and intercept of the line in Fig. 14, we get a value for $N(E_F)$ which is at best ten orders of magnitude too large ($> 10^{30}/$eV cm^3). Other authors[18,22,24] have obtained similarly large numbers. As was mentioned earlier, the difficulty has been attributed to the uncertainty in the evaluation of σ_0 in Eq. (10). The coefficient in the exponent of Eq. (10) is more generally agreed upon by theorists. If we match the slope of our line to this coefficient we get $N(E_F) = 1.64 \times 10^{23} \alpha^3$ (1/ eV cm^3) (α^{-1} in Å). If we assume a reasonable value of α^{-1},

say $\alpha^{-1} = 10$ Å, we get $N(E_F) = 1.64 \times 10^{20}/$eV cm^3, a reasonable result. Here α^{-1} is the characteristic decay length of the localized state wave function.

Stratton's theory[15] of the temperature dependence of the tunneling current is given in Eq. (7) and should be applicable at low temperature for thinner barriers. To check this theory the zero-bias conductance was plotted vs T^2 from 4.2–27.6 K. The results for a typical junction are shown in Fig. 15. If we calculate ϕ_0 from the line drawn in this figure using Eq. (7) we get 5.2 meV. If we substitute the corresponding value for B back into the full expression, Eq. (6), we get the theoretical curve shown in Fig. 15. This curve diverges from the data at ≈ 10 K. Other junctions behave similarly and yield values of ϕ_0 in the range 5–20 meV. Plots of the fractional change in current with temperature, $\dot{J} = [J(V,T_2) - J(V,T_1)]/J(V,T_1)$ for = $T_2 = 77$, 10, 4.2 K and $T_1 = 1.2$ K decreased monotonically and symmetrically from $V = 0$, revealing no structure at ϕ_0.

C. Electron spin polarization

The tunneling conductance vs voltage of Al/a-Ge/Fe and Al/a-Ge/Ni junctions was measured in a parallel magnetic field of 4 T. In contrast to previous measurements with Al_2O_3 barriers,[2] these ferromagnetic electrodes caused no noticeable spin polarization of the tunnel current through a-Ge barriers. This behavior is different from the behavior of

166
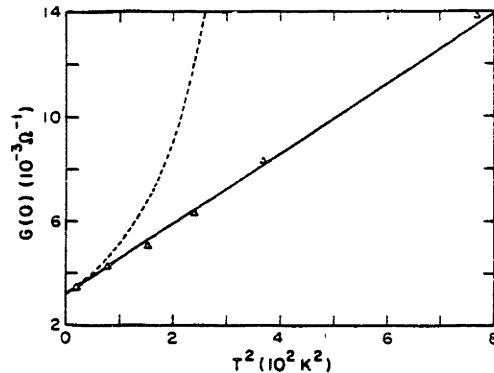
FIG. 15. Zero-bias conductance vs T^2 for a typical junction from 4.2–27.6 K. Triangles represent data. ϕ_0 was calculated from the line drawn through the data using the low temperature approximation to Stratton's theory [Eq. (7)]. However, when this ϕ_0 is used in the full expression [Eq. (6)] one gets the dashed line shown in the figure, which diverges from the data above approximately 10 K.

a-Si barriers in which spin polarization of the tunneling currents was seen in a few instances,[1] but not always. With a-Ge polarization was never seen.

V. DISCUSSION

First we consider to what extent the above data can be explained by a tunneling model. At 1.2 K we see in Fig. 6 the characteristic conductance curve expected for tunneling between two superconductors with equal energy gaps.[30] The sum peak at $eV = 2\Delta$ is present, although its breadth suggests that the superconductors are somewhat depaired or that an inelastic process is taking place in the tunneling. The small peak at $V = 0$ is characteristic of tunneling between superconductors when the energy gaps are equal and the temperature is not too low. The leakage current at low bias is small. The curvature of the conductance at higher voltage is consistent with a low tunnel barrier. Tunneling is indicated by the nearly exponential dependence of the resistance on the thickness of the a-Ge as shown in Fig. 7. Also, the barrier height calculated from the change in this resistance with barrier thickness is consistent with the barrier needed to roughly match the J vs V characteristic calculated for tunneling through a rectangular barrier. Overall, the data support the hypothesis that a low temperature the predominant conduction process is tunneling.

Values of the effective barrier height ϕ_0 are obtained by applying simple tunneling theory to the measured results. The average value of ϕ_0 obtained from Eq. (2) for a-Ge is the same as previously obtained for a-Si, implying the essential similarity of the conduction processes in these materials. It is important to note that in obtaining values of ϕ_0, all junctions showing shorted behavior when the Al films were superconducting were eliminated. Such shorts in parallel with the tunnel junction result in reduced curvature of the dJ/dV vs V curve at voltages above $2\Delta/e$ and give too high a value for the effective barrier. In spite of these precautions the scatter

with a-Ge junctions was greater than with a-Si. It is possible that this increase in scatter over that of a-Si resulted from the lesser stability of the structure of a-Ge as indicated by its lower annealing temperature. A value for the barrier height can also be obtained by fitting the measured resistance at $V = 0$ to Eq. (11) and using the value of s measured by the thickness gauge. The fact that $\phi = 57$ meV in Fig. 7 is consistent with all the data for $s = 54$ to 80 Å gives some confidence in this value of ϕ_0. This method is more direct than using the coefficients in Eq. (2) to obtain a value of ϕ and is probably more reliable. A similar conclusion was reached by Smith et al.[8] in their study of a-Si barriers. However it should be noted that ϕ_0 enters into this analysis only as the product $m^*\phi_0$, so that an effective mass m^* different from the free electron mass m would change the derived value of ϕ_0 as will be discussed below. The values of 57 meV is also consistent with the barrier heights needed to bring the current density vs voltage characteristics into rough agreement with Eq. (5). Another value of ϕ can be obtained from the Mott hopping model if we assume that it is equal to the energy separation of the localized states ΔE. In the previous publication on a-Si[1] the value of ϕ from this model was estimated to be 38 meV. The accuracy of this estimate is not high and probably applies equally well to a-Ge. Stratton's theory yields barrier heights of only 5–20 meV. This may be due to difficulties in determining the upper bound on the temperature range in which the theory is valid or related to the effective mass as explained later. Although there is a considerable difference in these values of the effective barrier height, we can conclude that the value is low, probably being in the range of 50 meV or less. The results also indicate that the effective barrier heights in a-Ge and a-Si are not significantly different.

A number of junctions were treated with glow discharges in N_2, O_2, or H_2, but no systematic study was made of the effect of preparation conditions. Nitrogen and oxygen increased the resistance over those which were untreated as shown in Fig. 12. The corresponding increase in ϕ is shown in Fig. 12. This result can perhaps be understood by the fact that the gas atoms partially passivate the dangling bonds of the a-Ge and thus lead to fewer localized states in the barrier with greater energy separation between them. In this model the average energy separation $\Delta E \approx \phi_0$. The decrease in the value of ϕ_0 with thickness as seen in Fig. 12 is also consistent with this model. However, the fact that in Fig. 13 ln R is proportional to s but with a smaller slope, does not follow from Eq. (11) with a larger value of ϕ_0.

At higher temperatues the dominant conduction process changes at a critical barrier thickness as shown in Fig. 8. Here the resistance vs thickness curve at 77 K has a sudden break at a thickness of 100 A. In the Mott model of hopping conduction, the mean hopping distance, L, increases with decreasing temperature. When L becomes comparable to the thickness of the barrier, tunneling between electrodes or through one localized state becomes important. A reasonable value of L at 77 K is 100 Å. For thicknesses above 100 Å the resistivity approaches a value independent of thickness. As the temperature was lowered the transition to Mott tunneling for such thick barriers rapidly increased to such high values that we could not observe it. The temperature depen-

167

dence of the conductance of *thick* barriers fits the functional form of the Mott model $G(T) = G_0 e^{-c/T^{1/4}}$ with a reasonable value of c at higher temperatures. For *thin* barriers the zero-bias resistance was exponential in thickness as expected from tunneling. Between 1.2 and 150 K, ln $G(0)$ vs $1/T$ was not found to be linear as would be expected from a simple temperature activated process.

One very noticeable property of the tunneling curves with a-Ge is that the current is symmetric with voltage about $V = 0$, a property which was observed also with a-Si. This symmetry is not affected by having metals with different work functions as electrodes. This symmetry was also seen in the junction in which the a-Ge was treated with a glow discharge in nitrogen, oxygen, or hydrogen even though a gradient in the density of localized states may have existed within the Ge barriers. It was previously conjectured[1] that this behavior is indicative of tunneling through localized states near the Fermi energy whose properties are not noticeably affected by the work functions of the electrodes.

The peak of the conductance at the sum gap of Al/a-Ge/Al junctions is wider and much lower than found for Al/Al_2O_3/Al junctions. This result is consistent with measurements previously made on Al/a-Si/normal metal junctions[1] in which the density of states peak was so broadened as to make it barely visible. The broadening of the density of states features on the conductance curve in Fig. 6 is qualitatively consistent with either a depairing of the superconducting electrodes or inelastic scattering in the tunneling process. Two reasons for depairing of the superconductor are suggested. (1) The magnetic moments associated with the dangling bonds of the amorphous Ge might act as magnetic impurities and cause depairing. (2) Interdiffusion between the metal and the Ge could give a normal metal layer at the surface of the superconductor and result in depairing because of a proximity effect. Hiraki *et al.*[31,32] showed that for semiconductors such as Si or Ge with a fairly small gap between the valence band and the conduction band, there was diffusion into films of Al, Au, Cu, and Pd, whereas for substances with a large gap such as SiO_2 there was no diffusion. If either of these two depairing mechanisms were present, the part of the ultrathin Al in contact with the Ge should have had a lower superconducting transition temperature than the remainder. Since two transitions of this sort were not observed, we favor the explanation that the broadening is produced by an inelastic process in the tunneling. Besides the broadening of the density of states features there was the observed lack of polarization of the tunneling currents from Ni and Fe electrodes. If interdiffusion of the ferromagnetic metal and the Ge took place, the lack of spin polarization could be attributable to the lack of ferromagnetism on the surface of the ferromagnetic electrode. On the other hand an inelastic process which scattered the spins in the tunneling process could also lead to a randomization of the spins of the tunneling electrons.

Although tunneling is the predominant conduction process at low temperature, the simple tunneling model through a rectangular barrier is not completely adequate. The observed increase of J as a function of V at high voltages was less than predicted by theory. This discrepancy between experiment and simple theory was not remedied by eliminating approximations that were unjustified because of the low effective barrier as was done in Eqs. (5). Also, although the zero-bias conductance had the expected T^2 dependence, the observed coefficient was much less than predicted by Stratton's theory.[15] The predicted peak in J [see (Eq. 8)] at $eV = \phi_0$ was not observed experimentally. Finally, the broadening of the dI/dV peaks corresponding to the sum gap of the superconductors also indicates complications that cannot be explained by a simple rectangular barrier.

Tunneling through a Schottky barrier at the metal a-Ge interface would seem to be a possibility. However, undoped a-Ge is an insulator at low temperature and such thin layers are incapable of transferring enough charge from the interior to the electrodes to lead to the band bending necessary to develop a Schottky barrier.[33] For a Schottky barrier one would *not* expect the following features which are observed for a-Ge: junction capacitance varying as the inverse thickness, resistance varying exponentially with thickness, and the symmetry of the conductance about $V = 0$ with electrodes having different work functions. The situation with a-Ge can be contrasted with that found in barriers of In_2O_3 studied by Magerlein[34] and Baker and Magerlein[35] where the In_2O_3 acted as a degenerate semiconductor and the presence of a Schottky barrier was signaled by the independence of the junction capacitance from the semiconductor thickness.

A more probable explanation of the deviations from a simple direct tunneling model is that the tunneling takes place through localized states in the a-Ge as was suggested in our previous study of a-Si.[1] Halbritter[36,37] and Kresin and Halbritter[38] have extensively treated the process of tunneling through localized states particularly with reference to Nb oxide barriers. In this model the localized states hybridize strongly with the conduction band of the electrodes and form surface or interface states which weaken the superconductivity in the electrodes. Resonant tunneling takes place through the localized states of thin barriers at low temperature where correlation effects do not dominate the tunneling process. Halbritter predicts a maximum in $d \ln(J/V)/dV$ at low voltage because of correlation effects, large leakage currents near $V = 0$, and resistance anomalies in the normal state. In the present experiments with Al/a-Ge/Al junctions no maximum was found in $d \ln(J/V)/dV$. There was no evidence of a resistance anomaly in the normal state other than the very small effect near $V = 0$ which is attributable to the extremely thin Al films. Also, leakage currents are often as low as 1%. This difference in the behavior of a-Ge with Al electrodes and Nb/Nb oxide/Nb junctions is probably attributable to properties of the Nb and its interface with the Nb_2O_5. Such junctions are known to have resistance anomalies and often have large leakage because of suboxides. The large dielectric constant of $Nb_2O_5 (\simeq 40)$ may account for the peak in $d \ln (J/V)dV$ as suggested by Halbritter.[37]

Although Halbritter's analysis does not explain the present data, tunneling through localized states near the Fermi energy seems to be a probable explanation of the conduction at low temperature. The overlap of the wave function of the localized states and the itinerant states in the

168

electrode would lead to a finite but perhaps long lifetime of the localized states. A long lifetime would limit the number of localized states available for tunneling at high current densities or temperatures. This model is qualitatively consistent with the observation that the current does not increase with voltage or temperature as fast as the simple tunneling model predicts. It also explains why the effective height as determined from the cubic term in Eq. (2) is smaller than the effective barrier determined from the zero-bias resistance and the measured thickness using Eq. (11).

Tunneling through a localized state could lead to an inelastic process. It is believed that the specific heat of amorphous sytems at low temperature[39] is dominated by excitations of two-level systems.[40,41] If, during its lifetime the localized state changes its energy by interaction with such an excitation, the conductance peaks would be broadened. Such an inelastic process could also cause spin scattering through the spin-orbit interaction with the lattice. In fact the spin relaxation time t_1 has been measured for a-Si and a-Ge by electron spin resonance[42] and the relaxation was attributed to interactions with excitations of a two-level system. It was found that the ratio of the relaxation time for a-Si to that of a-Ge varied inversely as their atomic spin-orbit coupling constants. Such a spin scattering process is consistent with the lack of electron polarization observed for Al/a-Ge/Fe and Al/a-Ge/Ni junctions in the present work and also for the polarization sometimes observed for Al/a-Si/Ni junctions,[1] since the spin-orbit interaction in Ge is about ten times that in Si.[42]

Another possible explanation of the less than expected increase in current with voltage is that the density of states has a local maximum near the Fermi energy as predicted by Mott and Davis.[43] Such a decrease in the density of states with voltage could lead to the observed slower increase of current with voltage, at least at fairly low voltages. A model related to that of Mott and Davis for transport in amorphous semiconductors has been proposed for a-Ge by Visćor.[44] In this model the lattice is assumed to be nonrigid and a strong interaction of the carriers with the lattice results in a band of small polarons, which at low temperature is centered on and pins the Fermi energy. This model claims (among other things) to resolve the difficulty about the prefactor in the Mott description of hopping mentioned in Sec. I, Eq. (10). Such a model offers the possibility of tunneling through the partially filled band of small polarons located symmetrically about the Fermi energy. Additional experimental and theoretical work are needed to test this proposed model for its pertinence to tunneling in a-Ge barriers.

Since the exact nature of the tunnel barrier and its dispersion relation[43] are unknown, the question as to what is the proper effective mass to use is still open. For tunneling in a-Ge at energies near the conduction band, it would be reasonable to use values of the effective mass which are only slightly modified from the crystalline conduction band value.[45] However, at low temperature the low voltages in undoped a-Ge the energies of the tunneling electrons fall in the band gap where the dispersion relation is unknown. If the tunneling is through localized states the mass of the free electron is more appropriate. Actually there is some internal

evidence in the present measurements and analysis which favors a value of m^* considerably larger than the free electron mass m. In analyzing measurements of the resistance of tunnel barriers using Eq. (11) m^* enters as $m^*\phi_0$ [see the Appendix, Eq. (A7)] and we could just as well treat ϕ_0 as an effective barrier height. However, the same effective barrier height would not apply to the temperature dependence of the tunnel current where m^* enters as m^*/ϕ_0 [see the Appendix, Eq. (A6)]. In addition, Eq. (2) gives us values of ϕ_0 and m^*/m which are essentially independent (see the Appendix, Eqs. (A4) and (A5)]. An interesting result is that the values $\phi_0 \approx 20$ meV and $m^*/m \approx 2.8$ are consistent with all the different types of measurements as is shown in the Appendix. Considering the very large scatter of some of the data, this value for m^*/m is extremely tentative. An effective mass larger than the free electron mass is perhaps consistent with the dispersion relation in the mobility gap of a-Ge or with the small polaron model of the tunneling process mentioned above.

In summary, we have measured the tunneling properties of junctions with a-Ge barriers. The results are very similar to those previously found for a-Si and are consistent qualitatively and semiquantitatively with tunneling. However, we have shown that even after eliminating unjustified assumptions for small barrier heights, the simple rectangular tunnel barrier model is insufficient to explain the results quantitatively. Possible explanations of these discrepancies are suggested, but the exact nature of the tunneling process remains to be clarified.

ACKNOWLEDGMENTS

APPENDIX

In this Appendix the main equations are rewritten with the effective mass m^* given explicitly so that the effect of changes in m^* can be seen. Equation (2) is

$$J = \alpha(V + \gamma V^3),\qquad (A1)$$

where

$$\alpha = \frac{(2m^*\phi_0)^{1/2}e^2}{sh^2}\exp\left(-\frac{4\pi s}{h}(2m^*\phi_0)^{1/2}\right),\qquad (A2)$$

$$\alpha = \frac{\pi^2 s^2 e^2 m^*}{3h^2\phi_0} - \frac{\pi s e^2 (2m^*)^{1/2}}{8h\phi_0^{3/2}}.\qquad (A3)$$

If we neglect the second term in Eq. (A3), we obtain from the first term in Eq. (A3) and Eq. (A2)

$$\phi_0 = -\frac{e}{4\sqrt{6}\gamma^{1/2}}\ln\left(\sqrt{\frac{3}{2}}\frac{1}{\pi}\frac{h^3\alpha\gamma^{1/2}}{e^3 m(m^*/m)}\right)$$

or   (A4)

$$\phi_0 = -\frac{0.1021}{\gamma^{1/2}}\ln\left(\frac{3.03\times10^{-10}\alpha\gamma^{1/2}}{m^*/m}\right),$$

where as before ϕ_0 is in electron volts, $\gamma^{1/2}$ is in volts, and α is

169

in A/cm^2. Equation (A4) shows that in this theory ϕ_0 is only influenced by m^*/m logarithmically. In the junctions considered here a change in m^*/m from 1 to 2 would decrease the value of ϕ_0 by only 3.4%.

The value of m^*/m is then given by the first term in Eq. (A3)

$$\frac{m^*}{m} = \frac{3h^2\gamma\phi_0}{\pi^2 ms^2 e^2} = 91.4\gamma\frac{\phi_0}{s^2}. \tag{A5}$$

In Fig. 10 the calculated value of the barrier thickness s_c obtained from Eq. (4a) is compared with the measured value s_m. The values s_c are quite scattered with an average of $(s_c/s_m)^2 = 2.8$. If we assume the s_m is the correct value, we can fit the data with the value of $m^*/m = 2.8$ with a standard deviation of ± 1.6. Because of the large scatter in the data this value of m^*/m cannot be taken very seriously.

Equation (7) is

$$J(V,T) = J(V,0)\left(1 + \frac{4\pi^2\beta^2\,\overline{\Delta s}^2 k^2 \times 2m(m^*/m)T^2}{3h^2\phi_0}\right). \tag{A6}$$

The coefficient of the temperature dependence contains the term $(m^*/m)s^2/\phi_0$. To keep the fit to the experimental data we can use the value of ϕ_0 obtained before $(2 \times 10^{-2}$ eV) and increase m^*/m to keep the coefficient the same. The values of m^*/m obtained thus are

$$1 < m^*/m < 4.$$

In Eq. (11)

$$R_1 = \frac{h^2 s}{e^2\sqrt{2m^*\phi_0}}\exp\left(\frac{4\pi s\sqrt{2n^*\phi_0}}{h}\right). \tag{A7}$$

The value of R_1 evidently depends on the product $m^*\phi_0$. The best fit of $\phi_0 = 57$ meV was obtained for different values of s assuming that $m^*/m = 1$. If we adopt the value of $\phi_0 = 20$ meV obtained from Eq. (A4), a value of $m^*/m = 2.85$ is required to fit the data given in Fig. 7. Thus all of these results are consistent with $\phi_0 \approx 20$ meV and $m^*/m \approx 2.8$. When we rewrite Eq. (5) to show m^*/m explicitly, we get

$$J(V) = \frac{6.16\times10^{10}}{s^2}\left(\left[\phi_0 - \frac{eV}{2} + \frac{2.93}{s}\left(\frac{m}{m^*}\right)^{1/2}\left(\phi_0 - \frac{eV}{2}\right)^{1/2} + \frac{2.86}{s^2}\left(\frac{m}{m^*}\right)\right]\left\{\exp\left[-1.025s\left(\frac{m^*}{m}\right)^{1/2}\left(\phi_0 - \frac{eV}{2}\right)^{1/2}\right]\right\}\right.$$
$$- \left[\phi_0 + \frac{eV}{2} + \frac{2.93}{s}\left(\frac{m}{m^*}\right)^{1/2}\left(\phi_0 + \frac{eV}{2}\right)^{1/2} + \frac{2.86}{s^2}\left(\frac{m}{m^*}\right)\right]$$
$$\times\left.\left\{\exp\left[-1.025s\left(\frac{m^*}{m}\right)^{1/2}\left(\phi_0 + \frac{eV}{2}\right)^{1/2}\right]\right\}\right), \quad (eV < \phi_0), \tag{A8}$$

$$J(V) = 3.36\times10^{10}\frac{F^2}{\phi_0}\left(\left[1 + 4.32\frac{F}{\phi_0^{3/2}}\left(\frac{m}{m^*}\right)^{1/2} + 6.23\frac{F^2}{\phi_0^2}\left(\frac{m}{m^*}\right)\right]\left\{\exp\left[-0.694\left(\frac{m^*}{m}\right)^{1/2}\frac{\phi_0^{3/2}}{F}\right]\right\}\right.$$
$$- \left[\left(1 + \frac{2eV}{\phi_0}\right) + 4.32\frac{F}{\phi_0^{3/2}}\left(\frac{m}{m^*}\right)^{1/2}\left(1 + \frac{2eV}{\phi_0}\right)^{1/2} + 6.23\frac{F^2}{\phi_0^3}\left(\frac{m}{m^*}\right)\right]$$
$$\times\left.\left\{\exp\left[-0.694\left(\frac{m^*}{m}\right)^{1/2}\frac{\phi_0}{F}\left(1 + \frac{2eV}{\phi_0}\right)^{1/2}\right]\right\}\right), \quad (eV > \phi_0). \tag{A9}$$

At very low voltages these equations reduce to Eq. (2) and in that region changes in m^*/m do not noticeably effect ϕ_0. At high voltages the terms with the product $(m^*/m)^{1/2}\phi_0^{3/2}s$ become important. Then the results are too complex to be simply characterized, but could be used to obtain numerical values.

[1] R. Meservey, P. M. Tedrow, and J. S. Brooks, J. Appl. Phys. 53, 1563 (1982).

[2] J. S. Moodera, R. Meservey, and P. M. Tedrow, Appl. Phys. Lett. 41, 488 (1982).

[3] I. Giaever and H. Zeller, Phys. Rev. Lett. 21, 1385 (1968).

[4] M. L. A. MacVicar, S. M. Freake, and C. J. Adkins, J. Vac. Sci. Technol. 6, 717 (1969).

[5] B. Konig, Phys. Lett. 39A, 117 (1972).

[6] W. H. Keller and J. E. Nordman, J. Appl. Phys. 44, 4732 (1973).

[7] J. Seto and T. Van Duzer, Appl. Phys. Lett. 19, 488 (1971).

[8] L. N. Smith, J. B. Thaxter, D. W. Jillie, and H. Kroger, IEEE Trans. Magn. MAG-18, 1571 (1982).

[9] H. Kroger, D. W. Jillie, L. N. Smith, L. E. Phaneuf, C. N. Potter, D. M. Shaw, E. J. Cukauskas, and M. Nisenoff, Appl. Phys. Lett. 44, 562 (1984).

[10] J. G. Simmons, J. Appl. Phys. 35, 2472 (1964); Phys. Rev. Lett. 23, 297 (1969).

[11] J. G. Simmons, J. Appl. Phys. 34, 1793 (1963).

[12] J. G. Simmons, J. Appl. Phys. 34, 238 (1963). In this paper the expression

taken from Holm in Ref. 13 is in error by having an extra term [the first term in Eq. (1)], which gives a negative dynamic resistance at $V = 0$ and by having an extra factor of 3/2 in the second term. These errors were corrected by Simmons in later publications. C. K. Chow [J. Appl. Phys. 34, 2490 (1963); 36, 559 (1965)] also has taken this additional factor of 3/2 from Holm.

[13] R. Holm, J. Appl. Phys. 22, 569 (1951).

[14] W. F. Brinkman, R. C. Dynes, and J. M. Rowell, J. Appl. Phys. 41, 1915 (1970).

[15] R. Stratton, J. Phys. Chem. Solids 23, 1177 (1962).

[16] J. G. Simmons, J. Appl. Phys. 35, 2655 (1964).

[17] N. F. Mott, Philos. Mag. 19, 835 (1969).

[18] P. Nagels, in Amorphous Semiconductors, edited by M. H. Brodsky (Springer, Berlin, 1979), p. 113.

[19] E. A. Davis, in Amorphous Semiconductors, edited by M. H. Brodsky (Springer, Berlin, 1979), p. 41.

[20] M. Pollak, M. L. Knotek, H. Kurtzmann, and H. Glock, Phys. Rev. Lett. 30, 856 (1973).

[21] N. F. Mott and E. A. Davis, Electronic Processes in Non-Crystalline Materials (Clarendon, Oxford, 1971), p. 285.

[22] S. K. Bahl and N. Bluzer, in AIP Conf. Proc. 20, Tetrahedrally Bonded Amorphous Semiconductors, edited by M. H. Brodsky, S. Kirkpatrick, and D. Weaire (American Institute of Physics, New York, 1974), p. 320.

[23] P. J Elliot, A. D Yoffe. and E. A. Davis, in AIP Conf. Proc. 20, Tetrahedrally Bonded Amorphous Semiconductors, edited by M. H. Brodsky, S. Kirkpatrick, and D. Weaire (American Institute of Physics, New York, 1974), p. 311.

[24] See review article by H Overof in Festkorperprobleme (Avances in Solid

1595 J. Appl. Phys., Vol. 58, No. 4, 15 August 1985

G. A. Gibson and R Meservey 1595

170

State Physics XVI), edited by J. Treusch (Vieweg, Braunschweig, 1976), p. 239.

[25]J. S. Brooks and R. Meservey, J. Vac. Sci. Technol. 20, 243 (1982).

[26]S. M. Sze, *Physics of Semiconductor Devices*, 2nd ed. (Wiley, New York, 1981), p. 849.

[27]K. H. Gundlach and G. Heldman, Solid State Commun. 5, 867 (1967).

[28]M. Born and E. Wolf, *Principles of Optics* (Macmillan, New York, 1964), p. 627.

[29]D. Adler, *Amorphous Semiconductors* (CRC, Cleveland, 1971), p. 28.

[30]S. Shapiro, P. H. Smith, J. Nicol, J. L. Miles, and P. F. Strong, IBM J. (January 1962), p. 34.

[31]A. Hiraki, K. Shuto, S. Kim, W. Kammura, and M. Iwami, Appl. Phys. Lett 31, 611 (1977).

[32]A. Hiraki, S. Kim, W. Kammura, and M. Iwami, Surface Sci. 86, 706 (1979).

[33]J. G. Simmons in *The Handbook of Thin Film Technology*, edited by L. I. Maissel and R. Glang (McGraw-Hill, New York, 1970), Chap. 14, p. 14–5.

[34]J. H. Magerlein, J. Appl. Phys. 54, 2569 (1983).

[35]J. M. Baker and J. H. Magerlein, J. Appl. Phys. 54, 2556 (1983).

[36]J. Halbritter, Solids State Commun. 34, 675 (1980).

[37]J. Halbritter, Surf. Sci. 122, 80 (1982).

[38]V. Kresin and J. Halbritter, *Proceedings of the International Low Temperature Conference*, edited by U. Eckern, A. Schmid, W. Weber, and H. Wühl (North Holland, Amsterdam, 1984), p. 1061.

[39]R. C. Zeller and R. O. Pohl, Phys. Rev. B 4, 2029 (1971).

[40]W. A. Phillips, J. Low Temp. Phys. 7, 351 (1972).

[41]P. W. Anderson, B. I. Halperin, and C. W. Varma, Philos. Mag. 25, 1 (1972).

[42]M. Stutzmann and D. K. Beigelsen, Phys. Rev. B 28, 6256 (1983).

[43]N. F. Mott and E. A. Davis, *Electronic Processes in Non-Crystalline Materials*, 2nd ed. (Clarendon, Oxford, 1979).

[44]P. Viscor, Phys. Rev. B 28, 927 (1983).

[45]G. W. Lewicki and C. A. Mead, Phys. Rev. Lett. 16, 939 (1966).

[46]S. Kielson and C. D. Gelatt, Jr., Phys. Rev. B 19, 5160 (1979).

171

STUDY OF LAYERED AND COEVAPORATED V(Mo)N AND (V/Si)N FILMS*

G.A. Gibson, J.S. Moodera, P.M. Tedrow and R. Meservey
Francis Bitter National Magnet Laboratory
Massachusetts Institute of Technology
Cambridge, Massachusetts 02139

Abstract

Layered and coevaporated V/Mo samples were nitrided and their T_c's and spin-orbit scattering rates were compared. This is of interest because of the close lattice match of VN with the postulated high T_c of cubic MoN. In no case was a T_c higher than that of VN obtained. The spin-orbit scattering rate was found to be larger in the layered (V/Mo)N samples than in the coevaporated ones.

We have compared (V/Mo)N and similarly made (V/Si)N multilayer films with theories for the critical field of such structures. Evidence for dimensional crossover was seen in the parallel critical field curve of (V/Mo)N films. Also, the T_c of thin (V/Si)N multilayers was found to be dependent on the Si layer thickness.

Introduction

The goals of this work are threefold. First, we are interested in studying multilayer systems with thin superconducting layers separated by either metallic or insulating layers. This allows comparison of proximity effect and Josephson coupling between the superconducting layers and their related dimensional crossover effects. Also, we are interested in comparing the spin-orbit scattering rates in layered films with those found for coevaporated ones. Previous experiments have shown that high atomic number impurities in transition metals do not seem to be as effective in increasing spin-orbit scattering[1] as in the ideal BCS superconductor Al.[2] There is some question as to whether spin-orbit scattering occurs as effectively in the interior of films as at the surface.[2] Finally, V(Mo)N films are of interest because of the postulated high T_c of cubic MoN (~30 K). The lattice constant of VN is close to that predicted for cubic MoN.[3] It was hoped that by substituting Mo at some of the V sites in VN or by nitriding Mo layers grown epitaxially between V layers that a high T_c phase could be stabilized.

Multilayer systems of superconductors separated by insulating or metallic layers (or even superconducting layers with a smaller pair potential) exhibit interesting behavior when the coherence length of the superconducting layers is on the order of their thickness. The theory for the upper critical field in the case where the alternate layers are insulators or semiconductors has been developed by Lawrence and Doniach[6] and Klemm, Luther and Beasley.[5] Here, the superconducting layers are coupled by Josephson tunneling. When the periodicity of the lattice is small compared with the coherence length in the direction of the layering, ξ_z, the superconducting properties of the structure are averaged over many layers and the result is effectively an anisotropic three-dimensional behavior. When the periodicity is large compared with ξ_z, the superconducting layers are decoupled and the behavior is two-dimensional. In between these limits is the interesting regime where the dimensional crossover occurs. The temperature

dependent coherence length, $\xi_z(T)$, is large near T_c so that one expects a linear, three-dimensional behavior near T_c. As the temperature is lowered and $\xi_z(T)$ decreases, the theory predicts a crossover to a two-dimensional square root-like critical field dependence on temperature. The strength of the interlayer coupling has been characterized by the parameter:[5]

$$r = \frac{4}{\pi}\left(\frac{\xi_z(0)}{\frac{S}{2}}\right)^2$$

where S is the periodicity. The exact shape of the parallel critical field curve depends on the intralayer pairbreaking and spin-orbit scattering (see ref. 5) but in general the dimensional crossover is most easily observable when r is on the order of one.

Takahashi and Tachiki[7] have recently developed a theory for the upper critical field in systems where the alternate layers are metals or superconductors with a smaller pair potential. Here the coupling is via the proximity effect. They predict several interesting effects. In systems where the diffusion constants of the two layer types are similar and the layers are sufficiently thin, one again finds a dimensional crossover in the parallel critical field. This occurs as the temperature dependent coherence length, $\xi_s(T)$, changes relative to the layer thickness. Takahashi and Tachiki[7] also show that in systems where the ratio of the diffusion constants in the layers, $\frac{D_N}{D_S}$, is large and the layers are thick compared to $\xi_N(0)$, one should observe a discontinuity of the slope of the $H_{c2\parallel}$ with an essentially two-dimensional temperature dependence both above and below the discontinuity. This discontinuity ___ ___ at the point where the nucleation of superconductivity switches from the centers of the normal layers to the centers of the superconducting layers. A large value for $\frac{D_N}{D_S}$ essentially decouples the layers, away from T_c, so that the perpendicular critical field approaches that of the superconducting layers. Takahashi and Tachiki also show that the onset of 3-D behavior with decreasing temperature in systems which do not exhibit this discontinuity (i.e., when the diffusion constants of the layers are similar) occurs at higher temperatures when the ratio of the density of states at the Fermi level, $\frac{N_N}{N_S}$, is small. Also, there is an enhancement in the ratio $H_{c\parallel}(0)/H_{c\perp}(0)$ for layer thicknesses near $\xi_S(0)$ when $\frac{N_N}{N_S}$ is small or when the so-called "normal" layers have a BCS electron-electron interaction constant, V_N, near zero. In this case, the transition temperature of the multilayer system decreases to zero as the layer thickness approaches $\xi_S(0)$ due to the proximity effect.

Results

We have made both layered and co-evaporated V/Mo

films by evaporation from e -guns. These films were
immediately nitrided by admitting grade 5 nitrogen to
the evaporator and raising the substrate temperature
to ~700°C. We have also deposited V/Si multilayer
films and nitrided them at up to 300°C. The ratio of
the constituents and the overall thicknesses were
varied in both cases. Preliminary data on layered and
coevaporated V(Mo)N and layered (V/Si)N films are as
follows. It was found for both coevaporated and
layered (V/Mo)N that in no case did the T_c exceed
9.25 K, the T_c of VN. The transition temperature as a
function of atomic percent Mo (before nitriding) for
coevaporated films on the order of 1000 Å thick is
shown in Figure 1. Initially, the T_c decreases with
increasing Mo concentration. However, at the same
time the perpendicular critical field at zero temper-
ature increases. In going from 0 to 24.7 atomic
percent Mo, for example, $H_{c\perp}(0)$ goes from about 8
to 11.4 tesla, whereas $H_{c||}(0)$ remains relatively
constant at 13.2 to 14 tesla. This is probably due to
an increase in the disorder of the films. The resis-
tivity of the films is greatest for films with roughly
equal concentrations of V and Mo, ~300 μΩ·cm, and
decreases to around 60 to 120 μΩ·cm for films on
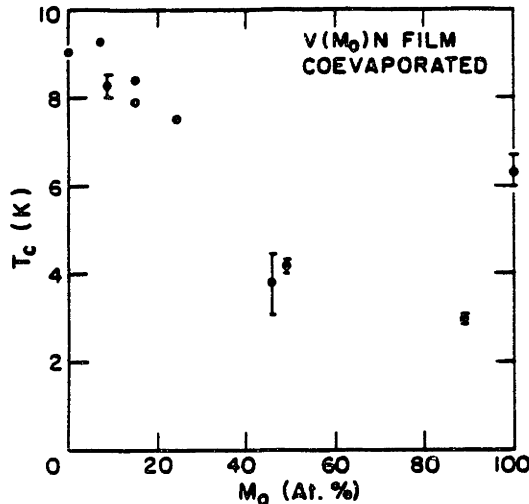either end of the Mo concentration.

Fig. 1. T_c vs. atomic percent Mo concentration for
coevaporated V(Mo)N films. All films were
nitrided at ~700°C for approximately 20
minutes.

A typical set of critical field curves for co-
evaporated V(Mo)N are shown in Figure 2. Data for two
films made in the same evaporation are shown. There
is a slight phase spread in composition between the
two. Nominally the films were 15.3% Mo and 670 Å
thick before nitriding. The perpendicular critical
field curve for one of the films has been fit using
the standard WHH[8] theory and agrees very well. These
curves should be compared with those shown in Figure 3
for layered films with a total of fifteen 50 Å layers.
As was mentioned earlier, $H_{c\perp}(0)$ is smaller in the
layered film. Furthermore, the parallel field curve
does not fit the standard WHH theory. At higher
temperature the $H_{c2}^{||}$ curve (Sample 1) appears linear
and then bends over to a square root-like dependence
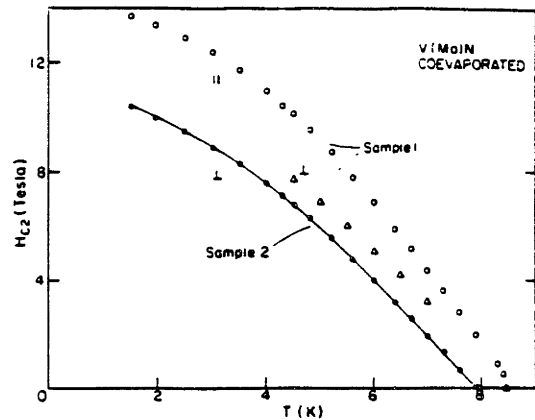at lower temperatures. This bend is reminiscent of

Fig. 2. Coevaporated V(Mo)N film with a total of
558 Å V and 111 Å Mo before nitriding.
Open symbols are for Sample 1 and closed
circles for Sample 2. Samples 1 and 2 were
made in the same evaporation but with
slightly differing Mo concentration. The
solid curve is a fit to the WHH theory (ref.
8) with λ_{so} = 2.3.
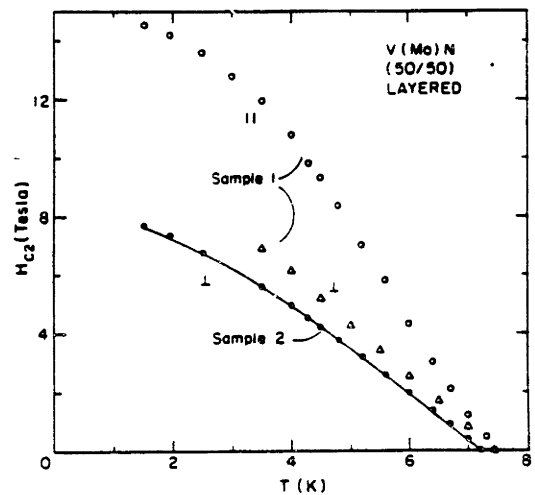
Fig. 3. Layered (V/Mo)N film with a total of fifteen
50 Å layers. Symbols o, Δ represent parallel
and perpendicular critical field, respec-
tively, for Sample 1. Closed circle is the
perpendicular H_{c2} for Sample 2. The solid
curve is a fit to the WHH theory with λ_{so} =
7.8.

the dimensional crossover predicted by Takahashi and
Tachiki. We can rule out spurious factors such as
edge effects because we don't see this effect in our
coevaporated films. In order to know whether we are
in the right regime to see the dimensional crossover
effects, it is necessary to know approximately the

values for $\frac{N_N}{N_S}$, $\frac{D_N}{D_S}$, $\frac{V_N}{V_S}$ and $\frac{d}{\xi_S(0)}$. Reliable knowledge
of these parameters requires further study as we do
not yet know even the exact composition of our layers.

We can say that complete interdiffusion of the vanadium and molybdenum layers during nitriding does not occur because of the clear differences in the perpendicular critical field curves for layered and coevaporated films. We suspect that our MoN may actually be fcc Mo$_2$N because of the transition temperature we find for pure MoN films (~6.6 K). Unfortunately, preliminary X-ray diffractometry measurements have been unable to confirm this. Figure 4 shows critical field curves for a MoN film with no vanadium made under similar conditions as the multilayer films.
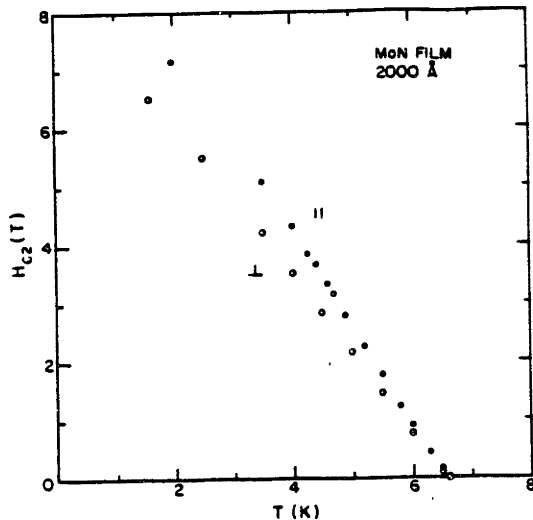

Fig. 4. Nitrided 2000 Å thick Mo film. (·), || critical field and (o), $\perp$ critical field.

If we assume that our MoN layers in the multilayer films are the same as this single thick MoN film, we can use it to estimate some of the parameters we would like to know. From the slope of the perpendicular critical field curve at T_c we get $D_{MoN_x} = .79 \frac{cm^2}{sec}$.

Similarly, using data from Moodera, Tedrow and Meservey,[9] we get $D_{VN} = .69 \frac{cm^2}{sec}$. From $H_{c\perp}(0)$ we get $\xi_{MoN}(0) = 66$ Å and $\xi_{VN}(0) = 56$ Å. The density of states at the Fermi level, N, is proportional to the electronic coefficient of specific heat, Y. Y has been measured for VN and found to be approximately 8.6 $\frac{mJ}{mol \cdot K^2}$.[10] We know of no such measurement on fcc Mo$_2$N. Since the T_c's and critical fields for the pure VN and MoN films are similar it is also reasonable to assume that $V_{MoN}^{BCS} = V_{VN}^{BCS}$. Given that the diffusion constants and BCS interaction constants are similar and that the coherence lengths are close to 50 Å, it would be reasonable to expect to see the dimensional crossover in the parallel critical field for the layered (V/Mo)N film in Figure 3 (see ref. 6). $H_{c||}(0)/H_{c\perp}(0)$ for this film is on the order of 1.5. For a 100 Å layer (V/Mo)N film $H_{c||}(0)/H_{c\perp}(0)$ was about 1.7. Thus, we don't see the enhancement of this ratio that one would expect if N_{VN} and N_{MoN} were greatly different.

Critical field curves for three (V/Si)N films

of different thickness are shown in Figures 5-7. In none of the parallel critical field curves is there evidence of the bend characteristic of the dimensional crossover. This is not surprising since even in the thinnest one the interlayer coupling is probably too weak. From $H_{c\perp}(3)$ we estimate that $\xi(0)$ is 62 Å. Using the ratio of the slopes of the paral-

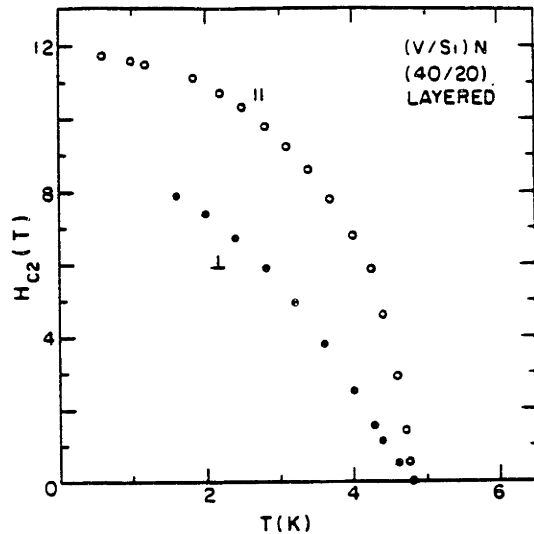Fig. 5. Layered (V/Si)N film with four 40 Å V layers and four 20 Å Si layers. Here (o), || critical field and (·), critical field.
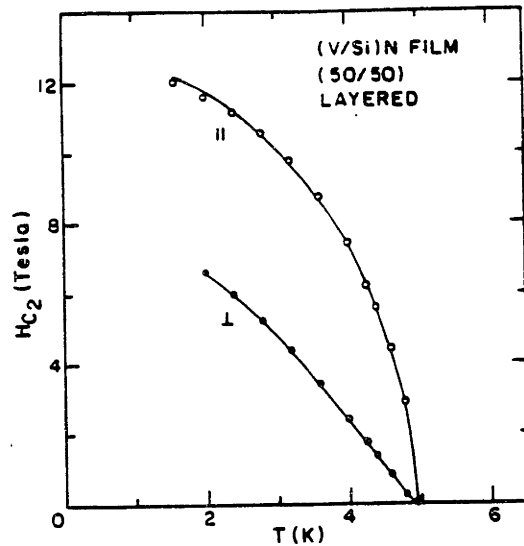

Fig. 6. Layered (V/Si)N film with a total of six 50 Å layers. (o), || critical field. (·) $\perp$ critical field. The solid curves are fits to the WHH theory. For the parallel case we used $C_F = 0.2$, $\lambda_{so} = 1.3$, whereas for the perpendicular case λ_{so} was 1.9.

lel and perpendicular curves very close to T_c, we get $\xi_\perp(0) = 14.0$ Å (see ref. 11, Eqs. 17 and 18). Thus, the interlayer coupling constant r is only .07. Despite this weak coupling, we do observe a decrease in T_c with increasing Si layer thickness for films with the same V layer thickness. For example, films with 40 Å V layers separated by 20 Å of Si had T_c's close to 6 K. When the Si layer thickness was increased to 35 Å the T_c decreased to 4.8 K.
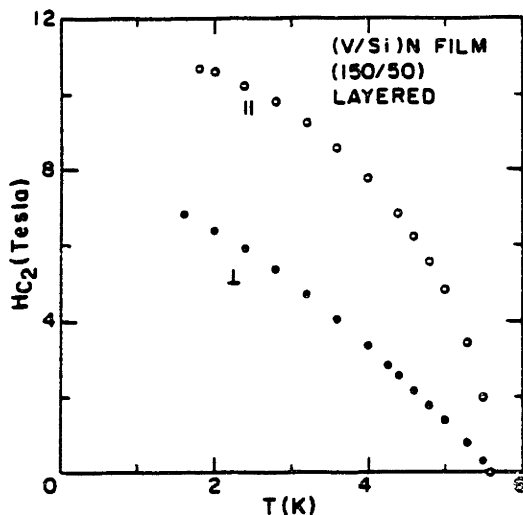

Fig. 7. Layered (V/Si)N film with three 150 Å V layers and three 50 Å Si layers. (o), $||$ critical field and (·), $\perp$ critical field.

In fitting the perpendicular critical field curves for the V(Mo)N samples shown in Figs. 2 and 3 to the WHH theory we got spin-orbit scattering values of λ ~ 2.3 for the coevaporated film and λ_{so} ~ 7.8 for the layered film, assuming no renormalization correction. Thus, spin-orbit scattering is stronger in the layered films. For the (V/Si)N film shown in Fiure 6 we got values of 1.3 and 1.9 for the parallel and perpendicular fits, respectively. One would expect a lower spin-orbit scattering rate at an interface with Si than with the higher atomic number element Mo. These values of λ_{so} are certainly higher than the λ_{so} of -0.4 we obtained for pure VN.*

In summary, we have studied both layered and coevaporated V(Mo)N samples and (V/Si)N multilayer structures. We have in no case obtained a T_c higher than that for VN in either our layered or coevaporated V(Mo)N films. We have seen evidence for dimensional crossover in the parallel critical field of a (V/Mo)N structure with 50 Å layers. We can rule out spurious factors such as edge effects because we don't see this behavior in our coevaporated films. Also, we have not seen any dimensional crossover effects in layered (V/Si)N samples of similar thickness. Perhaps this is because the proximity effect coupling in (V/Mo)N is much stronger than the Josephson coupling which occurs in (V/Si)N. Despite this, we have found that the T_c of (V/Si)N multilayers decreases with increasing Si layer thickness. This indicates that the VN layers are somewhat coupled. Thinner structures may show dimensional crossover effects. The spin-orbit scattering rate is significantly larger in the layered

(V/Mo)N films than in the coevaporated ones. (V/Mo)N multilayers also appear to have more spin-orbit scattering than the layered (V/Si)N films.

References

*Supported by AFOSR contract no. F49620-82-K-0028.

1. J.E. Tkaczyk and P.M. Tedrow, "Critical field measurements on very thin films of V-Ga superconductors," Advances in Cryogenic Engineering Materials, 32, 1093-1099, 1986.

2. P.M. Tedrow and R. Meservey, "Experimental test of the theory of high-field superconductivity," Phys. Rev. Lett., 43, 384-387, 1979; R. Meservey and P.M. Tedrow, "Surface relaxation times of conduction-electron spins in superconductors and normal metals," Phys. Rev. Lett., 41, 805-808, 1978.

3. W.E. Pickett, B.M. Klein, and D.A. Papaconstantopoulos, "Theoretical prediction of MoN as a high T_c superconductor," Physica, 107B, 667-668, 1981.

4. W. Lawrence and S. Doniach, "Theory of layer structure superconductors," Proc. of the 12th International Conference on Low Temperature Physics, E. Kanda, Ed., Academic Press of Japan, Tokyo, 361-363, 1971.

5. R.A. Klemm, A. Luther, and M.R. Beasley, "Theory of the upper critical field in layered superconductors," Phys. Rev. B, 12, 877-891, 1975.

6. S. Takahashi and M. Tachiki, "Theory of the upper critical field of superconducting superlattices," Phys. Rev. B, 33, 4620-4631, 1986.

7. S. Takahashi and M. Tachiki, "New phase diagram in superconducting superlattices," Phys. Rev. B, 34, 3162-3164, 1986.

8. N.R. Werthamer, E. Helfand, and P.C. Hohenberg, "Temperature and purity dependence of the superconducting critical field, H_{c2}. III. Electron spin and spin-orbit effects," Phys. Rev., 147, 295-302, 1966; P. Fulde, "High field superconductivity in thin films," Adv. in Physics, 22, 667-719, 1973.

9. J.S. Moodera, P.M. Tedrow, and R. Meservey, "Critical field studies of reactively sputtered and nitrided NbN, VN and V(Mo)N films," Advances in Cryogenic Engineering Materials, 32, 679-686, 1986.

10. N. Pessall, J.K. Hulm, and M.S. Walker, Final Report No. AF33, Westinghouse Research Laboratories, 1967.

11. S.T. Ruggiero and M.R. Beasley, "Synthetically layered superconductors," Chap. 10 in Synthetic Modulated Structures, L.L. Chang and B.C. Giessen, Eds.; Academic Press, Inc., New York, 1985.

Critical-magnetic-field anisotropy in single-crystal YBa2Cu3O7

J. S. Moodera, R. Meservey, J. E. Tkaczyk, C. X. Hao, G. A. Gibson, and P. M. Tedrow

Francis Bitter National Magnet Laboratory, Massachusetts Institute of Technology,
Cambridge, Massachusetts 02139

(Received 21 September 1987)

We have measured the critical magnetic fields $H_{c2\parallel}$ (parallel to a-b plane) and $H_{c2\perp}$ (perpendicular to a-b plane) of single crystals of YBa2Cu3O7 as a function of temperature in fields up to 19 T. The slope $-dH_{c2}/dT$ is greater by about a factor of 4 when the field is applied parallel to the a-b plane than when it is applied parallel to the c axis.

I. INTRODUCTION

One important aspect of the high-T_c oxide superconductors[1] is the degree of anisotropy of their electronic properties arising from their layered crystal structure. Measurements of the critical magnetic field of polycrystalline samples gave hints of anisotropy;[2] however, recent experiments on single-crystal specimens have begun to show directly the extent of this anisotropy.[3-6] We present here critical-field measurements as a function of field direction on single crystals of YBa2Cu3O7 grown in our laboratory.

II. EXPERIMENTAL TECHNIQUE

YBa2Cu3O7 single crystals were grown by two different methods. In the first method, during the formation of the Y-Ba-Cu-O compound for fabricating sintered pellet samples, crystals formed on the surface of the reacted powder. These crystals, $2 \times 2 \times 0.3$ to $\sim 1 \times 1 \times 0.1$ mm^3 in size, were carefully removed and annealed in O2. X-ray transmission Laue patterns showed them to be single crystals but with severe twinning. The second method of crystal growth was similar to that developed by Dinger, Worthington, Gallagher, and Sandstrom[7] and yielded many extremely flat, small crystals (area < 1 mm^2 and thickness $\lesssim 10$ μm), which were subsequently O2 annealed. Laue patterns of these samples proved them to be good single crystals with the c axis perpendicular to the flat face and with little twinning. Diagnostic susceptibility and resistivity measurements of these types of crystals showed them to be superconducting, with transition temperatures 92.5 ± 2 K for the twinned Y-Ba-Cu-O crystals (which we designate type B) and 89.7 ± 2.4 K for the less twinned crystals (which we designate type A). We present here critical field data for both types of crystal.

Gold wires were attached with silver paint to copper contacts evaporated onto the sample for four-terminal resistance measurement. The upper critical fields were determined by the resistive transition. Our earlier attempts with silver epoxy contacts invariably failed at low temperature, but with evaporated Cu contact pads, the leads remained good. For resistivity versus magnetic field measurements at various temperatures, the samples were mounted on a rotatable copper plate with a Pt resistance

thermometer adjacent to the sample. A small wire-wound heater supplied heat to the whole copper plate, thereby giving good stability in sample temperature. Helium exchange gas provided contact to the liquid-N2 bath. A superconducting magnet with a room-temperature bore provided a magnetic field up to 15 T, and higher fields were obtained in a water-cooled Bitter magnet. The sample temperature was swept through the transition at various fixed fields. Critical field data were taken for both orientations $H_{c2\parallel}$ and $H_{c2\perp}$ (parallel and perpendicular to the a-b plane, respectively) in the same run by changing the sample orientation.

III. EXPERIMENTAL RESULTS

A resistivity measurement done in the a-b plane of a type-A crystal in zero applied field is plotted against temperature in Fig. 1. At 280 K, ρ was estimated to be about 400 $\mu\Omega$ cm. The shape of the crystal was not ideal for determining the size of the conducting path, leading to a large uncertainty. The resistivity decreases linearly as T decreases with a slope of 1.46 $\mu\Omega$ cm/K, reaching a value of about 140 $\mu\Omega$ cm at 100 K. A line drawn through the data points extrapolates close to the origin. For comparison, the resistivity variation with temperature for a high-quality sintered pellet of Y-Ba-Cu-O is also shown in this
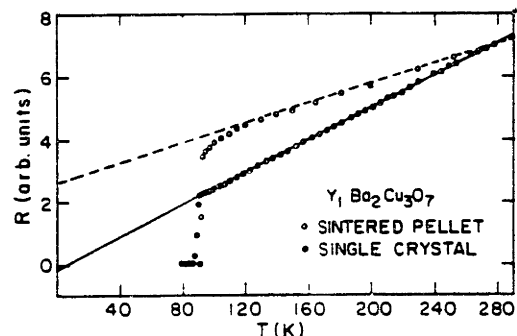

FIG. 1. Resistance vs temperature of a type-A single crystal and polycrystalline sample of YBa2Cu3O7.

figure. As in sintered pellets, ρ decreases linearly with T to about 120 K. However, below this temperature there is a deviation from the linear behavior in the pellet, which has been attributed[8] to superconducting fluctuations and which is not visible in the single-crystal data. The slope at $d\rho/dT$ is different in the two cases, which is not surprising since in the sintered pellet, grain boundaries play a significant role in the conduction process.

The measured upper critical fields of the type-A crystal as a function of temperature are shown in Figs. 2 and 3. The transition temperature $T_c(H)$ was taken to be that temperature at which the resistance dropped to half of its value in the normal state at a measuring current of 200 μA (≈ 10 A/cm^2). It was found that the T_c did not change with measuring currents from 100 μA to 500 μA, apparently eliminating the possibility of critical current or heating effects being significant. The temperatures have been corrected for the magnetoresistance of the Pt thermometer;[9] the corrections are as large as 1.2% at 15 T but decrease rapidly at lower fields. The transition temperature in zero-field $T_{c0}=89.7$ K with a transition width of 2.4 K. As the magnetic field increased, the transition width increased, too. The midpoint as well as the 10% and 90% points of the resistive transition are shown in Figs. 2 and 3. The resistance for the normal state at any temperature and field was taken to be the extrapolation of the normal state shown in Fig. 1 to lower temperatures. As the temperature is lowered below T, $H_{c2\|}$ rises sharply, with a positive curvature close to T_c. The slope $dH_{c2\|}/dT$
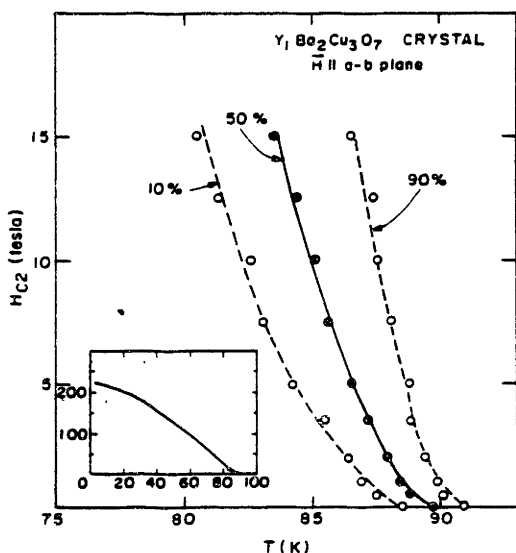

FIG. 2. Critical magnetic field vs temperature of a type-A crystal with the field in the a-b plane. The temperature at which 10%, 50%, and 90% of the normal-state resistance are restored are indicated for each field value. The inset shows the range of field and temperature covered by the measurements compared to the entire estimated phase boundary.
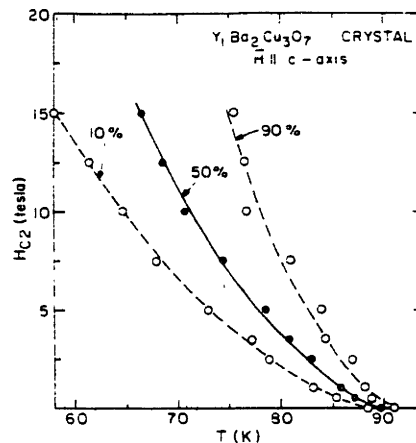

FIG. 3. Critical magnetic field vs temperature of a type-A crystal with the field perpendicular to the a-b plane. The temperatures at which 10%, 50%, and 90% of the normal-state resistance are restored are indicated for each field value.

near T_{c0} is -0.7 T/K, whereas at about 85 K the slope is about -3.6 T/K. For $H_{c2\perp}$ the curvature persists down to the lowest temperature at which $H_{c2\perp}$ could be measured. A slope of -0.2 T/K was found very close to T_{c0} and -1.1 T/K near 67 K. To estimate $H_{c2\perp}(0)$, the critical field at $T=0$, we use the formula $H_{c2\perp}(0)=0.69$ $[dH_{c2\perp}(T)/dT]T'$. Here the slope is chosen to be the tangent to the curve near the highest field (15 T) and T' is at the intersection of this tangent with the temperature axis. From this $H_{c2\perp}(0)=61$ T, giving a calculated coherence distance in the a-b plane $\xi_{ab}(0)=23$ Å. In a similar manner, $H_{c2\|}(0)$ is estimated to be 222 T. However, the small temperature range, combined with the arbitrary use of a resistance equal to one-half of the normal-state resistance as the criterion to determine $T_c(H)$, makes the uncertainty of $H_{c2}(0)$ as large as 25% even if the simple theory is valid for this material. With these reservations, and assuming there is strong Josephson coupling between layers and that $H_{c\perp}(0)/H_{c\|}(0) = \xi_c(0)/\xi_{ab}(0)$, the coherence distance perpendicular to the a-b plane $\xi_c(0)$ is probably no more than 6.3 Å. The transition width at $H_{c2\perp}$ becomes much wider than that at $H_{c2\|}$ over the field range available, but it should be noted that *as a function of temperature* the transition widths broaden at about the same rate below T_{c0}. The high anisotropy of these crystals is shown by the ratios $H_{c2\|}(0)/H_{c2\perp}(0) = \xi_{ab}(0)/\xi_c(0)=3.6$.

The critical field measurements for type-B crystals are shown in Fig. 4. In this case, two crystals from the same batch were mounted with their c axis perpendicular to each other, so that the two curves representing the two crystalline directions are for different but similar crystals. The behavior of H_{c2} is more conventional in appearance in this case, with $H_{c2\|}$ being nearly linear in T with a slope of -4 T/K, and $H_{c2\perp}$ having negative curvature with a slope of -0.96 T/K near T_{c0}. The conventional dirty-limit
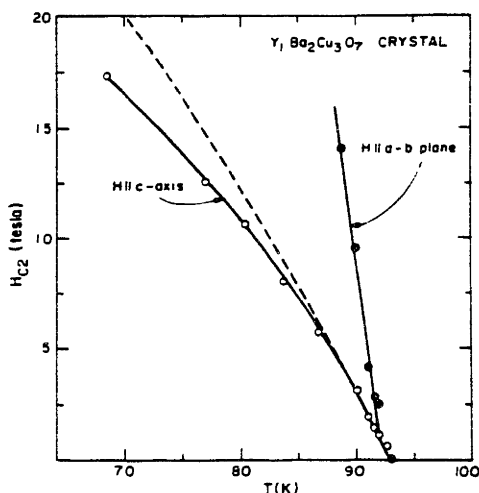
FIG. 4. Critical magnetic field vs temperature of a type-B crystal for the field in the a-b plane (◉) and perpendicular to the a-b plane (●). The dashed line is the calculated critical field using the slope near T_{c0} of the perpendicular data.

theory[10] with this slope is shown for comparison by the dashed line, although the dirty-limit theory may not apply to this material because of the short coherence length. The extrapolated values of $H_{c2\parallel}(0)$ and $H_{c2\perp}(0)$ are 256 and 62 T, respectively.

IV. DISCUSSION

As we have seen, the two types of crystal have values of dH_{c2}/dT and ξ for the respective directions which agree within about 10% in spite of the details of the temperature dependence near T_{c0}. Further work is needed to determine what part of the differences in the two kinds of crystal is fundamental and what part is materials related. The more nearly perfect crystal, type A, was presumably somewhat deficient in oxygen, judging from the slightly reduced T_{c0}. Inhomogeneity might lead to the positive curvature we observed. The inset in Fig. 2 makes an important point, however, indicating the range of field and temperature explored in this experiment. Many superconductors show nonconventional critical-field behavior this

close to T_{c0}.

A number of other groups have made measurements of H_{c2} on single crystals. Results by Iye, Tamegai, Takeya, and Takei[4] in fields up to 9 T are qualitatively very similar, showing the strong anisotropy and curvature near T_{c0} of both $H_{c2\parallel}(T)$ and $H_{c2\perp}(T)$. Analyzed in the same manner as our results, the data of Iye et al. give $H_{c\perp}(0){\approx}61$ T and $\xi_{ab}(0){\approx}23$ Å exactly as we obtained, whereas there is only 5% difference in the $H_{c2\parallel}$ values. [Iye et al. took $R{\approx}0$ to define $T_c(H,T)$, so their analysis is somewhat different.] Hidaka et al.[3] have also measured the critical fields of a single crystal of Y-Ba-Cu-O using the dc resistance method. They give a value of anisotropy factor of 5.5 in the critical fields; these data analyzed in the same way as ours appear to give a value of $H_{c\parallel}(0)/H_{c\perp}(0) \approx 7$. Both of these dc measurements were qualitatively similar to our results. There was strong anisotropy as well as strong curvature in both $H_{c\parallel}$ and $H_{c\perp}$ near T_{c0}. Also, there was an increased transition width as T was lowered below T_c. Worthington, Gallagher, and Dinger[5] have measured the critical fields of Y-Ba-Cu-O crystals by defining $T_c(H)$ as the temperature of the most rapid change in reflected power from a 0.70 MHz resonant coil surrounding the crystal. They obtain a value of $H_{c2\perp}(0){\approx}29$ T which implies $\xi_{ab}(0){\approx}34$ Å and $H_{c2\parallel}(0){\approx}140$ T, giving a value of $\xi_{\perp}(0){\approx}7$ Å. The critical fields show no curvature but $H_{c\perp}$ does not have a change of slope at 77 K. Noel et al.[6] have measured the anisotropy in the critical field to be about 8 for a single crystal of $TmBa_2Cu_3O_7$ by a resistive technique.

In summary, the various experiments give a value between 4 and 8 for the anisotropy in the critical field. As better characterized and more homogeneous samples become available, such matters as the details of the temperature dependence of H_{c2} can be cleared up. In addition, measurements to much higher fields are desirable as these would indicate the validity of the conventional theory[10] of the critical field at lower temperatures.

[1]J. G. Bednorz and K. A. Müller, Z Phys. B 64, 189 (1986); M. K. Wu, J. R. Ashburn, D. J. Torng, P. H. Hor, R. L. Meng, L. Gao, Z. J. Huang, Y. Q. Wang, and C. W. Chu, Phys. Rev. Lett. 58, 908 (1987); R. J. Cava, B. Batlogg, R. B. van Dover, D. W. Murphy, S. Sunshine, T. Siegrist, J. P. Remeika, E. A. Rietman, S. Zahurak, and G. P. Espinosa, ibid. 58, 1676 (1987).

[2]Y. Hidaka, Y. Enomoto, M. Suzuki, M. Oda, and T. Murakami, Jpn. J. Appl Phys. 26, L377 (1987); D. O. Welch,

M. Suenaga, and T Asano, Phys. Rev. B 36, 2390 (1987); T. P. Orlando, K. A. Delin, S. Foner, E. J. McNiff, J. M. Tarascon, L. H. Greene, W. R. McKinnon, and G. W. Hull, ibid. 36, 2394 (1987).

[3]Y. Hidaka, Y. Enomoto, M. Suzuki, M. Oda, A. Katsui, and T. Murakami, Jpn. J. Appl. Phys. 26, L726 (1987).

[4]Y. Iye, T. Tamegai, H. Takeya, and H. Takei, Jpn. J. Appl. Phys. 26, L1057 (1987).

[5]T. K. Worthington, W. J. Gallagher, and T. R. Dinger, Phys.

Rev. Lett. **59**, 1160 (1987).

[6]H. Noel, P. Gougeon, J. Padiou, J. C. Levet, M. Potel, O. Laborde, and P. Monceau, Solid State Commun. **63**, 915 (1987).

[7]T. R. Dinger, T. K. Worthington, W. J. Gallagher, and R. L. Sandstrom, Phys. Rev. Lett. **58**, 2687 (1987).

[8]P. P. Freitas, C. C. Tsuei, and T. S. Plaskett, Phys. Rev. B **36**, 833 (1987); J. S. Moodera, P. M. Tedrow, and J. E. Tkacyzk, *ibid.* **36**, 8329 (1987).

[9]H. H. Sample, B. L. Brandt, and L. G. Rubin, Rev. Sci. Instrum. **53**, 1129 (1982).

[10]N. R. Werthamer, E. Helfand, and P. C. Hohenberg, Phys. Rev. **147**, 295 (1966).

Electron-Spin Polarization in Tunnel Junctions in Zero Applied Field with Ferromagnetic EuS Barriers

J.S. Moodera, X. Hao, G.A. Gibson, and R. Meservey

Francis Bitter National Magnet Laboratory
Massachusetts Institute of Technology
Cambridge, MA 02139

Abstract

An electron-spin polarization P as much as 80% has been observed in the tunnel current in Au/EuS/Aℓ tunnel junctions. P can be explained by the different heights of the tunnel barriers for the two spin directions. The Zeeman splitting of the Aℓ quasiparticle density of states is greatly enhanced by the exchange interaction at the EuS/Aℓ interface. Spin polarization was even seen in zero applied field. The value of P calculated from the tunneling theory using known barrier heights in EuS is consistent with the measured values.

The discovery of Zeeman splitting of the quasiparticle density of states of superconducting Aℓ[1] immediately led to the ability to determine the electron-spin polarization P of tunnel currents. Using this technique, the value of P for electrons tunneling in $Aℓ/Aℓ_2O_3$/Ferromagnetic-metal junctions was extensively studied in Ni, Co, Fe and 3d alloys as well as in some rare-earth metals.[2-4] In these experiments the spin polarization was attributed to the difference in the spin densities of states of the itinerant electrons in the ferromagnets at the Fermi energy.[5] In contrast to these earlier results, the present experiments show for the first time electron-spin polarization of the tunneling current between nonferromagnetic electrodes. This effect can be explained by the different barrier heights for the two spin directions in the ferromagnetic insulator separating the metals. The barrier thus acts as a spin filter.

The EuS chalcogenides have been extensively investigated.[6,7] Several studies of EuS are closely related to the present observations. Esaki et al.[8] reported an internal field emission study of junctions having magnetic semiconductors EuS and EuSe as barriers 20 to 60 nm thick. They observed an increase of field emission current as the temperature was lowered to below the magnetic ordering temperature of the barrier and interpreted it as caused by the decrease of barrier height when spin ordering takes place. Similar results were obtained by Thompson et al.[9] with Schottky barriers made on n-type doped semiconducting single crystal EuS. Field emission studies[10-12] on EuS-coated tungsten tips showed a high degree of polarization of the field-emitted electrons below the Curie temperature of EuS, $T_c = 16.7$ K.[6] These results were explained by the spin filter effect in EuS below T_c.

In the present study, tunnel junctions were prepared in a conventional way by vacuum deposition on glass slides. Different types of junctions were made and in every case one of the metal electrodes was a 4 to 4.4 nm thick Aℓ film deposited on a liquid-nitrogen cooled substrate. The other electrode was a film of Au, Aℓ, or Fe. The tunnel barrier was an EuS film formed by evaporation using an electron gun on a pressed pellet of EuS. The average thickness of the EuS barriers used in this work was about 2.5 nm as determined by a rotating sector disk and a quartz crystal thickness monitor. The best tunneling results were obtained with junction resistances of 1 to 20 kΩ, for junction areas $\approx 4 \times 10^{-4}$ cm^2. The junctions fabricated were Au/EuS/Aℓ, Aℓ/EuS/Aℓ, Aℓ/EuS/Fe and Fe/EuS/Aℓ, where in each case materials are listed in the order in which they are deposited. Although usually all three materials were deposited on liquid-nitrogen-cooled substrates, in some cases the Au and EuS films were deposited at room temperature. Even though the yield of good tunnel junctions was greater on cold substrates, higher polarizations were found for the higher temperature depositions. X-ray diffraction of 100 nm EuS control films deposited at 80 K, 300 K, and 400 K all indicated the films to be polycrystalline and the line positions agreed with the diffraction pattern taken on an EuS powder sample. Selected junctions were cooled in a He^3 refrigerator equipped with a superconducting magnet, and conductance dI/dV versus V was measured at 0.4 K as a function of the magnetic field H applied parallel to the film surface. Current-voltage curves with bias up to 1 V were also made at various temperatures, from 1.1 K to 20 K. We present here mainly the results from the Au/EuS/Aℓ junctions; the other types of junctions showed qualitatively similar behavior. Two sets of Au/EuS/Aℓ junctions were carefully studied. We refer to them as set 1 and set 2. All three

materials in junctions of set 1 were deposited onto sub-strates at T ≈ 80 K, while in junctions of set 2 the Au and EuS films were deposited onto substrates at T ≈ 300 K.

Figure 1 shows measurements at 0.4 K of the differential conductance dI/dV vs. voltage V of a Au/EuS/Aℓ junction of set 1. The Aℓ film was superconducting with a transition temperature of 2.33 K. The curve labelled 0 was made before any magnetic field was applied, and the superconducting energy gap of Aℓ, 2Δ, is clearly seen. dI/dV at V = 0 was 1.4% of the normal state conductance, showing that the conduction process is almost entirely tunneling. As we applied a magnetic field H parallel to the plane of the junction, the conductance peaks were each split by the Zeeman energy because of the magnetic moment of the electron μ. At a value of H ≈ 1.5 T the paramagnetic limit is reached and the Aℓ film becomes normal. For a tunnel junction with a thin Aℓ electrode, a nonmagnetic barrier such as $Aℓ_2O_3$, and a normal metal counterelectrode, the Zeeman splitting in the superconducting quasiparticle density of states is equal to 2μH. However, the splittings shown in Fig. 1 are much greater than those corresponding to the applied field. This is similar to, although more extreme than, the enhanced Zeeman splittings found by Tedrow et al.[13] when Aℓ films are in contact with various rare-earth oxides. In this situation the conduction electrons of the thin Aℓ film are subjected to an effective internal field B caused by exchange scattering with the rare-earth ions in the insulator. The critical field of the Aℓ was reached when H ≈ 1.5 T which corresponds to a value of B ≈ 5 T, the paramagnetic critical field H_{cp} for Aℓ films of this thickness.[14] When H was reduced to zero (curve labelled 0' in Fig. 1) the Zeeman splitting persisted, corresponding to an effective internal field B ≈ 1.6 T. This effect was seen in all the EuS junctions studied, but had never

been observed previously with spin-polarized tunneling measurements. This hysteresis perhaps implies a remanent magnetization of the EuS as will be discussed below. A hysteresis in the resistivity of highly doped EuS reported by Shapiro and Reed[15] may be closely related. A striking feature of the data of Fig. 1 is the pronounced asymmetry which implies a large value of the electron-spin polarization of the tunneling current. A simple analysis neglecting spin-orbit scattering in the Aℓ film gives a value of P ≈ 74%. To obtain accurate values of P we used the complete theory[16,17] and fitted the curves; the best fit gave values of P = 55±5% and the spin-orbit scattering parameter $b = \frac{\hbar}{3\tau_{so}\Delta_o} = 0.05.$[17,18]

Figure 2 shows a characteristic junction from set 2 (Au and EuS deposited at 300 K). Zeeman splitting of the quasiparticle density of states in the superconducting Aℓ film and polarization of the tunnel current were present even before any magnetic field (other than the ambient field ≈ 1 Oe) had been applied. In this case, in an applied magnetic field as small as 0.15 T, H_{cp} was already reached. The polarization obtained by fitting the curves in Fig. 2 is P = 80±5%. This is the largest value of P obtained to date for a tunnel junction. The uncertainty in P comes from the fact that the effective internal field B is only known from the Zeeman splitting which is also affected by spin-orbit scattering, unlike previous experiments in which the internal field B is essentially equal to the applied field H. This situation is made worse in the present situation by the small range of B available before the H_{cp} of the Aℓ film is reached. Other types of junctions gave qualitatively similar results. For Aℓ/EuS/Aℓ, P ≈ 20%, for 80 K deposited Aℓ/EuS/Fe, P ≈ 40%, and P ≈ 65% for Fe/EuS/Aℓ with Fe and EuS deposited at elevated temperature. For the Fe electrode the

degree to which the Fe determined P is not yet known and is subject to further study.

The increase in P for the Au and EuS deposited at 300 K presumably results from the greater crystallite and domain size of the EuS when it is formed on Au of large crystallite size. A 30 nm thick Au film deposited on SiO_2 at room temperature has grains as large as 600 nm in size.[19] Conversely, Au deposited at low temperatures has a smaller grain size, and Aℓ and Fe are known to have an even smaller average crystallite size than Au when deposited at 80 K; these films probably introduce more disorder into the EuS film. For $T \ll T_c$ of EuS the spin-filter effect polarizes the tunnel current through each EuS domain even at H = 0, although the direction of the magnetization $\vec{M}$ may be different in each domain. If the characteristic domain size is L and the superconducting coherence distance is ξ, then for L $\ll \xi$ contributions of the exchange field to the effective field in the Aℓ film from differently oriented domains will tend to cancel over an Aℓ film area $\approx \xi^2$, leading to zero Zeeman splitting, and consequently polarization cannot be detected. On the other hand, for $L \geq \xi$ the B field in each area ξ^2 of the Aℓ film has a uniform direction and will lead to a large Zeeman splitting even when the direction of $\vec{M}$ varies between domains; in this case, polarization will be seen at H = 0. The hysteresis effect observed could be caused by remanent orientation of the domains. However, the present experiments cannot rule out a model in which the size of the domains is increased, even if their orientation is disordered when H returns to zero.

Independent of fitting the asymmetry of the superconducting tunnel conductance, we can estimate the expected value of P from known properties of EuS and from I versus V for voltages above the superconducting gap. For this analysis we assume for Au/EuS/Aℓ junctions a barrier of the form shown

in Fig. 3. Above the bulk EuS Curie temperature T_c = 16.7 K,[6] the barrier height (shown by the dashed line) is determined by the position of the bottom of the EuS conduction band with respect to the Fermi level of the metals. Using the values for the work functions $W_{A\ell}$ = 4.1 eV and W_{Au} = 5.0 eV,[20] and the electron affinity for EuS,[21] X_{EuS} = 2.5 eV, we infer values of the barrier heights at the interfaces of ϕ_1 = 2.5 eV and ϕ_2 = 1.6 eV. The average barrier height is thus ϕ = $(\phi_1 + \phi_2)/2$ = 2.05 eV. The tunnel current for such a barrier according to Simmons[22] is given approximately by

$$J = J_o(\phi - \frac{eV}{2})\exp\left[-A(\phi - \frac{eV}{2})^{\frac{1}{2}}\right]$$

$$- J_o(\phi + \frac{eV}{2})\exp\left[-A(\phi + \frac{eV}{2})^{\frac{1}{2}}\right] \tag{1}$$

where J_o = $(e/2\pi h)S^{-2}$ and A = $(4\pi S/h)(2m)^{\frac{1}{2}}$, with S being the thickness of the barrier and m the electron effective mass in the conduction band. At 20 K, which is above T_c, we can calculate values of ϕ and S which fit the measured values of $J(V)$. For two junctions of set 1 we obtained the values S = 1.76 nm, ϕ = 2.15 eV and S = 1.89 nm, ϕ = 2.015 eV. These values for ϕ differ by less than 5% from that obtained from the work function. The values of S are reasonable for the effective tunneling thickness in a junction of average thickness = 2.5 nm and are close to what one expects by comparison to $A\ell_2O_3$ barriers. The difference in m from the free electron mass is small and is assumed to be absorbed in an effective value of S. Below T_c, the conduction band of EuS is split by the ferromagnetic exchange interaction and the barrier is split in height for the two spin directions

as shown by the continuous lines in Fig. 3. Using the bulk value of the exchange splitting in EuS, ΔE_{ex} = 0.36 eV,[6] the calculated average barrier heights for the above junctions are $\phi\downarrow$ = 2.33 eV, $\phi\uparrow$ = 1.97 eV for S = 1.76 nm and $\phi\downarrow$ = 2.20 eV, $\phi\uparrow$ = 1.84 eV for S = 1.89 nm. Using Eq. (1) for each spin direction to calculate J↑ and J↓ we find that J = J↑ + J↓ agrees with the current measured at 1.1 K from 2×10^{-3} V to 0.4 V within about 10% in these two junctions. Values obtained for the polarization of the tunnel current P = (J↑ - J↓)/(J↑ + J↓) were 79% and 83%, respectively, with an uncertainty of 5%. These are maximum values for these junction parameters and assume that there is no spin scattering or other degrading effects. Since this measurement only relies on the normal state properties of the Aℓ electrode it is unnecessary for L to be larger than ξ to obtain the full spin-filter effect at H = 0. The agreement of this calculation with the value of 80±5% for the set 2 junctions is strong evidence for the correctness of the spin-filter model. Also, the temperature dependence of tunnel junction resistance is consistent with that expected from the temperature dependence of exchange splitting in the bulk EuS crystal.[23]

Very recently, tunneling in EuS/Aℓ/Aℓ$_2$O$_3$/Ag junctions has been investigated[24] in our laboratory: enhanced Zeeman splitting was observed in Aℓ but no polarization was detected. This shows that the polarization observed with EuS barrier is due to spin filtering; the exchange-induced splitting in Aℓ is a separate consequence of the ferromagnetic ordering of the EuS.

The high value of polarization obtained with EuS should be useful as a source of spin-polarized electrons in tunneling. Even higher values of P can probably be obtained with other ferromagnetic insulators or semiconductors. The method also provides a way of measuring the exchange splitting

for thin films of such substances. The ability to do spin-polarized tunneling studies in zero applied field will allow many new types of measurements of magnetic and superconducting materials.

References

1. R. Meservey, P.M. Tedrow, and P. Fulde, Phys. Rev. Lett. 25, 1270 (1970).

2. P.M. Tedrow and R. Meservey, Phys. Rev. B7, 318 (1973).

3. D. Paraskevopoulos, R. Meservey, and P.M. Tedrow, Phys. Rev. B16, 4907 (1977).

4. R. Meservey, D. Paraskevopoulos, and P.M. Tedrow, Phys. Rev. B22, 1331 (1980).

5. M.B. Stearns, J. Magn. Magn. Mat. 5, 167 (1977).

6. P. Wachter, Chapter 19, Handbook on the Physics and Chemistry of Rare Earths, edited by K.A. Gschneider, Jr. and L. Eyring, (North Holland, Amsterdam, 1979).

7. A. Manger and C. Godart, Phys. Reports 141, 51 (1986).

8. L. Esaki, P.J. Stiles, and S. von Molnar, Phys. Rev. Lett. 19, 852 (1967).

9. W.A. Thompson, F. Holtzberg, T.R. McGuire, and G. Petrich, in AIP Conf. Proc. No. 5, 827 (1971).

10. N. Müller, W. Eckstein, W. Heiland, and W. Zinn, Phys. Rev. Lett. 29, 1651 (1972).

11. E. Kisker, G. Baum, A.H. Mahan, W. Raith, and K. Schröder, Phys. Rev. Lett. 36, 982 (1976).

12. G. Baum, E. Kisker, A.H. Mahan, W. Raith, and B. Reihl, Appl. Phys. 14, 149 (1977).

13. P.M. Tedrow, J.E. Tkaczyk, and A. Kumar, Phys. Rev. Lett. 29, 1651 (1986).
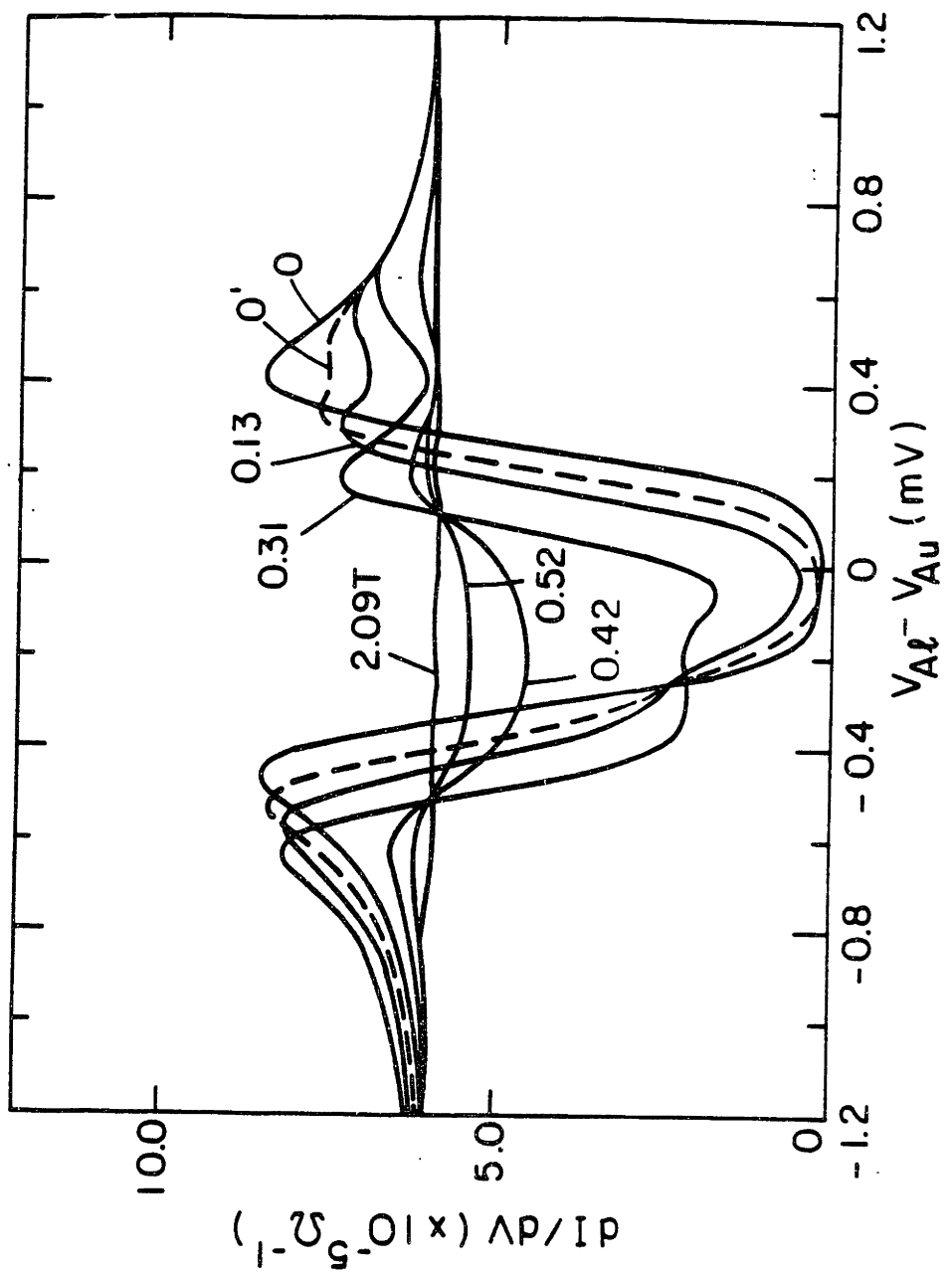
14. P.M. Tedrow, R. Meservey, and B.B. Schwartz, Phys. Rev. Lett. $\underline{24}$, 1004 (1970).

15. Y. Shapira and T.B. Reed, Phys. Rev. B$\underline{5}$, 4877 (1972).

16. J.A.X. Alexander, T.P. Orlando, D. Rainer, and P.M. Tedrow, Phys. Rev. B$\underline{31}$, 5811 (1985).

17. P. Fulde, Adv. Phys. $\underline{22}$, 667 (1973).

18. R.C. Bruno and B.B. Schwartz, Phys. Rev. B$\underline{8}$, 3161 (1973).

19. C.C. Wang, Ph.D. Thesis MIT (1986), unpublished.

20. S.M. Sze, Physics of Semiconductor Devices, 2nd ed. (John Wiley, New York, 1981), p. 396.

21. D.E. Eastman, F. Holtzberg, and S. Methfessel, Phys. Rev. Lett. $\underline{23}$, 226 (1969).

22. J.G. Simmons, J. Appl. Phys. $\underline{34}$, 2581 (1963).

23. P. Wachter, CRC Crit. Rev. in Solid State Sci. $\underline{3}$, 189 (1972).

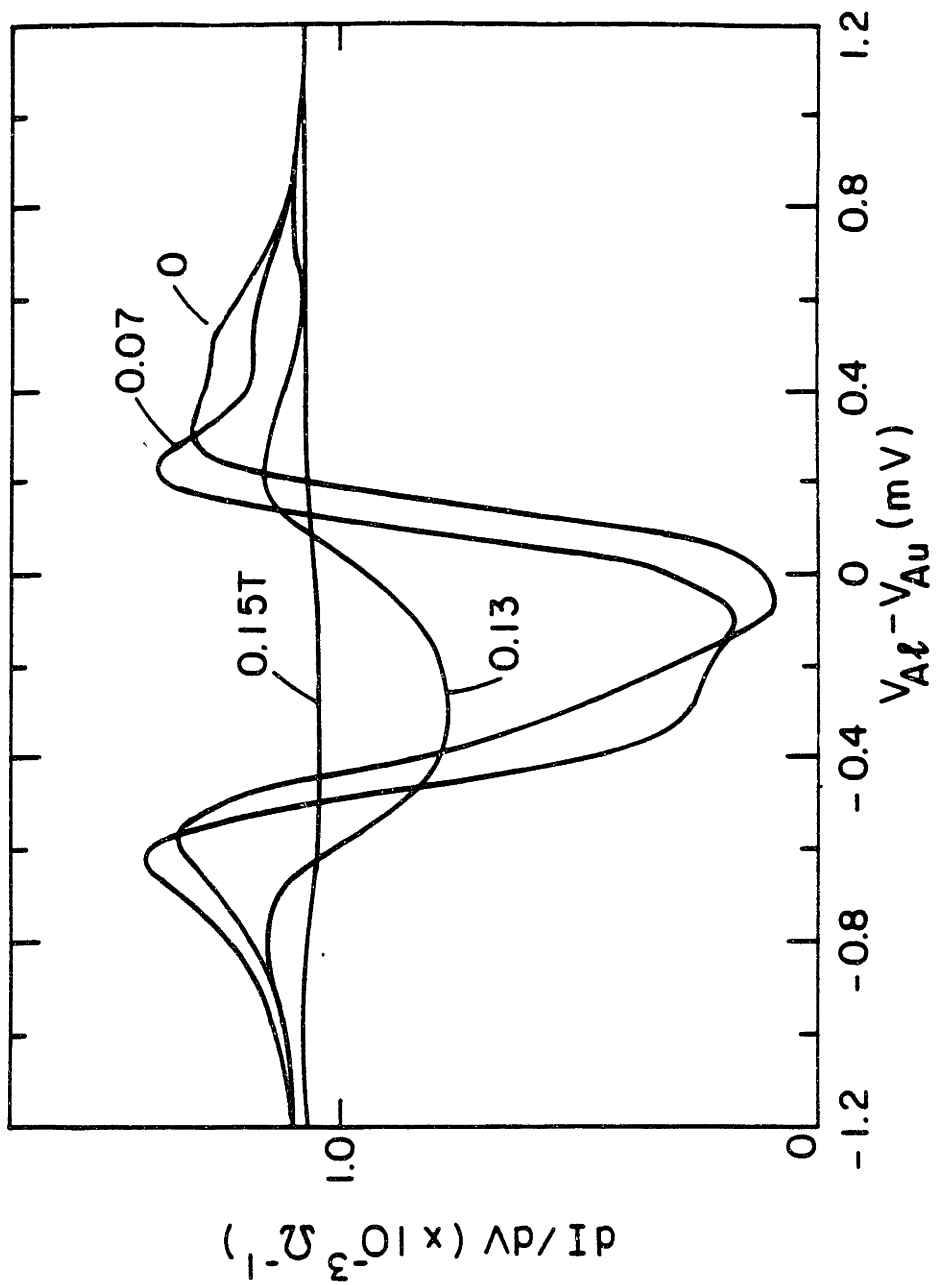24. J.E. Tkaczyk, Ph.D. Thesis, MIT, 1988, (unpublished).

Figure Captions

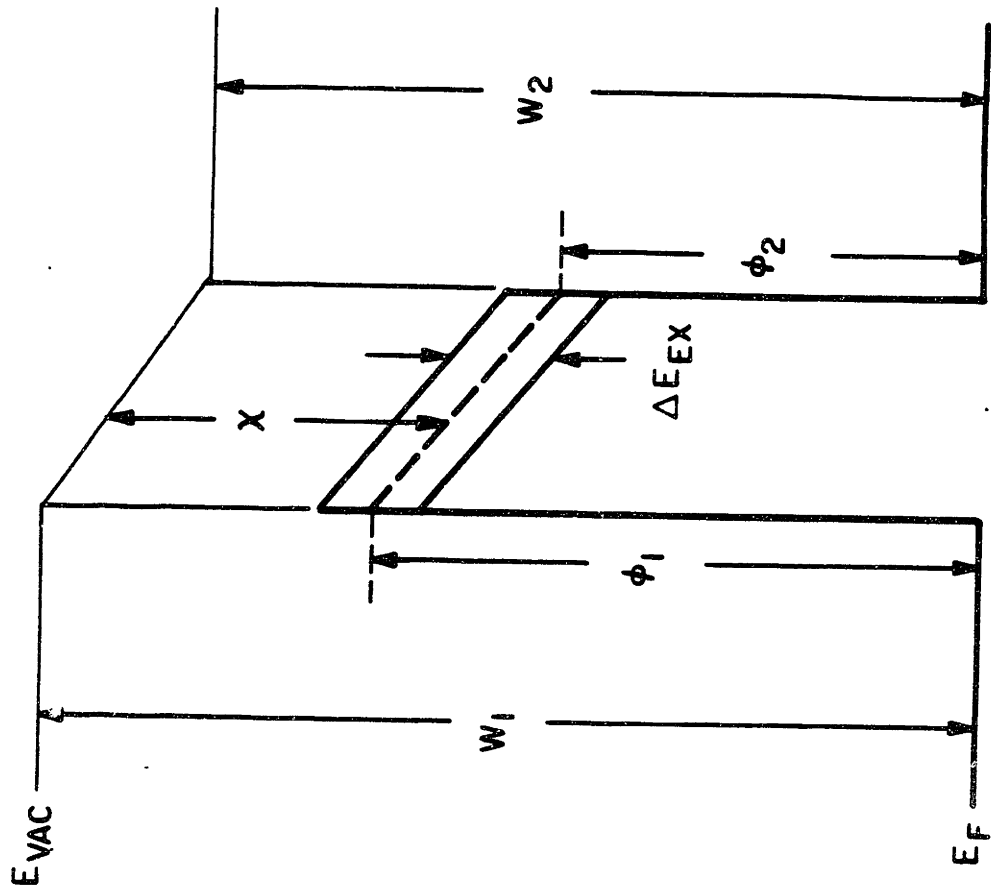Figure 1. Conductance versus voltage for a Au/EuS/Aℓ junction from set 1
(deposited at 80 K) at T = 0.4 K for various values of applied
magnetic field H indicated in teslas. Fitting theory to the
curves gives P = 55±5%. The curve H = 0 was made before a field
was applied. The dashed curve H = 0' was made after having
applied a field of 2.09 T and shows Zeeman splitting and
polarization on returning to zero field.

Figure 2. Conductance versus voltage for a Au/EuS/Aℓ junction from set 2
(Au and EuS deposited at 300 K) at T = 0.4 K for various values
of H. Fitting theory to the curves gives P = 80±5%. Curves were
all taken in increasing field. Hysteresis was observed in
decreasing H, but is not shown.

Figure 3. Schematic representation of the tunnel barrier of a Au/EuS/Aℓ
junction. W_1 and W_2 are the work functions of Au and Aℓ, respec-
tively. χ is the electron affinity of EuS. The barrier heights
at the Au and Aℓ interfaces are shown as ϕ_1 and ϕ_2 at the bottom
of the EuS conduction band (dashed) at T > 16.7 K. The bottom of
the two bands shown at T << T_c by the solid lines separated by
ΔE_{ex} are the barriers seen by the two spin directions.

The figure shows dI/dV ($\times 10^{-3}$ Ω^{-1}) plotted against $V_{A\ell} - V_{Au}$ (mV), with curves labeled 0, 0.07, 0.13, and 0.15T.

REFERENCES

● Abrikosov, A.A., and L.P. Gorkov, Zh. Eksp. Teor. Fiz. **42**, 1088 (1962) [*Soviet Physics* - JETP **15**, 752 (1962)].

● Alexander, J.A.X., T.P. Orlando, D. Rainer, and P.M. Tedrow, Phys. Rev. **B 31**, 5811 (1985).

● Alexander, J.A.X., Ph. D. thesis (unpublished), M.I.T. (1986).

● Allen, P.B., and R.C. Dynes, Phys. Rev. **B12**, 905 (1975).

● Altschuler, B.L., and A.G. Aronov, *Soviet Physics*-JETP **50**, 968 (1979).

● Altschuler, B.L., A.G. Aronov, and P.A. Lee, Phys. Rev. Lett. **44**, 1288 (1980).

● Baym, G., and C. Pethick, in *The Physics of Liquid and Solid Helium*, Part II, ed. K.H. Benneman, and J.B. Ketterson (John Wiley & Sons, New York, N.Y. 1978).

● Bergmann, G., Phys. Rev. **B7**, 4850 (1973).

● Berk, N.F., and J.R. Schrieffer, Phys. Rev. Lett. **17**, 433 (1966).

- Bowser, W.M., and W.H. Weinberg, Rev. Sci. Instru. **47**, 583 (1976).

- Bowser, W.M., and W.H. Weinberg, Surf. Sci. **64**, 377 (1977).

- Bowsio, L., A. Defrain, J. Keystone, and J. C. Vallier, Compt. Rend. **261**, 5431 (1965).

- Browne, D.A., K. Levin, and K.A. Muttalib, Phys. Rev. Lett. **58**, 156 (1987).

- Bruno, R.C., and B.B. Schwartz, Phys. Rev. **B8**, 3161 (1973).

- Bückel, W., and R. Hilsch, Z. Phys. **138**, 109 (1954).

- Burnell, D.M., J. Zasadzinski, R.J. Noer, and E.L. Wolf, Solid State Commun. **41**, 637 (1982).

- Chen, T.T., J.T. Chen, J D Leslie, and H.J.T. Smith, Phys. Rev. Lett. **22**, 526 (1969).

- Clogston, A.M., Phys. Rev. **125**, 439 (1962).

- Cohen, R.W., B. Abeles, and G.S. Weisbarth, Phys. Rev. Lett. **18**, 336 (1967).

- Crow, J.E., M. Strongin, and A.K. Bhatnagar, Phys. Rev. **B9**, 135 (1974).

- Daams, J.M., B. Mitrović, and J.P. Carbotte, Phys. Rev. Lett. **46**, 65 (1981).

- deGennes,P.G., *Superconductivity of Metals and Alloys*, ch. 8 (W.A. Benjamin, New York, N.Y. 1966).

- Dynes, R.C., J.P. Garno, G.B. Hertel, and T.P. Orlando, Phys. Rev. Lett. **53**, 2437 (1984).

- Dynes, R.C., V. Narayanamurti, and J.P. Garno, Phys. Rev. Lett. **41**, 1509 (1978).

- Eilenberger, G., Z. Phys. **214**, 195 (1968).

- Engler, H., and P. Fulde, Z. Phys. **247**, 1 (1971).

- Feder, J., S.R. Kiser, F. Rothwarf, J.P. Burger, and C. Valette, Solid State Commun. **4**, 611 (1966).

- Fulde, P., Adv. Phys. **22**, 667 (1973).

- Gallagher,W., Ph. D. thesis (unpublished), M.I.T. (1978).

- Gershenzon, M. E. , V. N. Gubankov, and M. I. Falei, Zh. Eksp. Teor. Fiz. **90**, 2196 (1986) [JETP **63**, 1287 (1986)].

- Gibson, G.A., and R. Meservey, J. of Appl. Phys. **58**, 1584 (1985).

- Gibson, G.A., and R. Meservey, Bull. Am. Phys. Soc. **31**, 437 (1986).

- Gibson, G.A., R. Meservey, and P.M. Tedrow, Bull. Am. Phys. Soc. **30**, 280 (1985).

- Gibson, G.A., R. Meservey, and P.M. Tedrow, Bull. Am. Phys. Soc. **33**, 263 (1988).

- Gladstone, C., M.S. Jensen, and J.R. Schrieffer, in *Supercon-ductivity*, R.D. Parks, ed. (Marcel Dekker, NY, 1969).

- Gurvitch, M., and J. Kwo, in *Advances in Cryogenic Engineer-ing*, ed. A.F. Clark and R.P.Reed (Plenum, N.Y.), **30**, 509 (1984).

- Hake, R.R., Phys. Rev. **158**, 356 (1966).

- Imry, Y., and A. Ovadyahu, Phys. Rev. Lett. **49**, 841 (1982).

- Jensen, M.A., and K. Andres, Phys. Rev. **165**, 545 (1968).

- Landau, L.D., Zh. Eksp. Teor. Fiz. **30**, 1058 (1956) [*Soviet Physics* - JETP **3**, 920 (1957)].

- Landau, L.D., Zh. Eksp. Teor. Fiz. **35**, 95 (1958) [*Soviet Physics* - JETP **8**, 70 (1959)].

- Landau, L.D., and E.M. Lifshitz, *Quantum Mechanics*, (Pergamon Press, NY, 1977), section 72.

- Larkin, A.I., and Yu. N. Ovchinnikov, Zh. Eksp. Teor. Fiz. **55**, 2262 (1968).

- Leavens, C.R., and A.H. MacDonald, Phys. Rev. **B27**, 2812 (1983).

- Leggett, A.J., Phys. Rev. **140**, A 1869 (1965).

- Leggett, A.J., Ann. Phys. **46**, 76 (1968).

- Leggett, A.J., Rev. Mod. Phys. **47**, 331 (1975).

- Leslie, J.D., J.T. Chen, and T.T. Chen, Can. J. of Phys., **48**, 2783 (1970).

- Lutskii, V. N., A. S. Rylik, and A. K. Savchenko, Pis'ma Zh. Eksp. Teor. Fiz. **41**, 134 (1985) [JETP Lett. **41**, 163 (1985)].

- Mackintosh, A.R., and O.K. Anderson, in *Electrons at the Fermi Surface*, ed. M. Springford, (Cambridge Univ. Press, NY 1980).

- McMillan, W.L., Phys. Rev. **167**, 331 (1968).

- McMillan, W.L., Phys. Rev. **B24**, 2739 (1981).

- Maki, K., Phys. Rev. **148**, 362 (1966).

- Meservey, R., D. Paraskevopoulos, and P.M. Tedrow, Phys. Rev. **B22**, 1331 (1980).

- Meservey, R., and P.M. Tedrow, Phys. Rev. Lett. **41**, 805 (1978).

- Meservey, R., P.M. Tedrow, and J.S. Brooks, J. Appl. Phys. **53**, 1563 (1982).

- Meservey, R., P.M. Tedrow, and R.C. Bruno, Phys. Rev. **B11**, 4224 (1975).

- Meservey, R., P.M. Tedrow, and R.C. Bruno, Phys. Rev. **B17**, 2915 (1978).

- Meservey, R., P.M. Tedrow, and J.S. Moodera, J. Mag. Mag. Mat. **35**, 1 (1983).

- Minnigerode, G.V., and J. Rothenberg, Z. Physik **213**, 397 (1968).

- Moodera, J.S., R. Meservey, and P.M. Tedrow, IEEE Trans. on Magnetics, MAG-21, 551-554, (1985).

- Moodera, J.S., private communication (1986).

- Moodera, J.S., private communication (1987a).

- Moodera, J.S., private communication (1987b).

- Naugle, D.G., and Glover, R.E., Physics Letters **28A**, 611 (1969).

- Orlando, T.P., E.J. McNiff, Jr., S. Foner, and M.R. Beasley, Phys. Rev. **B19**, 4545 (1979).

- Orlando, T.P., and M.R. Beasley, Phys. Rev. Lett. **46**, 1598 (1981).

- Platzman, P.M., and P.A. Wolff, in *Waves and Interactions in Solid State Plasmas*, Suppl. 13 of *Solid State Physics: Advances in Research and Applications*, ed. F. Seitz and D. Turnbull (Academic Press, New York, N.Y. 1973).

- Rietschel, H., and H. Winter, Phys. Rev. Lett. **43**, 1256 (1979).

- Rietschel, H., H. Winter, and W. Reichardt, Phys. Rev. **B22**, 4284 (1980).

- Serene, J.W., and D. Rainer, Phys. Rev. **101**, 221 (1983).

- Tedrow, P.M., J.T. Kucera, D. Rainer, and T.P. Orlando, Phys. Rev. **52**, 1637 (1984).

- Tedrow, P.M., and R. Meservey, Phys. Rev. Lett. **26**, 192 (1971).

- Tedrow, P.M., and R. Meservey, Phys. Rev. **B7**, 318 (1973).

- Tedrow, P.M., and R. Meservey, Physics Letters **51A**, 57 (1975a).

- Tedrow, P.M., and R. Meservey, Proc. LT-14, eds. M. Krusius and M. Vuorio (North-Holland, Amsterdam), Vol. 2, 75 (1975b).

- Tedrow, P.M., and R. Meservey, Physics Letters, **69A**, 285 (1978a).

- Tedrow, P.M., and R. Meservey, Solid State Commun. **27**, 1397 (1978b).

- Tedrow, P.M., and R. Meservey, Phys. Rev. Lett. **43**, 384 (1979).

- Tedrow, P.M., and R. Meservey, Phys. Rev. **B25**, 171 (1982).

- Tedrow, P.M., J.S. Moodera, and R. Meservey, Solid State Commun. **44**, 587 (1982).

- Teplov, A.A., M.N. Mikheeva, V.M. Golyanov, and A.N. Gusev, Sov. Phys. JETP **44**, 587 (1976).

- Tinkham, M., *Introduction to Superconductivity* (Robert Krieger Publishing C., N.Y., 1975), p. 270.

- Tkaczyk, J.E., Ph. D. thesis (unpublished) M.I.T. (1988)

- Usadel, K.D., Phys. Rev. Lett. **25**, 507 (1970).

- Vedeneev, S.I., and A.V. Pogrebnyakov, Sov. Phys. Solid State **20**, 1223 (1978).

- Vier, D.C., D.W. Tolleth, and S. Schultz, Phys. Rev. **B29**, 88 (1984).

- Werthamer, N.R., in *Superconductivity*, ed. R.D. Parks (Marcel Dekker, New York 1969), Vol.1, p.357.

- Werthamer,N.R., E. Helfand, and P.C. Hohenberg, Phys. Rev. **147**, 295 (1966).

- Wilkins, J.W., in *Electrons at the Fermi Surface*, ed. M. Springford (Cambridge University Press, London 1980).

- Wolf, E.L., *Principles of Electron Tunneling Spectroscopy*, (Oxford, New York, N.Y. 1985).

- Wolff, P.A., Phys. Rev. **120**, 814 (1960).

- Wuhl, H., J.E. Jackson, and C.V. Briscoe, Phys. Rev. Lett. **20**, 1496 (1968).

- Yafet, Y., Solid State Physics **14**, 1 (1963).

- Zasadzinski, J., D. M. Burnell, and E. L. Wolf, Phys. Rev. **B25**, 1622 (1982).